Technische Universität München

Fakultät für Maschinenwesen

TUM

Preview Feedforward Control for Active Vibration Damping of a Hybrid Suspension System

Johannes N. Strohm

Vollständiger Abdruck der von der Fakultät für Maschinenwesen der Technischen Universität München zur Erlangung des akademischen Grades eines

Doktor-Ingenieurs

genehmigten Dissertation.

Vorsitzender: Prof. Dr. phil. Klaus Bengler
Prüfer der Dissertation: 1. Prof. Dr.-Ing. habil. Boris Lohmann
2. Prof. Dr.-Ing. Ansgar Trächtler

Die Dissertation wurde am 06.04.2020 bei der Technischen Universität München eingereicht und durch die Fakultät für Maschinenwesen am 10.11.2020 angenommen.

"So ist die den Akt der Objektivierung abschließende Regelungstechnik die methodische Vollendung der Technik."

Denkschrift zur Gründung eines Insitutes für Regelungstechnik, Prof. Dr. Phil. Hermann Schmidt, Deutschlands erster ordentlicher Professor für Regelungstechnik, 1941

Hence, automatic control, which completes the act of objectification, is the methodical perfection of technology.

Memorandum on the foundation of an institute for automatic control, Prof. Dr. Phil. Hermann Schmidt, Germany's first full professor for automatic control, 1941

ABSTRACT

The question of how to increase driving comfort in road vehicles was already asked centuries ago. Back then, mechanical and later hydraulic solutions were found. In recent decades semi-active and active suspensions have been introduced, which alter their behavior during the ride. With those arose the need for suitable control laws.

In this thesis the focus is set on preview feedforward controllers for vibration damping of a quarter car. Assuming that environmental sensors in autonomous cars can also detect road irregularities, the road profile in front of the vehicle is considered to be known. To exploit this information, various feedforward controllers are proposed. All of them are model-based and require only few computational resources. The novelty is that pure feedforward controllers are used and that aspects are explicitly considered that are usually neglected, e.g., varying preview time and nonlinear dynamics in the spring and damper characteristics. Therefore, not only known schemes are applied but also new methods for the preview controller design are proposed.

Both, simulations and experiments show that a remarkable improvement of driving comfort can be achieved based on the road preview information only. Furthermore, the driving safety, which is the conflicting goal to driving comfort, is not decreased. It is also confirmed that considering the nonlinearities of the suspension in the controller design is advantageous compared to a linear treatment of the problem. Finally, the significant impact of the preview time on the performance is shown as well as the importance of taking the varying preview time explicitly into account to improve the driving comfort.

ACKNOWLEDGMENTS

CONTENTS

1 Introduction and Problem Statement

The suspension is one of the essential parts in todays cars. On the one hand manufacturers use it to establish a characteristic driving behavior of their cars. On the other hand a suspension is required to ensure driving comfort and driving safety –which is often advertised as sporty behavior– for various driving speeds, road types, or driving maneuvers. The driving comfort is characterized by the human body acceleration while the driving safety depends on the lateral and longitudinal forces that can be transmitted between the wheel and the road. The development from first simple suspensions to modern electronically controlled systems, which we consider in this thesis, took centuries. Along the way, not only the suspension components changed but also the objectives and technical possibilities. The short overview of the history of suspensions shows why it is still relevant to do research in the field of control of active suspensions and derives the today's challenges and goals.

The first suspensions date back to the Romans in the second century after Christ. They tried to decouple the movements of the body of their journey carriages from the wheel frame by mounting the body pendulously on leather belts [65]. Back then, the objective was clearly to improve driving comfort during long trips on roads in bad condition. With the advancement in coach technology the first metal leaf springs were introduced in the 17$^{\text{th}}$ century to ensure comfort at higher velocities. However, the average driving velocity of a coach was below 20 km/h such that driving safety, in terms of good road holding, did not play a role. This changed with the advent of faster motorized coaches at the beginning of the 20$^{\text{th}}$ century, when the objective had to be shifted from pure comfort maximization to comfort and safety maximization to ensure safe driving. At that time manufacturers began to mount both, springs and damping devices in vehicles to achieve this goal [17]. However, this so called passive suspension is only capable to maximize either driving comfort or driving safety: if a soft spring and a soft damper are used, the suspension can be easily compressed, for example in the case of a bump. Thus, the shock is absorbed which increases the driving comfort. However, the wheel tends to lose road contact, which means a loss of driving safety, if

the suspension is readily compressible. Vice versa, a harder suspension setting leads to good road holding, but to a worse comfort as road disturbances are easily transmitted to the chassis. Thus, driving comfort and driving safety are two conflictive objectives in passive suspension.

To further increase driving comfort without decreasing driving safety, semi-active and active suspensions were introduced. Semi-active suspensions incorporate a damper whose damping can be altered during the ride, while active suspensions contain actuators that can apply forces independently of the relative movement between the chassis and the wheel. With these components the suspension behavior can be adapted, for example to the current road condition and driving velocity such that the comfort is increased while maintaining sufficient driving safety. The first semi-active suspensions with variable damping were already developed and widely applied in the 1930s e.g., the Hartford Telecontrol [17]. With this system the driver could alter the normal force between the friction discs inside the dry friction damper via a Bowden cable during the ride and thus modify the damping according to the street conditions and driving velocity. In 1975, the company Automotive Products was the first to develop an active hydraulic suspension. This suspension could introduce additional forces between wheel and chassis via hydraulic cylinders. It was used in combination with a mechanical control valve to decrease the roll movement [31]. The first active suspension that was controlled electronically was built in a Lotus Esprit in 1983. The controller determined based on various sensor measurements the force that has to be applied via the actuators to level out the ride height. This car clarified that not only the hardware, i.e. the suspension, impacts the driving behavior but also the applied control algorithm. However, the Lotus remained a demonstrator and was never produced in series production [44].

The manufacturer's pursuit of increasing the driving comfort especially in upper class vehicles continued. Besides the cheaper semi-active suspensions, particularly active systems with an electronic controller as presented in the Lotus seemed to be promising regarding a comfort improvement without a decrease in driving safety. While Toyota used semi-active suspensions already in 1983 in series production cars [141] it took some time until the first active system was realized: In 1999 Mercedes introduced a slow active suspension to counteract road disturbances in series production cars. The system named Active Body Control (ABC) contains a controller that determines the force to be applied between the tire and the car body via a hydraulic cylinder [97].

Despite the remarkable performance of the ABC system the interest in bringing further, new active suspensions in series production decreased in the following years, as the comfort requirements of most drivers were met with the existing systems. Although

some new prototypes like the electro-mechanic ABC [86] and the active "ACOCAR™ damper" [125] have been developed, none of them was brought to series production. This changed from 2017 on when several companies began to present new active suspensions. The first one was Audi which announced its new approach "Audi AI active suspension" in 2017 [50]. In the following year 2018, Mercedes presented its completely revised "eABC" system [14]. Furthermore, in 2018 ZF revealed its new active damper "sMOTION" [145]. A similar approach was taken by the American start-up Clearmotion, which emerged in 2017 with its first active damper for cars [12]. Lately, the development of new active suspensions was also subject of scientific research. There are, for example, recent publications concerning a regenerative electromagnetic damper [38], a ball screw damper [46], and approaches comprising an electric motor with a lever in the suspension [4, 143]. Thus, the interest in active suspensions has grown again in industry and science in the last few years.

What is the cause for this renaissance of active suspensions? One motivation is autonomous driving which introduces new objectives as well as new technical possibilities. In an autonomous car the driver becomes a passenger. While a driver requires some feedback via car vibrations to perceive the road conditions and the current driving state, a passenger does not need to get this feedback. Furthermore, a passenger usually uses the time during a ride for activities like working, relaxing, or sleeping which requires the driving comfort to be as high as possible. Thus, the objective is shifted to pure maximization of driving comfort while sporty behavior in terms of good road holding for rapid acceleration and fast cornering maneuvers is not important any more. However, a certain level of driving safety is still required. To maximize driving comfort without losing driving safety an active suspension system is needed. As the development of autonomous driving advances fast, manufacturers' interest in active suspension systems is growing.

The application of active suspensions is only possible if these are combined with suitable software, namely a controller. It determines the input of the actuator, e.g., desired force or damping, based on measured quantities such as vertical chassis acceleration, vertical wheel acceleration, and suspension deflection to achieve a desired suspension behavior. Thus, the driving comfort is not only increased by the use of improved hardware, but also crucially affected by the chosen control algorithm. As updating the software to improve the performance is much cheaper than replacing the hardware, manufacturers' interest in advanced control strategies for active suspensions has also grown in the last few years.

In order to make a car drive autonomously lots of sensors are required for the de-

tection of lanes, obstacles, other cars, and humans. These lead to new possibilities regarding the controller design: Some of the sensors, i.e. cameras and Light Detection And Ranging (LIDAR) sensors, can also be used to detect the road profile in front of the car, see Figure 1.1. The road profile irregularities are the main disturbance regarding a vehicle's vertical dynamics. As this thesis focuses on the vertical dynamics it is legitimate to assume that the disturbance will be known within a certain range ahead of the autonomous car in the future. The question is, how the controller for the active suspension can exploit this knowledge to further increase driving comfort.
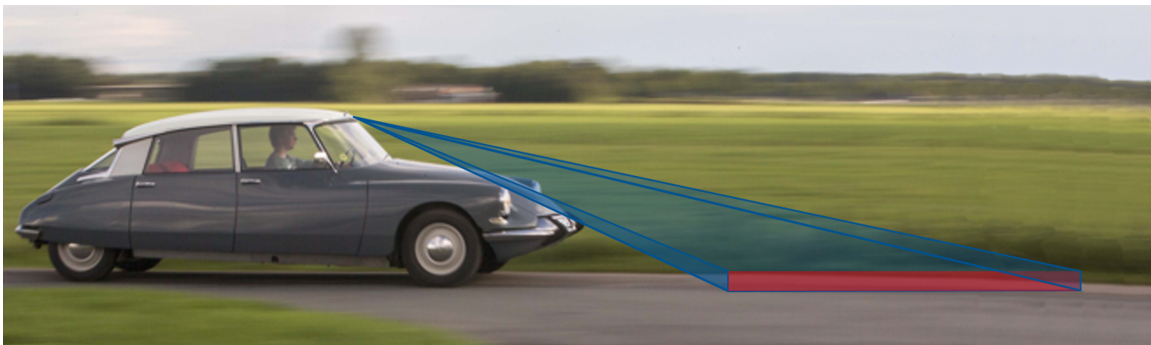
Figure 1.1: Preview horizon (red area) with camera behind rear view mirror

The present thesis provides answers to this question by proposing several so called preview feedforward controllers that calculate the suspension's actuator input based on the road profile preview information only. As only the vertical dynamics are to be considered it is sufficient to regard a quarter of a car, which consists of one wheel, one suspension and a quarter of the chassis mass. Furthermore, it is assumed throughout this thesis that the road profile is known up to a certain distance in front of the vehicle. Under these assumptions, the design of a preview feedforward controller that maximizes driving comfort without decreasing driving safety is still very challenging due to the following requirements:

○ The suspension deflection must not meet or exceed the deflection limits.

○ The chassis mass of a car changes due to different number of passengers or different loads. The controller has to improve the performance within a wide range of deviations from the nominal chassis mass.

○ The future disturbance is only known up to a certain distance in front of the car (horizon). The time span between the detection of the disturbance at the end of this horizon and the effect of that disturbance at the tire depends on the vehicle velocity. As the latter is never constant in a real car, this time span varies. From

the vehicle's view, the time span is the *preview time*. From the point of view of the detected disturbance at the end of the horizon, there is a *time delay*. Both terms are used interchangeably in this thesis.

○ Ideally, the inherent nonlinearities in the suspension, e.g., in the damper and spring characteristics, are included in the controller design to achieve the maximum performance.

○ As the controller should be applicable in a real world car it has to be insensitive to measurement noise, especially in the detected road profile.

○ The approaches have to work with limited computational resources.

○ The controlled active suspension has to improve comfort for various driving velocities and various road types.

○ The tuning parameters should be as intuitive as possible to facilitate the application into a real car.

The main contributions of this thesis to overcome these challenges are:

○ The development of a method to design analytically a proactive Finite Impulse Response (FIR) filter, which can be used as a preview feedforward controller.

○ The application of the proactive FIR filter in a linear proactive disturbance compensator for the quarter car in order to exploit the road profile preview. This led in experiments to an improvement of driving comfort of more than 50% compared to a passive suspension.

○ The development of a variant of the active noise canceling algorithm Filtered-x Least Mean Squares (FxLMS) that converges very fast.

○ The application of this variant for vibration damping of the quarter car. This led to an adaptive linear disturbance compensator that is capable of coping not only with slow changes in the road profile characteristics but also with jumps in the preview time.

○ The combination of a flatness based and a proactive FIR filter based disturbance compensator which results in a proactive nonlinear disturbance compensator. By considering the nonlinear dynamics of the quarter car this controller achieved in experiments a comfort improvement of almost 57% compared to a passive suspension.

○ The application of an H∞ control method for time delay systems to the quarter car. This results in a control-law which includes the preview time as an explicit parameter. Thus, only one parameter has to be changed if the preview time changes.

The thesis is structured as follows: Chapter 2 introduces the theoretical background of the applied methods, the considered quarter car models and existing approaches to active vibration damping. In Chapter 3 the accomplishments regarding preview control are presented in the form of summaries of the original publications reprinted in the Appendix. Chapter 4 puts these publications into one context, discusses the results of the presented approaches and shows the connection to existing literature. Furthermore, an outlook to further research directions is given based on this discussion.

2 PRELIMINARIES

The preview control methods presented in Chapter 3 are model based methods. They base upon different model types such as state-space models, time discrete transfer functions and time-delay state-space models, which are introduced in this chapter. Furthermore, the concepts of flat systems and of the Least Mean Square (LMS) algorithm are shown to facilitate the understanding of the methods derived and applied in this thesis. Besides the system theoretic fundamentals, various models of the quarter car as well as a description of the institute's test stand are presented. Moreover, the used road profiles are introduced and the considered performance criteria are explained. Finally, an overview of the existing feedforward and feedback control approaches with and without preview for vibration damping of the quarter car is given in this chapter.

2.1 Fundamentals of Systems Theory

The dynamics of a time invariant, input affine, possibly nonlinear system can be represented as a state-space model

$$\dot{\mathbf{x}} = \mathbf{f}(\mathbf{x}) + \sum_{i=1}^{m} \mathbf{g}_i(\mathbf{x}) u_i \tag{2.1}$$

$$\mathbf{y} = \mathbf{h}(\mathbf{x}, \mathbf{u}) \tag{2.2}$$

with the state vector $\mathbf{x} = [x_1,\ x_2, \cdots,\ x_n]^T \in \mathbb{R}^n$, the input $\mathbf{u} = [u_1,\ u_2, \cdots,\ u_m]^T \in \mathbb{R}^m$, and the output $\mathbf{y} = [y_1,\ y_2, \cdots,\ y_p]^T \in \mathbb{R}^p$. This representation is very convenient to understand the relation between input and state, and between state and output and is therefore often used for analysis as well as for controller design [49]. If the system has a linear behavior or can be locally approximated with linear behavior the dynamics can be expressed as a Linear Time Invariant (LTI) system

$$\dot{\mathbf{x}} = \mathbf{A}\mathbf{x} + \mathbf{B}\mathbf{u} \tag{2.3}$$

$$\mathbf{y} = \mathbf{C}\mathbf{x} + \mathbf{D}\mathbf{u} \tag{2.4}$$

with constant matrices $\mathbf{A}, \mathbf{B}, \mathbf{C}, \mathbf{D}$ of suitable dimensions. The dynamics (2.3),(2.4) can also be considered in discrete time

$$\mathbf{x}[k+1] = \mathbf{A}_d\mathbf{x}[k] + \mathbf{B}_d\mathbf{u}[k] \tag{2.5}$$

$$\mathbf{y}[k] = \mathbf{C}_d\mathbf{x}[k] + \mathbf{D}_d\mathbf{u}[k] \tag{2.6}$$

with the sufficiently small, fixed sample time T_s and the matrices $\mathbf{A}_d = e^{\mathbf{A}T_s}$, $\mathbf{B}_d = (\mathbf{A}_d - \mathbf{I})\mathbf{A}^{-1}\mathbf{B}$ with identity $\mathbf{I}$ of suitable dimension, $\mathbf{C}_d = \mathbf{C}$, and $\mathbf{D}_d = \mathbf{D}$ [89].

2.1.1 System Representation as a Matrix Product

Besides the representation of the system dynamics as a state space model it can also be expressed as transfer functions. These relate the input directly to the output and are usually given in the Laplace domain. In the Laplace domain a continuous time transfer function for a Single Input Single Output (SISO) system has the form [90]

$$G(s) = \frac{Y(s)}{U(s)} = \frac{b_0 s^q + b_1 s^{q-1} + \cdots + b_{q-1}s + b_q}{a_0 s^n + a_1 s^{n-1} + \cdots + a_{n-1}s + a_n} \tag{2.7}$$

and in the discrete time case in the z-domain [89]

$$G_d(z) = \frac{Y_d(z)}{U_d(z)} = \frac{b_{d,0} z^q + b_{d,1} z^{q-1} + \cdots + b_{d,q}}{z^n + a_{d,1} z^{n-1} + \cdots + a_{d,n}} \tag{2.8}$$

with constant coefficients $a_i, b_i, b_{d,i}$, and $a_{d,i} \in \mathbb{R}$ and $q, n \in \mathbb{N}_0^+$. We will take a closer look at the discrete time systems, as the proactive FIR filter that is developed in Chapter 3 is based on such a representation. The transfer function (2.8), which is also called a filter, has in general an infinitely long impulse response. If the transfer function is asymptotically stable, meaning all poles are within the unit disc on the complex plane, the impulse response converges to zero. For such systems, the system dynamics can be approximated with an FIR filter

$$G_{FIR}(z) = \frac{g_0 z^N + g_1 z^{N-1} + \cdots + g_N}{z^N}. \tag{2.9}$$

The FIR filter's coefficients g_i are the values of the sampled and after $N+1$ timesteps cut impulse response. Increasing N leads to an increasing accuracy of the approximation. For $N \to \infty$ the FIR filter exactly represents the transfer function (2.8). Basically, the FIR filter performs a convolution of the cut impulse response with an input sequence $u[k]$ of arbitrary length. Assuming a fixed length $M > 0$ of the input sequence, the

convolution can be expressed as a matrix product

$$\mathbf{y}_t = \begin{bmatrix} y[0] \\ \vdots \\ y[N+M] \end{bmatrix} = \begin{bmatrix} g_0 & & \\ \vdots & \ddots & \\ g_N & & g_0 \\ & \ddots & \vdots \\ & & g_N \end{bmatrix} \begin{bmatrix} u[0] \\ \vdots \\ u[M] \end{bmatrix} = \mathbf{G}\mathbf{u}_t \qquad (2.10)$$

with the „dynamic matrix" $\mathbf{G}$ [13], which has Toeplitz form. The length of the input sequence M is called „control horizon" in the context of model predicitve control [76]. Although this representation is based on the cut impulse response and on the assumption of a fixed length input sequence, it is very useful for further calculations.

2.1.2 Flatness

In this thesis we use the notion of flatness presented in the application article [100] as it is described very concisely: Given the dynamic system (2.1) and assuming that it is possible to find an output $\mathbf{y}_f = \mathbf{h}(\mathbf{x}, \mathbf{u}, \dot{\mathbf{u}}, \cdots)$ with $m = p$ such that the state $\mathbf{x}$ and input $\mathbf{u}$ can be expressed as a function of the output and its time derivatives

$$\mathbf{x} = \mathbf{a}(y_1, \cdots, \overset{(\alpha_1)}{y_1}, \cdots, y_m, \cdots, \overset{(\alpha_m)}{y_m}) \qquad (2.11)$$

$$\mathbf{u} = \mathbf{b}(y_1, \cdots, \overset{(\alpha_1+1)}{y_1}, \cdots, y_m, \cdots, \overset{(\alpha_m+1)}{y_m}) \qquad (2.12)$$

then the output $\mathbf{y}_f$ is a flat output and the system (2.1) is flat. The interested reader is referred to [24] and [23] in French for a more theoretic introduction to flatness.

Once a flat output is found, it can be used for the straightforward design of feedforward and feedback controllers, for example like in [100, 112], as well as of a disturbance compensator as shown in Chapter 3. However, the difficulty lies in finding the flat output as there is no procedure for its construction in general. For certain types of systems, for example, systems that are endogenous dynamic feedback linearizable, it is at least proven that they are flat [70]. For a subclass of these, the so called input-to-state statically feedback linearizable systems, there exist even methods for the construction of a flat output $\mathbf{y}_f$ [49, 105]. These systems have the property, that it is possible to find a controller $\mathbf{u} = \mathbf{f_u}(\mathbf{x}, \mathbf{v})$ with the new reference input $\mathbf{v} \in \mathbb{R}^m$, such that the controlled system is equivalent to a controllable LTI system. Interestingly, we found that the nonlinear quarter car model fulfills all the conditions of an input-to-state statically feedback linearizable system, so that a flat output can be constructed (see Chapter 3).

2.1.3 Least Mean Squares Algorithm for Active Noise Control

The field of Active Noise Control (ANC) deals with methods to actively cancel out an undesired noise. These can be applied to many different domains, e.g., air-acoustic, hydro-acoustic, and vibration ANC. The main idea is always the same: Reducing the noise by superposing a signal with the same amplitudes but opposite phase, which is known as antinoise [66]. The question is how to determine the antinoise. This can be done using the LMS algorithm shown in Figure 2.1: The filter $W(z)$ computes the antinoise $u(n)$ based on the known disturbance $x(n)$ so that the disturbance at the output $d(n)$ of the system $P(z)$ is canceled out $e(n) = 0$. Obviously, $W(z)$ has
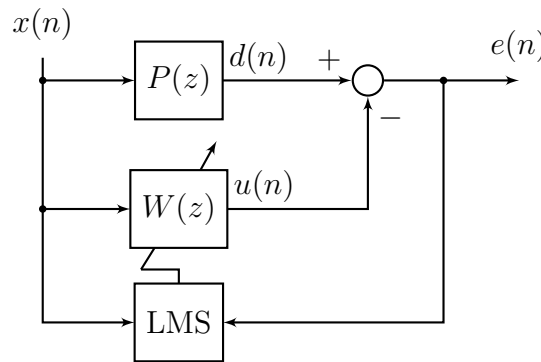
Figure 2.1: Block diagram of the LMS algorithm

to equal $P(z)$ to cancel the noise exactly. If $P(z)$ is unknown $W(z)$ can adapt this behavior using the LMS algorithm, which was first proposed in [137]. It has the goal to minimize the expected squared error $J = E[e(n)^2]$ by adapting the coefficients $\mathbf{w}(n) = [w_0(n) \ w_1(n) \cdots w_{L-1}(n)]^T$ of the FIR filter $W(z)$. The adaption is performed using the stochastic gradient descent to find the minimum. This means, that the gradient of J is approximated by the gradient of the instantaneous squared error $\tilde{J} = e(n)^2$ [66]:

$$\nabla \tilde{J} = 2[\nabla e(n)]e(n) = -2\mathbf{x}(n)e(n) \tag{2.13}$$

with $\nabla e(n) = \nabla(d(n) - \mathbf{w}^T(n)\mathbf{x}(n)) = -\mathbf{x}(n)$ and $\mathbf{x}(n) = [x(n) \ x(n-1) \cdots x(n-L+1)]^T$. According to the LMS algorithm the filter coefficients $\mathbf{w}(n)$ are shifted in each iteration a small step (step size μ) into the direction of the steepest decent $-\nabla \tilde{J}$ of the instantaneous error

$$\mathbf{w}(n+1) = \mathbf{w}(n) + \mu\mathbf{x}(n)e(n) \tag{2.14}$$

until the minimum is reached. In [136] it was shown that the expected value of the weight vector $\mathbf{w}(n)$ determined with the LMS algorithm (2.14) converges for stationary

input processes, with suitable step size μ, and with growing number of iterations to the optimal weight vector. Thus, the LMS algorithm is a very convenient way to determine the noise canceling FIR filter $W(z)$.

2.1.4 Time Delay Systems

Time delay models represent systems which incorporate a time delay in the state, the input, or the output. These exist in real world applications due to transport, actuator, or measurement delays. Linear time delay models can be divided into two types [26]: the retarded type in which the delay occurs in the state, e.g.,

$$\dot{\mathbf{x}}(t) = \mathbf{A}_0\mathbf{x}(t) + \mathbf{A}_1\mathbf{x}(t - \tau) + \mathbf{B}\mathbf{u}(t) \tag{2.15}$$

$$\mathbf{y} = \mathbf{C}\mathbf{x}(t) \tag{2.16}$$

and the neutral type systems, in which the delay can appear in the state and in the state derivative, e.g.,

$$\dot{\mathbf{x}}(t) = \mathbf{A}_0\mathbf{x}(t) + \mathbf{A}_1\mathbf{x}(t - \tau) + \mathbf{A}_2\dot{\mathbf{x}}(t - \tau) + \mathbf{B}\mathbf{u}(t) \tag{2.17}$$

$$\mathbf{y} = \mathbf{C}\mathbf{x}(t) \tag{2.18}$$

with square matrices $\mathbf{A}_0, \mathbf{A}_1, \mathbf{A}_2$, time delay τ, input $\mathbf{u}$, and state $\mathbf{x}$. The representation (2.15-2.16) is used to design the H∞ preview controller in Chapter 3.

To check the stabilizability of a retarded time delay system (2.15) the „γ-stabilizability" as presented in [92] can be used. The "γ-stabilizability implies the existence of $u(\cdot)$, $||u(t)|| < k_u e^{-\gamma t}$ such that the corresponding trajectory satisfies $||x(t)|| < k_x e^{-\gamma t}$ for some positive k_u, k_x and all $t > 0$" [92]. The system (2.15) is γ-stabilizable if and only if

$$\text{rank}([\mathbf{A}_t(s); \mathbf{B}]) = n \; \forall s \in \mathbb{C} \text{ with } \Re(s) \geq \gamma, \gamma \in \mathbb{R}_0^-, \tag{2.19}$$

where $\mathbf{A}_t(s) = \mathbf{A}_0 + e^{-s\tau}\mathbf{A}_1$. As the H$\infty$ controller for time delay systems presented in Chapter 3 is a combination of an observer and a controller, it is also important to verify the observability of the system. In contrast to LTI systems there are various notions of observability for time delay systems. In this thesis' context it is sufficient to regard the "strong observability". A system (2.15) with output (2.16) is strongly observable if

$$\text{rank}\left(\begin{bmatrix} s\mathbf{I} - \mathbf{A}_z(z) \\ \mathbf{C} \end{bmatrix}\right) = n \; \forall s, z \in \mathbb{C}, \tag{2.20}$$

with identity $\mathbf{I}$ of suitable dimension and $\mathbf{A}_z(z) = \mathbf{A}_0 + z\mathbf{A}_1$. The definition of the further observability notions and their relation can be found in [107].

2.2 Models and Test Stand

The driving comfort is affected by the heave, pitch, and roll movements of the car. In this thesis the focus is set on the heave modes while rolling and pitching are neglected. Thus, the relevant dynamics can be reduced to a quarter car. The quarter car is usually modeled as a two mass oscillator (e.g., [2, 39, 53, 127, 129, 139]). However, the chosen spring and damper characteristics (linear or nonlinear) of the suspension, tire model and actuator configuration vary broadly. The actuators are subdivided into two groups: the semi-active and active actuators. The former consist of variable dampers, that can alter their damping and thus, the damping force [103, 109]. The latter comprise all types of actuators that insert a force into the quarter car independently of the relative movement of the chassis and the wheel. In this thesis, a combination of active and semi-active actuators is considered. In the following, a short overview of different quarter car models is given. Furthermore, the institute's quarter car test stand, the used road profiles and their models are presented.

2.2.1 Linear Quarter Car Models

Figure 2.2a shows the scheme of a fully active linear quarter car with Gehmann model as tire model. "Fully active" refers to the actuator which is assumed to realize arbitrarily high forces $F(t)$, arbitrarily fast. The stiffness c_c and damping d_c of the suspension as
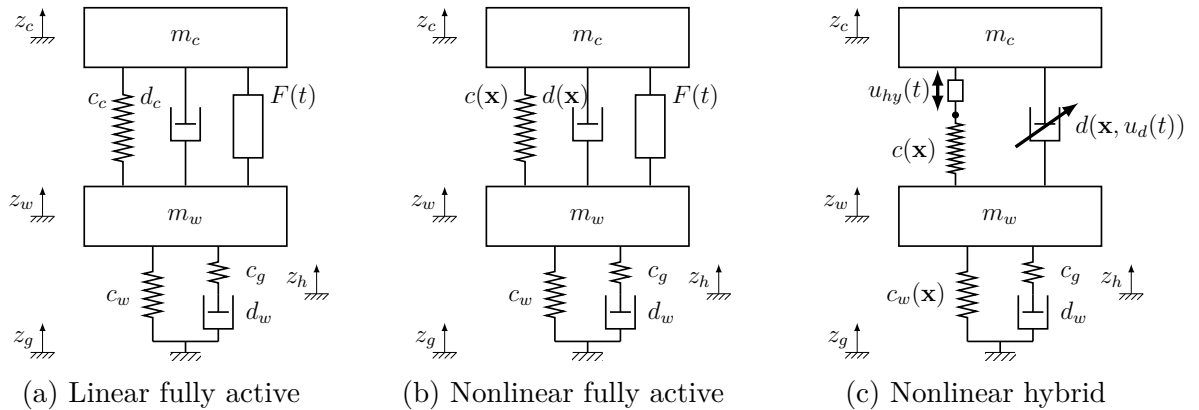

(a) Linear fully active   (b) Nonlinear fully active   (c) Nonlinear hybrid

Figure 2.2: Quarter car models

well as the tire stiffness c_w, Gehmann stiffness c_g, and tire damping d_w are assumed

to be constant in this model. The Gehmann model of the tire comprises a spring parallel to a series connection of a spring and a damper. This configuration emulates a frequency dependent damping coefficient in the tire model, which better represents the behavior of a rubber tire [82]. The state-space model is derived by using Newton's law and choosing the state vector to suspension deflection $z_c - z_w$, chassis velocity $\dot{z}_c$, tire deflection $z_w - z_g$, wheel velocity $\dot{z}_w$, and deflection of the Gehmann damper $z_h - z_g$:

$$\dot{\mathbf{x}} = \mathbf{A}\mathbf{x} + \mathbf{B}u + \mathbf{E}z, \text{ with} \tag{2.21}$$

$$\mathbf{x} = \begin{bmatrix} z_c - z_w & \dot{z}_c & z_w - z_g & \dot{z}_w & z_h - z_g \end{bmatrix}^T \tag{2.22}$$

$$\mathbf{A} = \begin{bmatrix} 0 & 1 & 0 & -1 & 0 \\ -\frac{c_c}{m_c} & -\frac{d_c}{m_c} & 0 & \frac{d_c}{m_c} & 0 \\ 0 & 0 & 0 & 1 & 0 \\ \frac{c_c}{m_w} & \frac{d_c}{m_w} & \frac{-c_w - c_g}{m_w} & \frac{-d_c}{m_w} & \frac{c_g}{m_w} \\ 0 & 0 & \frac{c_g}{d_w} & 0 & -\frac{c_g}{d_w} \end{bmatrix} \tag{2.23}$$

$$\mathbf{B} = \begin{bmatrix} 0 & \frac{1}{m_c} & 0 & -\frac{1}{m_w} & 0 \end{bmatrix}^T \tag{2.24}$$

$$\mathbf{E} = \begin{bmatrix} 0 & 0 & -1 & 0 & 0 \end{bmatrix}^T. \tag{2.25}$$

The input is the actuator force $u = F(t)$, the road profile velocity is the disturbance $z = \dot{z}_g$ and the parameters m_c and m_w denote the chassis mass and the wheel mass, respectively. The parameter values are given in Table 2.1. The choice of outputs depends on the control objectives. In this thesis the chassis acceleration, as measure for the driving comfort, the dynamic wheel load, as measure for the driving safety, and the suspension deflection are of interest (see Section 2.3)

$$y_1 = \ddot{z}_c = \begin{bmatrix} -\frac{c_c}{m_c} & -\frac{d_c}{m_c} & 0 & \frac{d_c}{m_c} & 0 \end{bmatrix} \mathbf{x} + \frac{1}{m_c}u \tag{2.26}$$

$$y_2 = F_{dyn} = \begin{bmatrix} 0 & 0 & -c_w - c_g & 0 & c_g \end{bmatrix} \mathbf{x} \tag{2.27}$$

$$y_3 = z_c - z_w = \begin{bmatrix} 1 & 0 & 0 & 0 & 0 \end{bmatrix} \mathbf{x}. \tag{2.28}$$

Based on the model (2.21), multiple simplified models can be derived. If, for example, the tire is to be modeled just as a stiffness without any damping, c_g has to be set to zero and the last state variable can be dropped. These linear models are used to design the proactive linear as well as the adaptive disturbance compensator. Moreover a time delay model is derived from these linear models.

2.2.2 Nonlinear Fully Active Quarter Car Models

Some of the controllers presented in this thesis base on the linear model. As the quarter car dynamics are – close to the equilibrium point – almost linear, this is a valid approach. However, the impact of the inherent nonlinear effects of the suspension gains importance, if the suspension deflection gets bigger. Therefore, it is not only necessary to model these nonlinearities but also to take them into account in the controller design. The main nonlinear effects are

- Progressive spring characteristic (see "total" in Figure 2.3a)

- Degressive damper characteristic (see characteristics for various damper valve currents i in Figure 2.3b)

- Dynamic kinematic transmission between suspension plane and tire plane [80]. The dynamic kinematic transmission is caused by the angle between the suspension and the direction of the heave motion (see Figure 2.4). Thus, only a fraction of the damper and spring forces takes effect in the direction of the heave motion. As the angle depends on the current suspension deflection the fraction of effective forces varies as well.

- Coulomb friction in the suspension

(a) Spring

(b) Damper
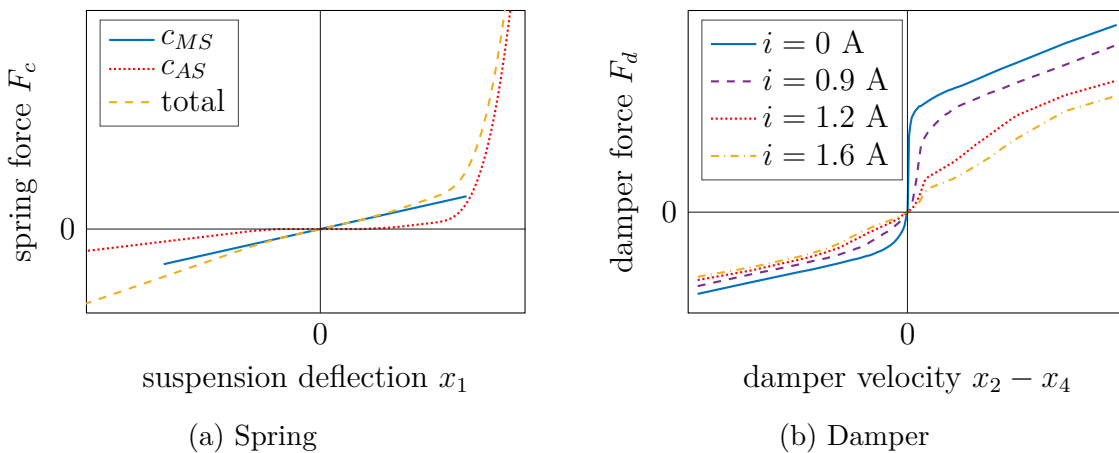
Figure 2.3: Nonlinear characteristics

Adding these nonlinearities to the model (2.21) leads to the configuration shown in Figure 2.2b: the nonlinear fully active quarter car. It is modeled as

$$
\dot{\mathbf{x}} = \begin{bmatrix} x_2 - x_4 \\ \frac{1}{m_c}(-\frac{i_x}{i_0}m_c g x_1 - F_d(\mathbf{x}) - F_c(\mathbf{x}) - F_r(\mathbf{x})) \\ x_4 \\ \frac{\frac{i_x}{i_0}m_c g x_1 + F_d(\mathbf{x}) + F_c(\mathbf{x}) + F_r(\mathbf{x}) + F_{dyn}(\mathbf{x})}{m_w} \\ \frac{c_g}{d_w}(x_3 - x_5) \end{bmatrix} + \begin{bmatrix} 0 & 0 \\ \frac{1}{m_c} & 0 \\ 0 & -1 \\ -\frac{1}{m_w} & 0 \\ 0 & 0 \end{bmatrix} \begin{bmatrix} u \\ z \end{bmatrix} \tag{2.29}
$$

$$
y_1 = \ddot{z}_c = \dot{x}_2 = \frac{-\frac{i_x}{i_0}m_c g x_1 - F_d(\mathbf{x}) - F_c(\mathbf{x}) - F_r(\mathbf{x}) + u}{m_c} \tag{2.30}
$$

$$
y_2 = F_{dyn}(\mathbf{x}) \tag{2.31}
$$

$$
y_3 = x_1 \tag{2.32}
$$

with the nonlinear forces

$$
F_d(\mathbf{x}) = i_{dyn}(x_1) \cdot d(i_{dyn} \cdot (x_2 - x_4)) \tag{2.33}
$$

$$
F_c(\mathbf{x}) = i_{dyn}(x_1) \cdot (c_{MS} i_0 x_1 - c_{AS}(-i_0 x_1)) \tag{2.34}
$$

$$
F_r(\mathbf{x}) = F_{r,max} \tanh(c_r \cdot (x_2 - x_4)), \tag{2.35}
$$

the kinematic transmission

$$
i_{dyn} = \frac{\dot{z}_c^{SP} - \dot{z}_w^{SP}}{\dot{z}_c - \dot{z}_w} = \frac{F}{F^{SP}} = i_0 - i_x(z_c - z_w) = i_0 - i_x x_1, \tag{2.36}
$$

and the dynamic wheel load

$$
F_{dyn} = -c_w x_3 - c_g \cdot (x_3 - x_5). \tag{2.37}
$$

Quantities with the superscript SP are in the suspension plane, without superscript in the tire plane (see Figure 2.4). The damping characteristic in (2.33) of a passive, non-actuated damper corresponds to the one with $1.2\,\mathrm{A}$ in Figure 2.3b. The spring characteristic consists of a constant stiffness c_{MS} and an additional nonlinear stiffness c_{AS} (see Figure 2.3a). The term $\frac{i_x}{i_0}m_c g x_1$ represents the gravitational forces that arise due to the kinematic transmission during suspension deflection. The parameter values for the model (2.29), which is used for the nonlinear disturbance compensator design, are stated in Table 2.1.
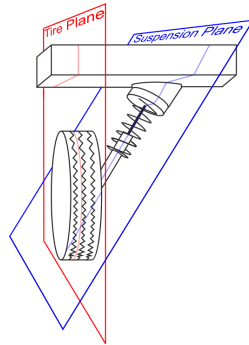
Figure 2.4: Suspension and tire plane

Table 2.1: Nominal Parameters

Description	Parameter	Value
Chassis mass	m_c	$507\,\text{kg}$
Wheel mass	m_w	$68\,\text{kg}$
Linear suspension stiffness	c_c	$24000\,\text{N/m}$
Linear suspension damping	d_c	$1400\,\text{Ns/m}$
Tire stiffness	c_w	$378\,000\,\text{N/m}$
Tire damping	d_w	$130\,\text{Ns/m}$
Gehmann stiffness	c_g	$52\,900\,\text{N/m}$
Constant transmission factor	i_0	0.685
Variable transmission factor	i_x	$0.309\,\text{1/m}$
Gravitational acceleration	g	$9.81\,\text{m/s}^2$
Max. Coulomb-friction	$F_{r,max}$	$65\,\text{N}$
Friction coefficient	c_r	0.04

2.2.3 Test Stand

The linear fully active and the nonlinear fully active model are both built under the assumption of an arbitrarily fast actuator between the chassis mass and the wheel mass. The driving comfort concerning the vertical dynamics has to be considered in a frequency range up to 25 Hz [82]. Thus, fully active actuators must have a cut off frequency of at least 25 Hz. If they are too slow, they act like a solid connection between wheel and chassis leading to a loss of driving comfort in the case of high frequency disturbances. There are only few realizations of such actuators, e.g., the Bose adaptive suspension [51]. Their main problems are the high energy consumption and packaging space. Therefore, a second type of active systems was introduced, the so called slow-active and hybrid configurations [59, 110, 129]. The slow-active suspension comprises an actuator with a small bandwidth (<25 Hz) mounted in series with the main spring which avoids the stiffening for high frequencies. Additionally to this actuator,

(a) Test stand   (b) Hybrid suspension

Figure 2.5: Quarter car test stand

the hybrid configuration incorporates a variable hydraulic damper whose damping can be modified by altering the current of the solenoid valve (see Figure 2.2c). This configuration was first developed at the author's institute [58] and also realized in a quarter car test stand (see Figure 2.5a). The suspension comprises a hydraulic Spring Mount Adjustment (SMA) from Mercedes' ABC [97] (Figure 2.5b blue frame) and a continuously variable damper from a BMW 7 series sedan (Figure 2.5b red frame). Due to the combination of these two actuators the suspension's performance is almost as good as a fully active one's, but requires considerably less energy [58]. In experiments, the chassis acceleration, the wheel acceleration and the suspension deflection are measured for feedback control. The controllers are implemented on a dSpace DS1103 PPC Controller Board and executed with a sample time of 1 ms. Details on the test stand, the actuator models and the low level actuator controllers are given in [56, 57, 94].

2.2.4 Nonlinear Hybrid Quarter Car Model

The hybrid model, which models the test stand most accurately, contains the same nonlinearities as the nonlinear fully active model. However, the real actuators are included, namely the SMA (cutoff frequency $\approx 5\,\mathrm{Hz}$) and the variable damper with characteristics as shown in Figure 2.3b. This model is used for simulation purposes

only, considers tire lift-off (for details see [114]) and additionally includes a quadratic tire stiffness. To apply a controller designed with one of the fully active models to the hybrid model or to the test stand, the calculated input force has to be split up into two portions: one for the SMA and one for the variable damper. This is done in a dynamic optimal fashion. In a first step, the SMA tries to realize the entire force. The high frequency parts that cannot be applied with the SMA are then used as the commanded input for the variable damper. Further details and other variants of the control allocation, e.g., the energy optimal control allocation, are given in [114].

The performance of the proposed controllers is always compared to the performance of a passive suspension when discussing the results. The nonlinear hybrid quarter car model is used with constant $1.2\,\mathrm{A}$ damper valve current and a fixed SMA to simulate the passive suspension. The same settings are chosen at the test stand for experiments with a passive suspension.

2.2.5 Road Profiles

Throughout this thesis two types of road profiles are used: measured and synthetic profiles. The measured road profile was recorded on a real existing country road in a bad condition (see Figure 2.6). It has very high amplitudes especially in the frequency range from $0.5\,\mathrm{Hz}$ to $10\,\mathrm{Hz}$ and is therefore, very well suited to test which amount of the road disturbance the controller is able to compensate. The synthetic road profiles
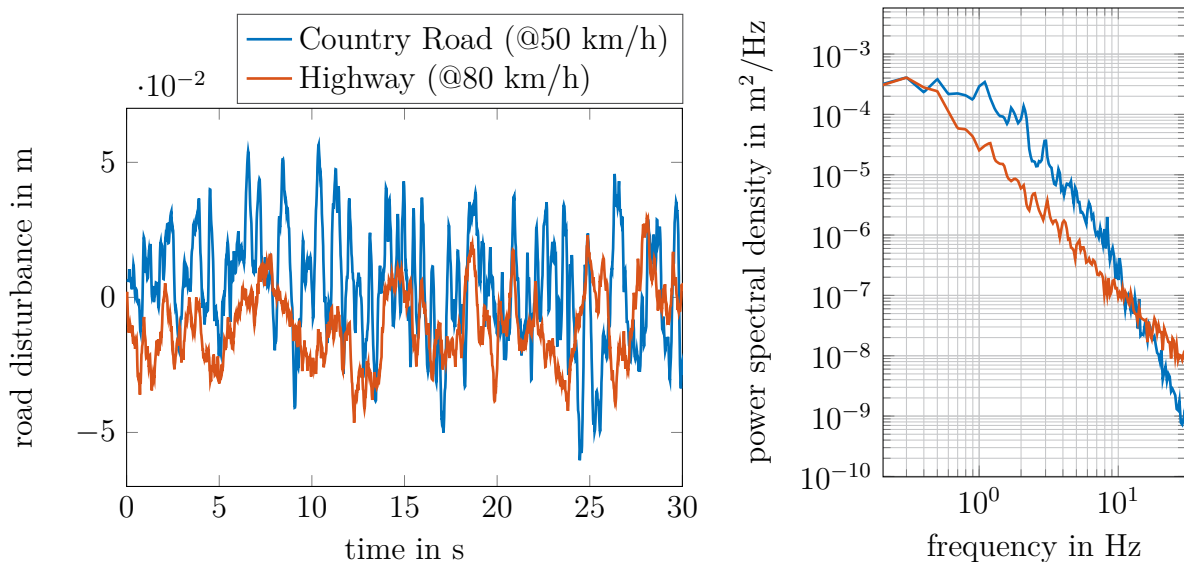
Figure 2.6: Road profiles

are generated by filtering a Gaussian white noise. As measured data has shown that

road profiles vary in their power spectral density depending on the road type, the filters are designed to generate profiles with power spectral densities $\Phi(\Omega)$ according to the desired road type [22, 82]

$$\Phi(\Omega) = \Phi(\Omega_0) \left[\frac{\Omega}{\Omega_0} \right]^{-w} \tag{2.38}$$

with angular spatial velocity Ω, waviness w, roughness $\Phi(\Omega_0)$ and the reference wave number $\Omega_0 = 1\,\mathrm{m^{-1}}$. For highways, for example, the waviness ranges between $w = 1.5$ and $w = 2.6$ and the roughness between $\Phi(\Omega_0) = 0.3\,\mathrm{cm^3}$ and $\Phi(\Omega_0) = 7.8\,\mathrm{cm^3}$. As the synthetic road profiles are more generic due to their stochastic nature, they are used for the controller tuning. An exemplary profile of a synthetic highway with parameters $w = 2.4$ and $\Phi(\Omega_0) = 5.3$ is shown in Figure 2.6.

2.3 Performance Criteria

The main goal of active suspension control in cars is to increase driving comfort, without losing driving safety. To quantify these objectives, measurable performance criteria have to be introduced. According to [48, 133] the driving comfort corresponds to the human body acceleration, which equals in the case of the quarter car the chassis acceleration $\ddot{z}_c$. The lower the amplitudes of acceleration, the higher the comfort. Furthermore, [48, 133] state that human's perception of oscillations depends on the frequency and direction. Oscillations in vertical direction are particularly uncomfortable in the range between $4\,\mathrm{Hz}$ and $8\,\mathrm{Hz}$. Thus, to further objectify the subjective perception of vibration, a frequency weighting filter with the magnitude plot shown in Figure 2.7 can be used. The chassis acceleration that was filtered with this frequency weighting is denoted $\ddot{z}_{c,comf}$.

Figure 2.7: Frequency weighting according to [133]

The driving safety is influenced by the tire-road contact. The better the contact, the better longitudinal and lateral forces can be applied during acceleration, breaking, and cornering. The 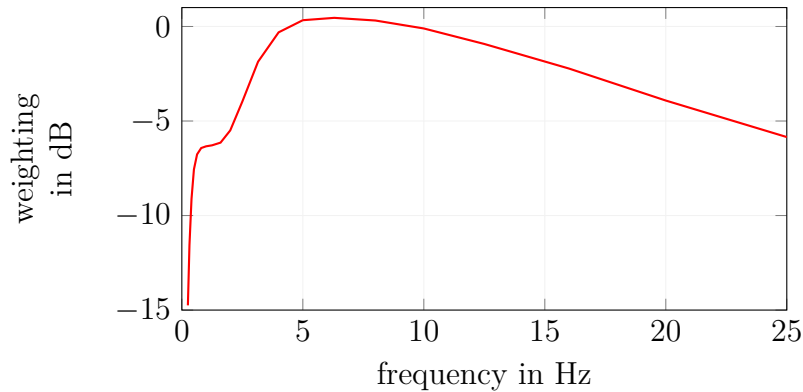tire-road contact corresponds to the normal force. Without any road disturbance the normal force between road and tire equals the static wheel force: the gravitational force of the quarter car $F_{stat} = (m_c + m_w)g$. It is reduced by the dynamic portion of the wheel force F_{dyn} in the case of wheel oscillations resulting from road disturbances. In the worst case, the dynamic wheel force becomes bigger than the negative static one ($F_{dyn} > -F_{stat}$) and the tire loses contact to the ground. Thus, to improve driving safety, the amplitudes of F_{dyn} have to be kept as small as possible such that $F_{dyn} < -F_{stat}$ is guaranteed.

Besides these two objectives, a third quantity has to be taken into account: the suspension deflection. In contrast to the chassis acceleration and the dynamic wheel load the suspension deflection $x_1 = z_c - z_w = z_{cw}$ does not have to be minimized. Instead, it is more important not to exceed the compression and rebound limits of $-10\,\mathrm{cm}$ and $11\,\mathrm{cm}$, respectively, as this leads to shocks in the chassis and thus, to low comfort.

In this thesis, the simulation runs and experiments are performed with road profiles with a length between $60\,\mathrm{s}$ and $100\,\mathrm{s}$. To compare for example multiple simulation runs performed with the same road profile but with different controllers, the trajectories of the objectives ($\ddot{z}_c, F_{dyn}, z_{cw}$) have to be summarized by one number, i.e. the Root Mean Square (RMS) value

$$|x|_{RMS} = |x| = \sqrt{\frac{1}{N} \sum_{i=1}^{N} (x_i)^2}. \tag{2.39}$$

As the absolute RMS values are not only depending on the controller performance but also on the road disturbances, they cannot be used to draw general conclusions. Therefore, we introduce the criterion

$$\Gamma(\cdot) = 1 - \frac{|\cdot|_{controlled}}{|\cdot|_{passive}} \tag{2.40}$$

which relates the RMS value of one quantity of the controlled active suspension to the RMS value of the same quantity of the passive suspension. A value of $\Gamma > 0$ indicates an improvement compared to the passive quarter car, $\Gamma < 0$ a decrease in performance. Thus, it is possible to examine the controller performance independently of the road disturbance.

2.4 Controllers for Active Suspensions

Control laws are the essential part of active suspension systems. First approaches to preview control date back to 1968 [6]. Since then many different methods were developed and applied in both, academia and industry. Those differ in many aspects, e.g., static/adaptive, linear/nonlinear controller, analytical/numerical solution, with/without preview, number of required measured quantities, and computational demand. Below, the most prominent approaches as well as those needed to understand and to classify the methods developed in this thesis, are presented.

2.4.1 Methods without Preview

A very early feedback controller for the quarter car is Karnopp's "Skyhook-Controller" [54]. The idea is to emulate via the semi-active or active suspension a quarter car, which has an additional damper mounted between the vehicle chassis and the sky (see Figure 2.8). Its damping force $F_{sky} = d_{sky}\dot{z}_c$ only depends on the Skyhook-damping d_{sky} and on the absolute chassis velocity and reduces the chassis movements. The analogue for decreasing the wheel movement is the "Groundhook-Controller", which adds a virtual damper between the wheel and the ground [132] or between the wheel and an inertial reference frame [63]. Due to the simple structure of the controllers and the intuitive tuning via the Skyhook/Groundhook damping these approaches are broadly used in series production cars (an overview is given in [131]).
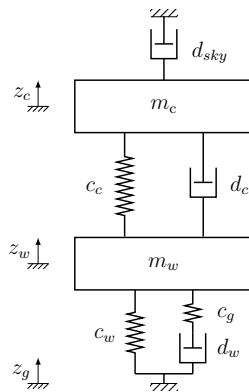

Figure 2.8: Skyhook damper

An often used model based linear control approach is the Linear Quadratic Regulator (LQR). Based on the fully active linear system (2.21) a constant controller gain **K** is determined via the solution of the algebraic Riccati equation that minimizes a quadratic cost function [40, 45, 126, 144]. The cost function comprises quantities that

relate to driving comfort and driving safety e.g., tire and suspension deflection, chassis acceleration, dynamic wheel load and the input force. The suspension behavior can be set by altering the weighting of these. The LQR was not only successfully applied to fully active suspensions but also as "clipped optimal control" to semi-active suspensions by clipping the non dissipative control force [131]. Furthermore, the LQR was used for the hybrid configuration (see Figure 2.2c) as well: In [59] it was shown that controlling the hybrid suspension with an LQR leads to a performance close to that of the fully active suspension (see Figure 2.2b). However, there are two main drawbacks of the LQR when applied to the quarter car: It is not possible to consider nonlinearities in the suspension and – as the LQR is a state-feedback controller – the whole state vector of the quarter car must be measured or estimated. Measuring the state vector requires many sensors, which leads to high costs, and is therefore, not an option for production cars. For this reason, researchers have put a lot of effort into designing linear [27, 108, 142] and nonlinear [37, 61, 96] estimators for suspension systems.

In this thesis the LQR as presented in [95] is deployed as benchmark controller $u = -\mathbf{k}\mathbf{x}_{LQR}$ with $\mathbf{k} = [-3504\ 3094\ 9873\ 733]$. The state $\mathbf{x}_{LQR} = [z_c - z_w\ \dot{z}_c\ z_w - z_g\ \dot{z}_w]^T$ is assumed to be known exactly in simulations. At the test stand we derive these quantities based on the measured signals, i.e. z_{cw}, $\ddot{z}_c$, and $\ddot{z}_w$. While $z_c - z_w$, $\dot{z}_c$, and $\dot{z}_w$ are obtained through filtering, combining, integrating and/or deriving the measured quantities, $z_w - z_g$ has to be reconstructed using model knowledge. Assuming that the tire in the linear fully active quarter car is modeled just as a spring with stiffness c_w, the equilibrium of forces regarding the wheel mass yields

$$c_w(z_w - z_g) = -m_w\ddot{z}_w + c_c(z_c - z_w) + d_c(\dot{z}_c - \dot{z}_w) - F = -m_w\ddot{z}_w - m_c\ddot{z}_c. \quad (2.41)$$

Since $\ddot{z}_w$ as well as $\ddot{z}_c$ are measured, the state variable $z_w - z_g$ can be determined by dividing (2.41) by c_w.

A further approach that is also often applied to active vibration damping in a quarter car, is robust control. Robust control methods design a controller that minimizes the maximum gain – the H∞ norm of the transfer function – between an unknown disturbance and the outputs to be controlled (objectives) based on the measured outputs (for details see [19, 113, 146]). To set the controller performance the objectives can be weighted with constant factors or transfer functions. These "H∞ controllers" were successfully applied to many different suspension configurations, with various measured and controlled outputs [68, 98, 102, 140]. The advantages of H∞ controllers are their robustness against unknown disturbances and the great freedom in the choice of

weighting functions of the objectives.

Another possibility to cope with changes e.g., in the system dynamics or in the road profile is the use of adaptive controllers. In [40] multiple optimal controllers are designed for different road types and vehicle velocities. The switching between them according to the road condition and the vehicle velocity leads to an adaptive behavior. An adaptive Skyhook controller with gain scheduling based on road disturbance frequencies is proposed in [69]. Koch presents in [62] the reference model based adaptive controller, which actuates the SMA and the variable damper such that the controlled hybrid suspension emulates a passive reference model that is comfort optimal according to the current driving state. To adapt not only to the current road excitation, but also to changes in the system dynamics the LMS algorithm is successfully applied to a fully active quarter car in [122].

The controller design methods presented so far are all linear. Therefore nonlinear behavior as e.g., in the spring and damper characteristics cannot be considered. Thus, nonlinear schemes have to be used to further improve the performance. In [95] the nonlinear quarter car is modeled in the Takagi-Sugeno framework [123], which represents the nonlinear dynamics as an interpolation of linear models. For each of these linear models an LQR is designed. Interpolating between these controllers results in the nonlinear parallel distributed compensator. Another approach to include the nonlinear dynamics is Nonlinear Model Predictive Control (NMPC): In each time step the behavior of the system is predicted within the prediction horizon and the control sequence is optimized within the control horizon to minimize a cost function. Afterwards, the first step of the control sequence is applied to the system and the numerical optimization starts again with the current state as initial state. The nonlinear dynamics as well as state and input constraints can be considered in the optimization problem. This approach was applied in an offline variant in [115] and in a parametrized form in [99]. The challenge of online NMPC is to solve the optimization problem fast enough [77].

2.4.2 Methods with Preview

In 1968 Bender posed the question how to exploit road profile preview in a controller to enhance driving comfort [6]. Today, this questions becomes more relevant than ever, as the road profile in front of the car is indeed measurable with environment detecting sensors installed e.g., in an autonomous car as shown in the following literature: In [35] an algorithm was developed, which determines the road profile height based on data from a camera mounted behind the windshield. Also, LIDAR sensors can be

used to detect road irregularities in the millimeter range, as presented in [104]. In [5] camera data is combined with measurements from the accelerometers and gyroscopes in the car to improve the quality of the road profile estimation. Donahue showed in [18] that the road profile can be reconstructed from radar data as well. A possibility to gain preview information about road disturbances without environment detecting sensors is the wheel based preview. The idea is to reconstruct the road profile based on acceleration and deflection measurements at the front wheel and exploit this knowledge with the active suspension at the rear wheel. This can be realized for example with a Kalman filter [114], an adaptive observer [130], or a neural network [84]. Consequently, the assumption that the information about the future road profile will be available in cars is valid.

The controller proposed by Bender to answer his question is a linear optimal controller which was designed using Wiener filter theory. He modeled the quarter car as a damped harmonic oscillator and showed the positive effects of incorporating preview information [6]. Tomizuka used the same model and stated that an optimal discrete preview controller can achieve the same performance as Bender's continuous-time controller [128]. The first time the quarter car was modeled as a two mass oscillator in the context of preview control is in [127]. Based on the Hamilton-Jacobi-Bellmann equation (for details see [55]) an optimal linear preview feedforward controller is designed and applied for vibration damping. The latter two approaches were implemented in a military vehicle with active suspension in [67]. In this publication, the controller of [127] seemed to be more promising than the controller in [128] as the latter needed too much suspension space. Later on, the Riccati equation was applied to design an optimal feedback controller with a preview feedforward portion in [41]. The disadvantages of these early approaches are that they are neither applicable to nonlinear systems nor adaptive.

A possibility to apply standard linear control methods for the design of preview controllers is to include the time delay τ between the detection and the effect of the disturbance (= preview time τ) in the linear state space model used for the controller design. In continuous time this can be done with a Padé approximation [7] of the time delay τ

$$e^{-\tau s} \approx \frac{1 - k_1 s + k_2 s^2 + \cdots + (-1)^b k_b s^b}{1 + k_1 s + k_2 s^2 + \cdots + k_b s^b}. \tag{2.42}$$

The coefficients k_i can be determined e.g., according to [36]. The higher the delay, the higher the order b of (2.42) has to be chosen to sufficiently approximate the delay. Once the delay is expressed as the linear transfer function (2.42), the system (2.21) can be

easily extended with it. A second way to include the time delay into an LTI system is to discretize the system dynamics and augment it with N additional states. For the model of the discrete-time fully active linear quarter car (2.21) with sample time T_s and system matrices $\mathbf{A}_d \in \mathbb{R}^{n \times n}$, $\mathbf{B}_d \in \mathbb{R}^{n \times 1}$, $\mathbf{E}_d \in \mathbb{R}^{n \times 1}$, the augmented system is

$$
\mathbf{x}_a[k+1] = \begin{bmatrix} \mathbf{A}_d & \mathbf{E}_d & \mathbf{0}_{n \times N-1} \\ \mathbf{0}_{N-1 \times n} & \mathbf{0}_{N-1 \times 1} & \mathbf{I}_{N-1 \times N-1} \\ \mathbf{0}_{1 \times n} & 0_{1 \times 1} & \mathbf{0}_{1 \times N-1} \end{bmatrix} \mathbf{x}_a[k] + \begin{bmatrix} \mathbf{B}_d \\ \mathbf{0}_{N \times 1} \end{bmatrix} u[k] \\
+ \begin{bmatrix} \mathbf{0}_{n+N-1 \times 1} \\ 1 \end{bmatrix} z[k+N]
$$

(2.43)

with N equal to the closest positive integer value to $\bar{N} = \tau/T_s$ and the state $\mathbf{x}_a[k] = [\mathbf{x}[k]^T \ z[k] \ z[k+1] \cdots z[k+N-1]]^T$. Thus the augmented state contains the system state and the sampled road profile between the tire and the currently measured preview point. Both approaches work well with a fixed time delay. However, as soon as the time delay changes, the Padé approximation or the number of augmented states changes, which alters the augmented model. Hence, a new controller has to be designed for the altered augmented model to keep the same level of performance for the new preview time.

Based on the presented schemes to include the preview in an LTI model, various LQRs [21, 73, 111] as well as H∞ controllers [3, 11] were successfully applied to active suspensions. The main drawbacks of these controllers are that they are designed only for one fixed preview time and that they do not consider the nonlinearities.

A further optimal control method which is capable of using preview information and which considers state and input constraints is Model Predictive Control (MPC). The knowledge about the future road disturbance can be easily included into the prediction step even if the preview time is variable. In [81] MPC is applied to a linear, fully active half car model, in [10] to a linear fully active quarter car, in [34] to a linear slow-active full car, and in [33] to a linear full car with semi-active, hybrid or fully active suspension. Nonlinear dynamics are considered in [78](NMPC). The performance of these controllers is very promising. However, there is no guarantee in general that the optimization yields a feasible, optimal solution in the required time. Furthermore, the required computing power is much higher than that of a standard control unit in a today's series production car.

Besides NMPC, only very few approaches to nonlinear preview control of the quarter car have been made. One is presented in [83] and is based on several neural networks, which are used as system model, controller, and soft sensor for the road profile. The

drawback of this approach is that it is difficult to include knowledge about the model and the high number of design parameters. Furthermore, neural networks carry the risk of unforeseen behavior.

An adaptive preview feedforward controller is presented in [64]. Using the FxLMS algorithm (for details see [66]) an FIR filter is adapted online, such that the chassis velocity is minimized. This filter determines the actuator force based on the knowledge about the future road disturbance. For slow changes in e.g., the system dynamics and the preview time, this linear approach works quite well. However, the convergence is too slow to compensate fast and abrupt changes in the preview time.

3 Accomplishments

This chapter presents the fundamental contributions of this thesis by summarizing the content of each of my papers and establishing a relation between these papers. The papers are reprinted with kind permissions of the publishers in Appendix A.

3.1 Optimal Feedforward Preview Control by FIR Filters [118]

The main contribution of this paper is a new method for designing an FIR filter as an optimal feedforward preview controller for asymptotically stable LTI SISO systems. The need for a preview feedforward controller is motivated by the fact, that in control applications in various domains the exploitation of preview information is either required or at least beneficial [20, 75, 104, 134].

First, it is shown how to exploit the matrix product representation of the system's dynamics (see Section 2.1.1) to design an FIR filter as feedforward controller through inversion of the dynamic matrix. As this approach is only feasible if the system's impulse response is monotonically decreasing [25] and preview information cannot be considered, the optimization based method is presented. Again, the matrix product representation is used to analytically derive via optimization a formula to determine an optimal proactive deconvolution matrix. Subsequently, it is shown how to construct the preview FIR filter for a specific preview time from the deconvolution matrix. Moreover, it is presented and discussed, why the deconvolution matrix has a Toeplitz-like structure with decreasing elements in each column, which is a necessary condition for the derivation of the preview FIR filter.

Afterwards, the design method is illustrated with a time discrete, second order sample system with zeros outside the unit disk. It is shown that the deconvolution matrix has the required structure, that it is possible to design preview FIR filters for various preview times with this method, and that these filters exhibit a proactive behavior. Finally it is sketched, how to extend the cost function to improve the steady state behavior and an outlook is given concerning the application of this method for the problem of vibration damping.

3.2 Proactive Disturbance Compensator for Vibration Damping of a Quarter-Car [119]

The contribution of this manuscript is twofold: On the one hand it is presented how to design a linear proactive disturbance compensator based on the preview FIR filter developed in the preceding paper [118]. On the other hand, the paper shows for the first time the application of the proactive disturbance compensator to the problem of vibration damping of a quarter car based on preview information about the future road surface.

To meet the increased comfort requirements in autonomous cars a proactive disturbance compensator can be used to exploit the available preview data. Such a compensator can be derived based on the design scheme of the preview FIR filter which is shortly summarized at the beginning of this paper. Afterwards, the proactive disturbance compensator is introduced by analogy with the dynamic disturbance compensator for LTI systems [74]. The dynamic disturbance compensator first determines the effect of the known current disturbance on the output and then realizes the negative effect via the actuator at the output. Due to the superposition principle in LTI systems, the effect of the actuator cancels out the effect of the disturbance exactly and the output remains undisturbed. To realize the negative effect of the disturbance with the actuator the system inverse is used as feedforward controller in the dynamic disturbance compensator. As the inverse is not always realizable and as the goal is to exploit preview data, it is replaced with the preview FIR filter.

In the next step, the proactive disturbance compensator is applied to the quarter car. The compensator design is based on the linear fully active quarter car model with Gehmann tire model (see Section 2.2.1). To show the influence of the design parameters simulations are performed with a synthetic road profile (see Section 2.2.5), the nonlinear quarter car models (see Sections 2.2.2 and 2.2.4), and various parameter sets for e.g., the cost function, the control horizon, and the preview time. The results of the simulations are: 1. The weighting in the cost function can be used to set a desired performance regarding driving safety or driving comfort in a certain range. 2. There is a minimum required control horizon length to achieve the optimal performance. 3. The longer the preview time the better is the performance, at least until a certain point. Increasing the preview time beyond this point does not further improve the performance.

The proactive disturbance compensator was first parametrized based on the results of the simulations with the synthetic road profile. To test the sensitivity to different road types it was then used in simulations and experiments with the real road profile

of the country road (see Section 2.2.5). Assuming an ideal preview time of 1.5 s an improvement of comfort of 60.4% could be achieved simultaneously to an increase of driving safety of 38.8%. This underlines the superior performance of the proactive disturbance compensator in comparison with the LQR (comfort: 53.5%, safety: 10.9%) and Skyhook controller (comfort: 31.6%, safety: 15.2%) (see Section 2.4.1). The experiments presented in this publication confirm the simulation results. Using the proactive disturbance compensator at the quarter car test stand leads to a comfort improvement of up to 51.8% (LQR: 45.1%, Skyhook controller: 22.9%) and to an increase in driving safety of 6.3% (LQR: 1.9%, Skyhook controller: 7.5%).

3.3 A Fast Convergence FxLMS Algorithm for Vibration Damping of a Quarter Car [120]

This publication's contribution comprises a methodical part and an application-oriented part. The former is the development of an algorithm that leads to a fast converging, adaptive feedforward controller. Through application of this method to the quarter car we show that it can be used to adapt to fast changes of the system, i.e. jumps in the preview time, within milliseconds.

The main idea is to modify the normalized leaky-ν FxLMS algorithm such that it re-initializes the adaptive FIR filter with initial guesses close to the optimal values each time a sudden change is detected in the preview time. The derivation is as follows:

First, the normalized leaky-ν FxLMS algorithm (see [9, 32, 43, 66, 87] for details) is presented, which is an extension of the LMS algorithm introduced in Section 2.1.3. Afterwards its structure is compared with the structure of the proactive disturbance compensator designed in [119]. As they are basically the same, it seems likely to use the proactive disturbance compensator, which is determined based on a system model, to somehow initialize the FxLMS algorithm. In this publication we prove that the adaptive FIR filter does converge towards the proactive disturbance compensator, if the same cost function is to be minimized. Thus, we can use the information of the offline designed proactive disturbance compensator as initial guesses for the FxLMS algorithm. The re-initialization after a sudden change in the preview time has to be included in the adaption algorithm. For this purpose, we propose the so called fast convergence Filtered-x Least Mean Squares (fcFxLMS) algorithm.

For the application of the fcFxLMS to the quarter car the comfort optimal proactive disturbance compensator is designed based on the linear fully active quarter car

model with Gehmann model for the tire dynamics. From this disturbance compensator the necessary initial guesses for the fcFxLMS algorithm for various preview times are extracted. In this publication, the adaptive FIR filter is used in simulations with the nonlinear hybrid quarter car model covering two scenarios. In the first scenario the vehicle travels on the country road (see Section 2.2.5) with a constant preview time. It is shown that the improvement of comfort is 3 percentage points (pp) higher than that of the static disturbance compensator and that of the standard FxLMS algorithm due to the faster convergence at the beginning of the adaption. In the second scenario the behavior of the fcFxLMS in the case of a jump in the preview time is tested. It is shown that this jump has, contrary to the FxLMS algorithm, almost no effect on the driving comfort. This results in a 10 pp higher improvement of the comfort than with the standard FxLMS algorithm.

3.4 A Proactive Nonlinear Disturbance Compensator for the Quarter Car [121]

The contribution of this publication is the application of a nonlinear proactive disturbance compensator to the quarter car. The nonlinearities of the quarter car (see Section 2.2.2) were not considered in the former publications and are now taken into account with the nonlinear flatness based disturbance compensator presented in [15, 72]. The preview capabilities are added by extending this compensator with the linear proactive disturbance compensator proposed in my publication [119].

To use this approach the system has to be flat and thus, a flat output has to exist. Such an output is determined for the nonlinear fully active quarter (see Section 2.2.2) car by construction of an output with full relative degree [1, 70]. The designed flatness based disturbance compensator decouples the chassis completely from the wheel. However, the compensator is an unstable linear system and the complete decoupling leads to a loss of driving safety.

Therefore, a virtual controller that stabilizes the flatness based compensator is introduced. Furthermore, the linear proactive disturbance compensator is added to determine the desired trajectory for the flatness based disturbance compensator. In this way, the comfort performance is decreased to a level, at which the driving safety equals the safety of a passive quarter car. These three components (flatness based compensator, linear proactive compensator, virtual controller) together build the proactive nonlinear disturbance compensator.

To investigate the influence of the design parameters simulations are performed with the active and the hybrid quarter car. The results for the active quarter car show that the virtual controller can be tuned to stabilize the flatness based compensator without altering the behavior significantly. Furthermore the input weighting in the cost function of the linear proactive disturbance compensator can be used to set an arbitrary behavior regarding driving comfort or driving safety. The results of the simulations with the hybrid quarter car exhibit the same tendencies, but a lower performance due to the non ideal actuators.

In further simulations with the hybrid quarter car we examine how the preview time, errors in the road profile signal, and changes in the chassis mass influence the performance regarding comfort and safety. In the paper, the following conclusions are deduced from the simulation results: The performance of both, comfort and safety converge with increasing preview time to a constant value. The proposed nonlinear proactive disturbance compensator is little sensitive to changes in the chassis mass, to slow drift and to noise in the road profile signal. However, deviations between the assumed and the real preview time deteriorate the driving safety. Nevertheless, the driving comfort was improved in all test cases.

Last, we compare simulation results to results of experiments at the quarter car test stand. In both, the nonlinear proactive disturbance compensator outperforms the comfort oriented LQR (see 2.4.1). Furthermore, the improvement of comfort in experiments is less than that in simulations due to non-modeled effects e.g., damper hysteresis, actuator dynamics, and tire behavior. Still, the comfort is increased by almost 57% without decreasing driving safety.

3.5 Preview H∞ Control of a Hybrid Suspension System [117]

The contribution of this paper is the treatment of the problem of vibration damping in a quarter car from the perspective of time delay systems. Choosing not the driver, but the newly detected road disturbance in front of the car as the point of view results in a time delay between the detection and the effect of the disturbance on the quarter car. In this publication we apply an H∞ controller design method for time delay systems presented in [106] to design one H∞ preview controller that can be used with arbitrary time delays.

The in [106] proposed method results in an observer-controller which incorporates the time delay as an explicit parameter. This enables the observer-controller to be used in a vehicle traveling at varying speeds and thus with varying time delay, if the time

delay is known. In the case of a change of the time delay, only the time delay parameter has to be adjusted. This is an advantage in comparison with other preview controllers (see Section 2.4.2), which need to be completely recalculated or which change their structure in the case of a change in the preview time.

As benchmark controllers an H∞ controller without preview and one, with the constant preview time modeled via a Padé approximation (see [3, 11] and Section 2.4.2) are designed based on the linear fully active quarter car model without Gehmann model. Both were determined using standard H∞ design methods implemented in MATLAB's *Robust Control Toolbox*. To use the time-delay controller design method proposed in [106] a time delay model of the quarter car is required. It can be derived from the fully active linear model by choosing the time derivative of the road profile as disturbance and introducing a new state variable which integrates the time derivative of the road profile. This state variable effects then via the delayed state $\mathbf{x}(t-\tau)$ the system. In this way, the time delay is included as parameter τ in the system. The observer-controller for such a system is determined by iteratively solving a Linear Matrix Inequality (LMI) [106, 117].

For this manuscript we designed a pure feedback and a pure feedforward controller for the case "no preview". For each of the cases "preview with constant preview time" (modeled via Padé approximation) and "preview with variable preview time" (modeled via a time delay system) a feedback controller with feedforward portion and a pure feedforward controller are derived. The aim is to compare these controllers. For this, simulations with the nonlinear hybrid quarter car model (see Section 2.2.4) and the country road (see Section 2.2.5) as road profile are performed. The results show that the pure feedforward controllers can achieve, under the assumption of a perfectly known road profile and a constant preview time, almost the same performance as the feedback controllers. Furthermore it is presented that the time delay controller designed according to [106] achieves the goal of a steady performance for various preview times, even in the case of differences between the controller design model and the simulation model. However, the sensitivity to these differences is bigger for the time delay H∞ controller than for the standard H∞ controllers. A further result of this paper is that the standard H∞ controller outperforms the time delay H∞ controller for many preview times – as long as the standard H∞ controller was simulated with the time delay for which it was designed. In the case of deviations between the actual time delay and the delay for which the standard H∞ controller was determined, the time delay H∞ controller has advantages. Thus, it is concluded, that the ability of the time delay H∞ controller to

include the preview time via one parameter comes to the prize of a slightly decreased performance.

4 Discussion and Outlook

4.1 Discussion

The present thesis investigated various approaches to feedforward control for vibration damping in a hybrid suspension using preview road profile data. The contributions are partly of methodical and partly of application related nature. In this section, the results of the developed disturbance compensators are discussed in light of the related literature.

4.1.1 Methodical Contributions

The first methodical contribution of the thesis is the preview FIR filter in [118]. Existing approaches to preview control can be divided in inversion based methods and optimization based methods. The former design the feedforward controller based on the inversion of the system dynamics, as in [16, 47, 79]. Optimization based schemes minimize a cost function analytically or numerically to build the feedforward controller [124, 135, 147]. There are inversion based methods that result in a preview FIR filter [79]. However, there are not any optimization based methods that generate directly an optimal preview FIR filter. This was also mentioned in [135], in which the same approach was taken to determine the optimal deconvolution matrix, as we use in [118]. However, the step back to an FIR filter was not done in [135]. We close this gap by showing how to derive a preview FIR filter from the optimal deconvolution matrix.

The proposed scheme is very similar to early MPC namely, Dynamic Matrix Control (DMC) [13]. The DMC design procedure yields a feedback controller for one specific preview time conducting one optimization. Our approach, in contrast, leads to a feedforward controller which can be parametrized according to the preview time without rerunning the optimization. The main difference to modern MPC methods (see Section 2.4.2) is that we neglect constraints to be able to analytically derive the preview controller. In this way, no numerical optimization is required online, which makes the proposed preview controller very well suited for the use in applications with limited computational resources.

The proposed method requires the approximation of the impulse response and is only applicable to asymptotically stable systems. However, it is still very desirable to design preview controllers as FIR filters because of their inherent stability, which makes them especially as feedforward controllers very convenient. Furthermore, adaptive approaches to active noise canceling are also based on FIR filters. This correlation is exploited in the second methodical contribution of this thesis to speed up the convergence of the adaption.

The second methodical contribution is the fcFxLMS algorithm which is based on the LMS and the FxLMS algorithm. Both algorithms are well established and broadly used for active noise canceling [9, 32, 43, 66, 87]. Classical applications are in the acoustic field, e.g., in noise canceling headphones [29, 66, 101]. The FxLMS algorithm is further successfully applied for vibration control, e.g., of a cantilever beam [91] and in the automotive field for damping of motor vibrations [93], seat vibration [30, 138] or chassis vibration [64]. The vibration damping works well as long as the variations to which the controller is supposed to adapt, are sufficiently slow [43]. In [91] it is stated, that it takes a few seconds until considerable damping is achieved and also in [93] it is shown, that especially fast changes in the system behavior, i.e. vibrations, deteriorate the performance. To achieve high performance from the beginning on and after fast changes the convergence speed has to be improved. However, it is not possible to arbitrarily increase the convergence speed by enlarging the step size of the iterative gradient descent algorithm (see Section 2.1.3) of the FxLMS as the algorithm can become unstable.

An effective way to speed up convergence is to find good initial guesses for the FIR filter, which is adapted by the FxLMS algorithm. In this thesis it is shown for the first time, how to determine these initial guesses analytically based on the newly developed preview FIR filter [118]. This approach is advantageous particularly in the case of many different possible preview times as our method proposed in [118] yields the initial guesses for a whole range of preview times. Moreover these initial values can be used to reinitialize the filter after sudden changes in the preview time. In contrast to our model based approach the initial guesses are determined based on premeasured data in [52]. However, this method is only beneficial if there are no fast changes in the system behavior such as jumps in the preview time. These require that initial guesses are found a priori for each possible preview time. Since the initial guesses are determined based on premeasured data in [52] an experiment has to be conducted for each possible preview time, which is very time consuming.

The proposed fcFxLMS algorithm was designed for fast variations in the preview time, which occur frequently in applications with moving vehicles. As environment

sensors, such as LIDARs and cameras, usually have a fixed maximum preview length, the preview time depends on the velocity of the vehicle on which the sensors are mounted (e.g., car, airplane, robot). Furthermore, sudden changes of the preview time caused by a change of the preview length also arise in various applications, e.g., due to obstacles, sharp corners, other vehicles, or clouds. Hence, the fcFxLMS algorithm is not limited to the field of automotive control, but can also be effective in avionics and robotics.

4.1.2 Application Based Contributions

The goal of this thesis was to propose preview controllers for vibration damping of the quarter car. As the focus was set on controllers, which can be applied in a real car, the constraint of limited computational resources was introduced. Therefore we investigated model-based preview controllers that can be determined offline [117, 119] or require only very few resources for online optimization [120]. The MPC schemes with [10, 33, 78, 81] and without preview [99, 115] (see Section 2.4) are not considered, as their computational requirements are to demanding for control units of series production cars – at least at the moment. However, with growing computational power in the car and with further advances in fast model predictive control methods, e.g., [85], these might become applicable in the future. Nevertheless, the methods presented in this thesis will still have their advantages, as MPC schemes can not generally guarantee that a solution of the optimization problem is found in each time step. Moreover, stability analysis of the MPC approaches is often a challenge, due to the numerical online optimization.

Many feedback controllers for vibration damping without preview are optimal controllers, such as the LQR and robust H_∞ controllers (see Section 2.4.1). The LQR has the advantage that it is optimal according to a cost function and thus, can be easily tuned by changing the weighting of the terms in the cost functions. As the cost functions are usually interpreted physically, the desired behavior can be set quite intuitively. The tuning of the H_∞ controllers is also very transparent, as it is done by changing the weighting functions of the outputs on which the disturbance's influence is to be minimized. Moreover, optimal approaches are also widely used in preview control for active suspensions. As the system behavior is optimized over a time horizon, it is obvious that preview information can be considered. For this reason, optimal approaches have been used in preview vibration control of quarter cars for decades [3, 6, 11, 21, 41, 73, 111, 127, 128]. Due to these two positive properties, all proposed feedforward controllers also contain an optimal control component.

Until now, almost all preview controllers for the quarter car (see Section 2.4.2) are a combination of a feedback and a feedforward controller. Rare exceptions are for example [64, 83]. In this thesis the performance of pure feedforward controllers is investigated, which do not require a state measurement or estimation. The only quantity needed is the road profile in front of the car. The presented results allow the conclusion that preview feedforward controllers lead to a similar or even higher driving comfort than standard feedback controllers – as long as the road profile can be accurately detected.

Throughout this thesis it is assumed that the road profile is exactly known to derive a conclusion about the best possible performance. Furthermore, this facilitates the comparison between the proposed approaches. Clearly, this assumption does not hold in a real application. However, it was shown in [116, 130] that it is already possible to detect stochastic road profiles with an error smaller than 1 cm. In the future it might be possible, that a high-accuracy road profile is stored in a cloud and sent to the vehicles [71]. Thus, the gap between the currently achievable accuracy and a perfectly known road profile can be decreased.

Most publications regarding analytical preview controllers, e.g., the approaches with augmented systems as presented in Section 2.4.2 and the early schemes in [6, 127, 128] do not consider the problem of varying preview time and the nonlinear behavior. In this thesis these two aspects are not only examined but also taken explicitly into account in the design of the controllers. The results confirm that it is important to consider the nonlinearities and the varying preview time for further performance improvement and that the proposed controllers can successfully treat these challenges.

The results of the linear proactive disturbance compensator [119] show that a pure feedforward controller surpasses the performance of standard feedback controllers such as LQR or Skyhook in simulations and experiments – under the assumption of a perfectly known road profile. Although neither constraints, nor actuator dynamics, nor nonlinear dynamics are considered, the experimental performance almost reaches the best MPC-type feedback controller without preview that was tested with the same test stand and same road profile in [114] ($\Gamma(\ddot{z}_c) = 53.0\%$, $\Gamma(F_{dyn}) = 4.0\%$). This underlines the big potential of road profile preview controllers. The controller fulfills the goal of a proactive behavior, is easily tunable, can be derived analytically and does not need much computational resources. However, it does not consider nonlinearities and variable preview time.

For the first time, a model based approach to design a proactive nonlinear disturbance compensator for a quarter car is presented in [121]. In contrast to [83] its design is model based and the performance can be set with only one parameter. Due to the consideration

of the nonlinear behavior, the performance at the test stand is increased to $(\Gamma(\ddot{z}_c) = 56.5\%, \Gamma(F_{dyn}) = 7.2\%)$ which is 4.7 pp higher in comfort than the linear compensator and 3.5 pp higher than the best MPC-type feedback controller [114]. Furthermore, it is shown that this approach is insensitive to measurement noise or drift, variations in chassis mass, and different road profiles. However, the changes in preview time are not taken into account.

These are considered in the adaptive controller proposed in [120]. Existing approaches to preview control of a quarter car are not adaptive, except the controller proposed in [64], which leads to very promising results. However, this controller follows the classical FxLMS method, which adapts too slowly to sudden changes in the preview time. Here, we present for the first time an FxLMS which is able to adapt to fast changes in the preview time. Simulation results confirm the good performance of the FxLMS algorithm and highlight the performance improvement based on the proposed fcFxLMS. It is capable to adapt to different road profiles and fast changes in the preview time. Due to the simple update law, it does not require much computational resources. However, the fcFxLMS does not consider the nonlinearities in the suspension.

For the first time, a time delay H∞ controller is applied in [117] to the problem of vibration damping in the quarter car with variable preview time. This is a first step towards the use of controller design methods for time-delay systems for that purpose. The results demonstrate that the goal of decoupling the performance from the time delay can be achieved, but that the performance is worse than that of a controller designed for one specific preview time e.g., using system augmentation or the Padé approximation (see Section 2.4.2). This is the consequence of the time delay controller's property to be valid for arbitrary preview times without changing any controller gains ("delay independent controller"). Furthermore, it is shown that the sensitivity of this observer controller to model mismatch is too high to be applied in a real quarter car. Moreover, nonlinear dynamics are not considered and it is not clear how errors in the road profile or in the assumed time delay deteriorate the performance.

4.2 Outlook

This thesis shows that pure feedforward preview controller achieve a remarkable performance regarding improvement of driving comfort. However, the performance depends crucially on the available road preview data. Linear analysis and simulations state that the in [121] proposed controller is quite insensitive to measurement errors such as noise or drift. However, a thorough nonlinear analysis to theoretically confirm these results

has not been performed yet. Likewise, it has to be examined, how accurate road profile signals can be detected with the sensors in an autonomous car. In [35] a linear Kalman filter is used for road profile estimation. A very high estimation accuracy for a quarter car without preview was achieved via an Extended Kalman Filter and an Unscented Kalman Filter in [96]. Therefore, we recommend to test the road profile estimation accuracy of an Extended Kalman Filter and an Unscented Kalman Filter, and to combine these with the proposed controllers.

A further interesting aspect is how recorded data of numerous vehicles that detected the same road profile can be combined in a cloud to further improve the accuracy of the estimated road profile. In this context it is also necessary to investigate how road profile information that has been sent from the cloud to a car has to be combined with vehicle position estimates to avoid a misalignment between the true and the received profile. Last but not least, a thorough analysis of different error types in the detected future road profile could lead to further requirements for the preview controller design.

The simulation results presented in this thesis lead to the conclusion that considering the true preview time is crucial for a good performance. Therefore, the focus of future research has to be set on how to incorporate the preview time, when the preview controller is to be applied on a real car. One possibility when using the linear or nonlinear proactive disturbance compensator presented in [119] and [121] could be to switch between controllers for specific preview times. These methods are well suited for this approach, as the optimization in [118] determines FIR preview controllers for a specific preview time range. In this case the challenge is how to implement the large number of controllers in an efficient and lean way. Moreover it needs to be tested whether the switching leads to undesired behavior. This can be done, for example, with a common Lyapunov function approach, which was presented in [60] for the switching of multiple LQRs. The second possibility is to use the proposed fcFxLMS algorithm which led to very promising results even for fast changing preview times. However, this adaptive controller does not consider the nonlinearities. To further improve the performance it is recommended to incorporate the fcFxLMS algorithm in place of the linear proactive disturbance compensator in the nonlinear proactive disturbance compensator introduced in [121]. Another approach to include the nonlinearities in an adaptive controller is to update the weights of a neural network online (as in [42, 88]). Here, the challenges are the big amount of required computational resources and the slow convergence, which pose a problem in the case of rapidly varying preview times.

The proposed controller for time delay systems can handle varying preview time, but the controller gains are independent of the preview time. Thus, the controller is a

compromise for all time delays. To improve the performance of a time delay controller there are approaches, which include further information about the time delay such as its maximum rate of change or an upper bound (so called "delay-dependent controllers" [8, 28]). This thesis showed that time delay controllers can be used for active vibration damping in a quarter car. Based on this insight these delay-dependent schemes seem to be a promising way to go for further performance improvement. Furthermore, it has to be examined, how robust these controllers are regarding model mismatch, disturbances in the road profile signal or deviations in the preview time.

To apply the presented controllers in a real car the road profile in front of all four wheels has to be known, either estimated or received from the cloud. Furthermore, the controllers have to be applied to all four suspensions. The simple use of the proposed controllers independently at all suspensions could be a first approach but does not consider the coupling between the four actuators. Moreover, the suppression of roll and pitch movements is not incorporated in the controllers. Therefore, the next step is to apply the shown concepts to a full car model. The extension of the proactive FIR filter to the Multi Input Multi Output (MIMO) case should be straightforward. The FxLMS algorithm does already exist for multiple error sources, sensors, and actuators [66]. However, the challenge is that for example the front left suspension actuator influences also the vibrations at the front right and at the rear suspension and vice versa. Hence, it may occur an undesired feedback. The MIMO extension of the fcFxLMS should be realizable based on the extended proactive FIR filter.

In the long term the holistic view on all vehicle dynamics control systems in a car will be of interest. Especially the driving comfort and driving safety can be heavily influenced by the chosen trajectory of an autonomous car. In some cases, it might be more reasonable to slightly alter the trajectory to avoid a pothole instead of using much energy to compensate the pothole with the active suspension. Conversely, the suspension controller can use information from the planned trajectory to determine how much forces have to be realized between the wheel and the road. This will help to adjust the controller online to increase the comfort as much as possible without losing the ability to transfer the required forces to the road.

Appendix A

Reproduction of publications

A.1 Optimal Feedforward Preview Control by FIR Filters

Contributions: The idea of using an impulse response representation was raised by Prof. B. Lohmann. The development of the preview FIR filter, the theoretical considerations, analysis, implementation, simulations and writing have been done predominantly by the first author.

Optimal Feedforward Preview Control by FIR Filters

Johannes N. Strohm* Boris Lohmann*

* Institute of Automatic Control, Technische Universität München,
85748 Garching, Germany (e-mail: johannes.strohm,
lohmann@tum.de)

Abstract: The paper presents a new method for designing an optimal feedforward preview controller for asymptotically stable single-input single-output (SISO) systems. We conduct an optimization based on an impulse response representation of the system's dynamics for a chosen control horizon. This leads to an optimal deconvolution that proactively exploits the reference or disturbance signal's preview information to calculate the control input for a desired output. In order to extend this deconvolution to arbitrarily long input signals, we show that, under certain circumstances, a finite impulse response (FIR) filter can be build from it. This filter can be seen as the system's optimized inverse, which also applies to non-minimum phase systems. Since optimization is done offline, the resulting filter is computationally inexpensive and easily implemented. Its effectiveness is shown by applying the proposed method to a sample system.

1. INTRODUCTION

For many control applications, the future reference signal is known. For power plant control, for example, the energy that a city needs during the course of a day is well known (see e.g. Vosen (1999)). Beginning well ahead of time with a required change of the plant's operating point is thus advantageous. Preview data is also available in the field of autonomous driving: self-driving vehicles use various sensors to detect their environment and extract information about the road's future course from the acquired data. Driving a car without this preview information is impossible even for humans (see MacAdam (1981)). Furthermore disturbances can sometimes be measured before they impact a system. For example, Mercedes Benz' Magic Body Control (MBC) scans the road in front of the vehicle, so that the variable suspension can be adjusted before the tire reaches the pothole (see e.g. Schindler (2009)). For wind power plants researchers are currently trying to find opportunities to detect wind fields in front of the plant and to use this information to control blade pitch before the gusts reach the tower (see e.g. Dunne and Pao (2016)). Summed up in one sentence: preview information is sometimes necessary and often beneficial for efficiently achieving one's control objectives. The challenge is to use the preview data to effect an adequate system reaction in a timely way. This can be tackled with non-causal feedforward control methods, which exploit knowledge about the future trajectory or disturbance to influence the system in advance.

In this paper, we propose a design technique for optimal, non-causal, finite impulse response (FIR) filters used as feedforward controllers for asymptotically stable SISO systems. The remainder of the paper is organized as follows: In section 2 we summarize some known methods for designing feedforward controllers. Section 3 describes,

how to build the optimal FIR filter. We introduce the needed system dynamics representation, then develop an optimal proactive deconvolution, and lastly derive the optimal proactive FIR filter. An example for the presented design procedure is shown in section 4 for a nonminimum phase system. Section 5 contains some concluding remarks.

2. STATE OF THE ART

Several approaches exist to using preview data for proactive controller behavior. The most popular is Model Predictive Control (MPC). It predicts the plant model's future output for the prediction horizon and optimizes the plant's discretized input signal for the control horizon such that an objective function is minimized. Available knowledge about future disturbance or reference signals can be easily included in the plant's predicted behavior and is thereby considered during optimization. One early approach to MPC is the so called Dynamic Matrix Control (DMC)(see Cutler and Ramaker (1980)). This method (i) features a step- or impulse-response model to represent the system dynamics, (ii) it computes the minimization problem's solution analytically (for the unconstrained case), and (iii) it finally derives a feedback control law (which can perform unstably). We will make use of DMC steps (i) and (ii) in section 3.

Feedforward control for linear time-invariant (LTI) systems is often done by system inversion. Non-causal inversion, which needs preview data, was introduced (e.g. in Devasia et al. (1996), Hunt et al. (1996), Marro et al. (2002)) to cope with nonminimum phase systems. There are also optimal inversion-based methods, which minimize an objective function (see e.g.Zou and Devasia (2004)). However, none was found leading to an optimal proactive FIR filter.

One early method for designing optimal FIR filters for feedforward control is presented in Takegaki and Matsui (1985). Unfortunately, it is available in Japanese only. As far as we could understand the text, the FIR filter coefficients are optimized directly under the assumption of a specific form of disturbance (e.g. step/ colored noise disturbance). The optimization itself uses the same objective function as that in DMC and in our approach; however, the resulting filter is causal and thus not proactive.

Wagner gives a good overview of FIR filters for building or approximating the inverse dynamics of discrete systems in Wagner (1999). He also compares deconvolution methods (steps (i) and (ii) of DMC above) with FIR filters. The latter are built via direct optimization of the filter coefficients. In contrast to Takegaki and Matsui (1985), a delay is taken into account and the amplitude of the input is not considered during optimization. As the input is not weighted and the filter remains causal, the feedforward control leads to huge control input signals when used with nonminimum phase systems. Furthermore, preview information cannot be used. The deconvolution methods, on the other hand, are based on a matrix vector product through which the input sequence needed for a desired output trajectory is calculated. As the input amplitude is incorporated in the objective function the resulting behavior is proactive, which leads to the possibility of controlling nonminimum phase systems with admissible input values. Wagner (1999) also shows that deconvolution without input weighting can be transformed into the direct optimization of FIR filter coefficients. However, no transformation to an FIR filter is presented for the proactive variant of the deconvolution. While these deconvolution methods can only use a desired trajectory of fixed length, the representation as a FIR filter has the advantage of being able to process arbitrarily long trajectories and of always being stable, as will be seen in section 3.

Developing an optimal preview FIR filter from the known optimal deconvolution is the main contribution of this paper. In subsequent sections, we will clarify the above-mentioned optimization and explain how to create the optimal proactive FIR filter.

3. FILTER DESIGN

Below we will first describe the representation of the system dynamics needed and how to calculate the inverse dynamics. The next step consists of building the optimal proactive deconvolution. Lastly we will show how to derive the final FIR filter.

3.1 System Dynamics Representation

LTI system dynamics is fully described by its impulse response. In discrete time, the impulse response, $g[n]$, takes the form

$$g[n] = g_0\delta[n] + g_1\delta[n-1] + \cdots + g_n\delta[n-N] \quad (1)$$

with the unit impulse $\delta[n]$ at time n and $N \to \infty$ for an exact representation. The input sequence $u[n]$ can be expressed as a series of impulses, u_i, where $0 \le i \le \infty$,

$$u[n] = u_0\delta[n] + u_1\delta[n-1] + \cdots + u_m\delta[n-M] \quad (2)$$

with $M \in \{0, 1, 2, \cdots\}$. The system output, $y[n]$, can be interpreted as the sum of with u_i weighted and shifted

impulse responses, which is the convolution of (1) with (2):

$$y[n] = u_0g[n] + u_1g[n-1] + \cdots + u_Mg[n-M]. \quad (3)$$

Now, we make an approximation and two restrictions. The approximation is to neglect elements g_i of the impulse response $g[n]$ for $i > N$. To keep this approximation's error small, we have to restrict ourselves to asymptotically stable systems. For these systems the impulse response converges to zero so that the error can be made arbitrarily small for a suitable choice of N. Taking the elements g_i as the numerator coefficients a_i of the FIR filter

$$G_{FIR}(z) = \frac{a_0z^N + a_1z^{N-1} + \cdots + a_N}{z^N} \quad (4)$$

leads to a fast, easy to implement approximation of the original system. The second restriction concerns the input sequence. Up to now, we've regarded an arbitrarily long sequence $u[n]$. However for the further steps, it is necessary to choose $M \neq \infty$ and consider only a limited period of $u[n]$. In MPC, this period is called "control horizon".

With $N, M < \infty$, we can rewrite the convolution (3) as a matrix vector product:

$$\mathbf{y} = \begin{pmatrix} y_0 \\ \vdots \\ y_{N+M} \end{pmatrix} = \begin{bmatrix} g_0 \\ \vdots & \ddots \\ g_N & & g_0 \\ & \ddots & \vdots \\ & & g_N \end{bmatrix} \begin{pmatrix} u_0 \\ \vdots \\ u_M \end{pmatrix} = \mathbf{Gu}. \quad (5)$$

It can be seen that $\mathbf{G}$ is a Toeplitz matrix and each column consists of the finite impulse response padded with zeros. Comparing (5) with (4) it becomes clear that (5) is just another representation of (4) with the disadvantage of a finite input sequence. In DMC the matrix $\mathbf{G}$, the so called "dynamic matrix", is usually built with the step-response. Equation (5) predicts the output y_i for the next $N + M$ time steps (the so called "prediction horizon"). As we are not interested in the decaying behavior, which is represented by the last $M - N$ rows, we will use a square $(M + 1) \times (M + 1)$ matrix for our subsequent calculations:

$$\mathbf{G}_{\square} = \begin{bmatrix} g_0 \\ \vdots & \ddots \\ g_N & & g_0 \\ & \ddots & \vdots & \ddots \\ & & g_N & \cdots & g_0 \end{bmatrix} \quad (6)$$

with $M \ge N$.

An intuitive approach to determine the input $\mathbf{u}$ for a desired output $\mathbf{y}_d$ is to simply build the inverse [1] of $\mathbf{G}_{\square}$:

$$\mathbf{u} = \mathbf{G}_{\square}^{-1}\mathbf{y}_d, \quad (7)$$

which is called deconvolution. In Ford et al. (2014) it is shown that the inverse of a lower triangular Toeplitz matrix again has lower triangular Toeplitz form. It is furthermore proven that for monotonically decaying $g_0 \ldots g_N$, the inverse's columns decay also monotonically. A monotonically decreasing impulse response thus leads to a monotonically decreasing impulse response of the inverted system

---

[1] If $g_0 = 0$, then $\mathbf{G}_{\square}$ is singular and $y_1 = 0$. By removing the first row and the last column from (5), a corresponding non-singular square matrix (6) results and (7) is to be modified correspondingly. Thereby, the next steps can easily be adapted to cases where the first elements of $g[n]$ are zero.

(in the following called "inverse impulse response"), which is represented by the first column of the inverse matrix $\mathbf{G}_\square^{-1}$. Due to this structure the matrix vector product again represents a convolution like (3) and can therefore be transformed back to an FIR filter by taking the elements of the first column of the inverse matrix $\mathbf{G}_\square^{-1}$ as filter coefficients. In other words, we approximate the inverse system dynamics by an FIR filter that is based on the inverse impulse response. This transition is necessary to enable use of arbitrarily long desired trajectories, $\mathbf{y}_d$, which cannot be done with the deconvolution in (7).

The practicability of this method is only secured for a very small number of systems with monotonically decreasing impulse responses. As soon as the impulse response has an over- or undershoot, the elements of the first column of $\mathbf{G}_\square^{-1}$ and thus the inverse impulse response possibly diverge. This makes the back transformation to an FIR filter impossible, as an infinite number of filter coefficients would be needed. Furthermore, the inputs determined with (7) will then tend to infinity too, which makes them inapplicable for a real system. Especially for nonminimum phase systems the inverse impulse response always diverges. This is exactly the behavior we expect for systems with zeros outside the unit circle, as these "unstable" zeros become poles of the inverted system. To also use this method for systems with over- and undershoot and to keep the input values small, we introduce an optimization.

3.2 Optimal Proactive Deconvolution

To tackle the above mentioned problems, we have to move away from the idea of perfect trajectory tracking. It is often sufficient to follow a given trajectory approximately so that we allow an error

$$\mathbf{e} = \mathbf{y}_d - \mathbf{G}_\square \mathbf{u}. \tag{8}$$

The aim of the optimal FIR filter is to follow the desired trajectory as well as possible while minimizing the needed input effort and rate of change. Mathematically, this is achieved by minimizing the objective function

$$J = \mathbf{e}^T \mathbf{Q} \mathbf{e} + \mathbf{u}^T \mathbf{R} \mathbf{u} + \Delta\mathbf{u}^T \tilde{\mathbf{R}} \Delta\mathbf{u}, \tag{9}$$

where $\mathbf{Q}, \mathbf{R}$ and $\tilde{\mathbf{R}}$ are positive definite weighting matrices for the error, the input and the change of input respectively. The rate of change of the input can be calculated by

$$\Delta\mathbf{u} = \begin{bmatrix} 1 & & & \\ -1 & 1 & & \\ & \ddots & \ddots & \\ & & -1 & 1 \end{bmatrix} \mathbf{u} = \mathbf{D}\mathbf{u}. \tag{10}$$

To minimize J, we insert (8) and (10) in (9) and differentiate (9) with respect to $\mathbf{u}$. Equating the derivative to zero and rearranging the terms, we get

$$\mathbf{u}^* = (\mathbf{G}_\square^T \mathbf{Q} \mathbf{G}_\square + \mathbf{R} + \mathbf{D}^T \tilde{\mathbf{R}} \mathbf{D})^{-1} \mathbf{G}_\square^T \mathbf{Q} \mathbf{y}_d = \mathbf{F} \mathbf{y}_d. \tag{11}$$

Again, we have a deconvolution as in (7). However, the optimized deconvolution matrix $\mathbf{F}$ (in contrast to $\mathbf{G}_\square^{-1}$) is not a lower triangular Toeplitz matrix, but dense. The structure can resemble a Toeplitz matrix, but it has deviations mainly in the first and last columns. The upper triangular entries of F are obviously responsible for the proactive behavior. These elements describe, how future values of the desired trajectory influence the current input.

In DMC, only the first row of $\mathbf{F}$ is taken to calculate the optimal input u in each time step. As the influence of former input values on the current output is not included implicitly, those have to be fed back (see figure 1). This can lead to instability, which is the main disadvantage of DMC as feedforward control.

Wagner (1999) derives the above deconvolution in the same way and mentions that it is deployable only for trajectories of finite length. The longer the desired $\mathbf{y}_d$ the bigger the deconvolution matrix and the more memory is needed. To remove these disadvantages we show in the next section how to build, based on the optimal proactive deconvolution, an FIR filter that can handle arbitrary long desired trajectories.
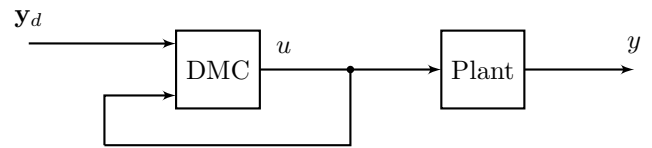

Fig. 1. Feedforward dynamic matrix control

3.3 Optimal Proactive FIR Filter

Section 3.1 showed that, under the restriction of a finite length input signal, an FIR filter can be represented as a matrix vector product with the convolution matrix in lower triangular Toeplitz form. We also mentioned that if we have a monotonically decreasing lower triangular Toeplitz deconvolution matrix, then we can use its elements as filter coefficients for a deconvolving FIR filter with arbitrary input length. To build such an FIR filter from the deconvolution matrix $\mathbf{F}$ we have to ensure that $\mathbf{F}$ has "Toeplitz-like" form and that its rows converge to zero. For the following considerations we exploit the properties of LTI systems, e.g. the principle of superposition. Each desired output sequence $\mathbf{y}_d$ can be seen as a sequence of single impulses. According to the principle of superposition, we can calculate the input sequence needed for each of these single impulses and determine the total input $\mathbf{u}$ by shifting the single input sequences in time and adding them up. It is thus sufficient to regard in the following only the case of a single impulse as desired trajectory.

To show that a row in the middle of $\mathbf{F}$ converges to zero, we have to assume that

- the control horizon $\mathbf{M}$ is long enough;
- the weighting matrices $\mathbf{Q}, \mathbf{R}$ and $\tilde{\mathbf{R}}$ are diagonal and of the form $k\mathbf{I}$ with a positive scalar weighting factor k and the identity matrix $\mathbf{I}$;
- the impulse response, $g[n]$, converges to zero.

The first two assumptions concern parameters to be chosen and the last is always true because we restricted this method to asymptotically stable systems earlier. The first step is to rewrite (11) as

$$(\mathbf{G}_\square^T \mathbf{Q} \mathbf{G}_\square + \mathbf{R} + \mathbf{D}^T \tilde{\mathbf{R}} \mathbf{D})\mathbf{u}^* = \mathbf{G}_\square^T \mathbf{Q} \mathbf{y}_d, \tag{12}$$

and to assume as desired output an impulse in the middle $(M/2)$ of the control horizon:

$$\mathbf{y}_d^T = [0 \ \cdots \ 0 \ 1 \ 0 \ \cdots \ 0]^T. \tag{13}$$

The resulting vector on the right-hand side is

$$\mathbf{y}_{RHS}^T = q[0 \; \cdots \; 0 \; g_N \cdots \; g_0 \; 0 \; \cdots \; 0]^T \qquad (14)$$

with q as the weighting factor of $\mathbf{Q}$. In the next step, we try to determine the structure of the resulting matrix on the left-hand side of (12). $\mathbf{R}$ is diagonal and $\mathbf{D}^T\tilde{\mathbf{R}}\mathbf{D}$ is a tridiagonal matrix with positive values on the main diagonal and half of these values negated on the secondary diagonals. Since $\mathbf{Q}$ is of the form $q\mathbf{I}$, it does not change the structure of $\mathbf{G}_\square^T\mathbf{Q}\mathbf{G}_\square$ so that it is sufficient to inspect the term $\mathbf{G}_\square^T\mathbf{G}_\square$. This expression equals the autocorrelation matrix. The autocorrelation function is a convolution with the mirrored signal itself. Calculating the first column of $\mathbf{G}_\square^T\mathbf{G}_\square$ is the same as convolving the impulse response $g[n]$ with the mirrored impulse response, $g[M-n]$. For column L, we have to convolve $g_L[n]$ with $g[M-n]$, where $g_L[n]$ is the impulse response shifted by $L-1$ zeros and cut after M elements. For better understanding, this procedure is shown for a sample system in fig. 2. The left two plots show

Fig. 2. Illustration of autocorrelation

the calculation of the first column ($L = 1$) of $\mathbf{G}_\square^T\mathbf{G}_\square$ and the ones on the right show how the $L = M/2^{\text{th}}$ column is determined. The blue impulse response represents $g_L[n]$, whereas the red impulse responses show for some time steps how the impulse response $g[n]$ is shifted during convolution. The result of the convolution is shown in the lower plots (red circles mark the value corresponding to one red impulse response). According to the third assumption $g[n]$ will converge to zero, like in the example in fig. 2. This obviously leads to entries whose absolute values increase the closer they are to the diagonal and decrease the farther away. By choosing M big enough, we can make the absolute values of the columns in the middle of $\mathbf{G}_\square^T\mathbf{G}_\square$ start at approximately zero, increase towards the diagonal entries and then converge back to zero. For oscillating impulse responses, the convolution also oscillates. However, the general trend remains the same for the amplitude of the oscillation. Altogether, because adding $\mathbf{R}$ and $\mathbf{D}^T\tilde{\mathbf{R}}\mathbf{D}$ increases the diagonal values, the structure of the matrix on the left-hand side of (12) resembles

$$\mathbf{G}_{LHS} = \begin{bmatrix} & & & & \\ & & & & \\ & & & & \\ & & & & \\ & & & & \end{bmatrix}, \qquad (15)$$

where the size of the circles represents the absolute values of the entries in the corresponding areas of the matrix. It remains to be shown, what the optimal input sequence $\mathbf{u}^*$ will be for the desired right hand side (see (14)). As $\mathbf{u}$ should stay as small as possible and as $\mathbf{y}_{RHS}^T$ has only non-zero entries in the center, the input sequence $\mathbf{u}^*$ must have - considering the structure of $\mathbf{G}_{LHS}$ - very small values at the beginning and at the end. The big diagonal values of $\mathbf{G}_{LHS}$ are to be exploited to minimize the needed input while effecting the non-zero entries in $\mathbf{y}_{RHS}$. This leads to non-zero values in the middle of the input so that all in all it will be of the form:

$$\mathbf{u}^{*T} = [\bigcirc \; \cdots \; \bigcirc \; * \; \cdots \; * \; \bigcirc \; \cdots \; \bigcirc]^T, \qquad (16)$$

where $\bigcirc$ and $*$ are almost zero and non-zero values respectively. Going back to the deconvolution (11), we can conclude that a column in the center of $\mathbf{F}$ has to have the same structure as the optimal input in (16), because the desired output, $\mathbf{y}_d$, (see (13)) picks one column out of $\mathbf{F}$ to determine $\mathbf{u}^*$.

So far we have shown that the columns in the center of $\mathbf{F}$ start at and converge to zero. The last step is to illustrate why the deconvolution matrix will have a Toeplitz-like structure. Again, due to the principle of superposition, it suffices to regard a single impulse as desired output. We assume that we have enough time before and after the single impulse to alter the input in advance or afterwards ($\Leftrightarrow M$ big enough). Then, it does not matter when exactly the desired impulse is planned. The optimal input must always be the same sequence shifted in time, because we regard only linear time invariant systems. To achieving this, the matrix $\mathbf{F}$ must have a Toeplitz-like structure. The structure is just Toeplitz-like, because the areas in the upper left and lower right corners of $\mathbf{F}$ do differ from exact Toeplitz structure and because the elements far away from the diagonal are only almost zero and not exactly zero. The former is not a bug, but a feature. If an impulse in the output is demanded just for the next time step, then there is no time to "prepare" this output in advance. The input must react immediately and thus, has to be different compared to the case in which there is enough time to do something in advance. This is considered implicitly in the deviations from the Toeplitz-structure. The first column of $\mathbf{F}$ represents the input sequence for a desired instantaneous impulse. As this column starts with a diagonal value, no future information is considered thereby precluding proactive behavior. The entries therefore have to be different from the ones in the next column to achieve an impulse in the output. The same is true for columns that describe the input needed for a desired impulse a very short time ahead.

Summarizing the above, it was shown that as long as the LTI system is asymptotically stable, the weighting matrices are of the form $k\mathbf{I}$ and the control horizon M
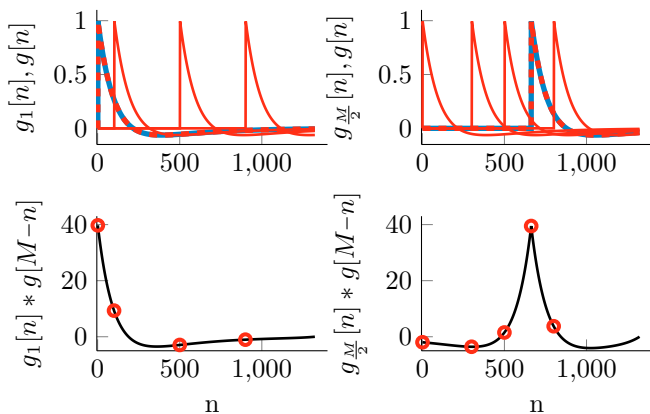
is sufficiently large, the deconvolution matrix $\mathbf{F}$ will have a Toeplitz-like structure with converging columns thus enabling transformation into an FIR filter.

In the case of unoptimized deconvolution (7), $\mathbf{G}_\square^{-1}$ is a lower triangular Toeplitz-matrix and therefore proactive behavior could not be achieved. Since the first column contains the most non-zero entries and thus the most information, we clearly picked this one to use its values as coefficients of the FIR filter. The choice of column is a little less straight forward for the back transfomation of the optimized deconvolution matrix $\mathbf{F}$. A column out of the center of $\mathbf{F}$ is best generally speaking, because the Toeplitz structure there is the most distinct and we have approximately the same number of entries weighting the future desired outputs (elements above the diagonal) and weighting the past desired outputs (elements below the diagonal). If M is furthermore large enough, the absolute values of the center columns will decrease the closer they are to the border of the matrix. The error we make by using a finite number of coefficients will thus be very small. When the input is determined via the deconvolution (11), the $M/2^{\text{th}}$ column is multiplied by the $M/2^{\text{th}}$ value of the desired output. This value thus effects the current input, so we need to know it $M/2$ time steps in advance. What if the desired output is not known $M/2$ steps in advance? Given the case that there is no knowledge about the future output, taking just the diagonal value and the values below of the $M/2^{\text{th}}$ column is not recommended. The results are much better if we use the first column of the matrix $\mathbf{F}$ as filter coefficients. This column takes into consideration that we know nothing in advance so that as already described, the reaction to a desired output will be faster. Furthermore, all M entries in that column can be used and not just $M/2$ of them, which makes the filter more exact. Thus, for each length of preview time there is one corresponding column in $\mathbf{F}$, which contains the (according to the objective function) optimal inverse impulse response. The following formula is used to design the proactive FIR filter based on the entries f_i of the pth column of $\mathbf{F}$:

$$F_z(z) = \frac{f_{-p+1}z^M + \cdots + f_{-1}z^{M-p+2}}{z^{M-(p-1)}} + \cdots$$
$$\cdots + \frac{f_0 z^{M-p+1} + f_1 z^{M-p} + \cdots + f_{M-p+1}}{z^{M-(p-1)}}, \quad (17)$$

where negative i describe the elements f_i above and positive i below the diagonal entry of $\mathbf{F}$. It can be easily seen that as soon as $p > 1$, $F_z(z)$ becomes an improper transfer function and thus proactive (by using future values of y_d gained from preview). In summary, we build the optimal deconvolution matrix $\mathbf{F}$ and derive from it an optimal proactive FIR filter. This is an important difference to the approach taken in Takegaki and Matsui (1985), where the filter coefficients are included in the objective function and are thus directly optimized under the assumption of a known form of the desired output.

Throughout the analysis, we postulated that the control horizon M is greater or equal to the impulse response length N and that M is long enough. How to identify, whether or not M is "long enough"? If the optimized inverse impulse response were known a priori, then we would have to choose M just a little longer than that. Unfortunately, we do not know the optimized inverse

impulse response in advance, because we are trying to determine it. Fixing M is thus an iterative procedure. We chose an $M \geq N$ and calculate the optimized inverse impulse response. If it starts at and converges smoothly to zero, then we are done. If not, then we have to choose a bigger M and restart the whole procedure.

4. EXAMPLE

We take the continuous time nonminimum phase system as an example:

$$G_1(s) = \frac{-3s + 2}{(s+1)(s+2)}. \quad (18)$$

To design the optimal proactive feedforward control via the FIR filter, $F_z(z)$ (see fig. 3), we transform $G_1(s)$ to a discrete time transfer function (sample time $T_s = 10^{-2}$) and determine the impulse response (see fig. 4).
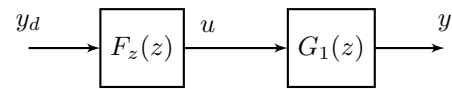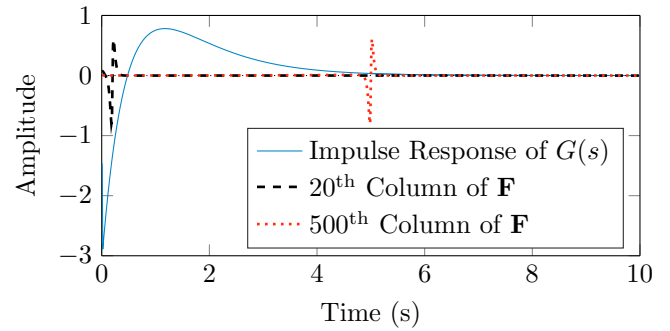

Fig. 3. FIR feedforward control

Fig. 4. (Optimized inverse) impulse response of $G_1(s)$

After 10 seconds, the impulse response is close enough to zero to clip it without a large error. This leads to a length of $N = 10/10^{-2} = 1000$. The impulse response is used to assemble the dynamic matrix, $\mathbf{G}_\square$, for which we chose the length of the control horizon to $M = N = 1000$. The objective function is of the form of (9) with $\mathbf{Q} = \mathbf{I}$ and $\mathbf{R} = \tilde{\mathbf{R}} = 0.01\mathbf{I}$. This choice ensures that all weighting matrices are as demanded in section 3.3. The matrix $\mathbf{F}$ is calculated using (11). The amplitude of its elements is depicted in fig. 5. It has the structure shown in (15), and the values of its center columns start at and converge to zero. $\mathbf{F}$ is thus Toeplitz-like, which confirms that our choice of the length of the control horizon, M, was large enough. Figure 4 also illustrates the 20th and the 500th columns of $\mathbf{F}$, which can be interpreted as optimized inverse impulse responses of $G_1(s)$. The actual inverse impulse response would be unstable, whereas the optimized ones remain bounded. Furthermore, there is -except the time shift- a remarkable similarity between the two columns of $\mathbf{F}$, which once more proves the Toeplitz-like structure.

We take the elements of the 500th column as FIR filter coefficients. According to the sample time, T_s, this leads to a preview time of 5 seconds. Now we demand a step in the output at 6 seconds. Figure 6 shows the resulting input and output when simulating with the discretized system. The input already starts to rise 5 seconds before the desired
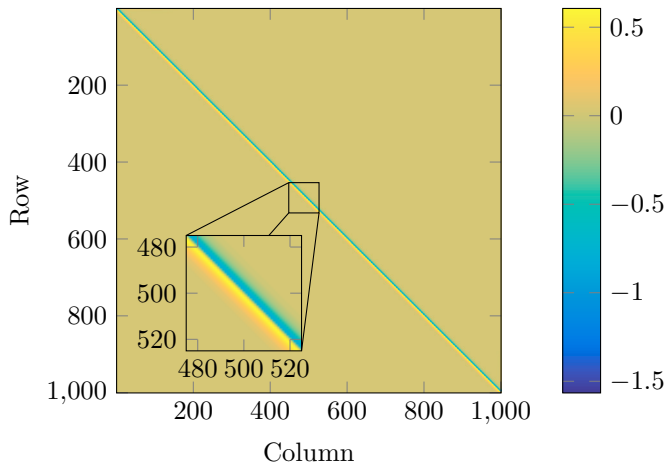
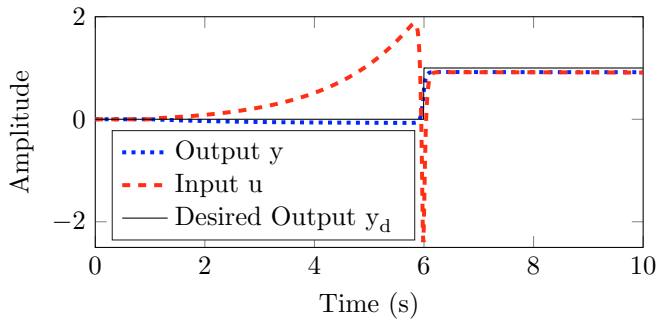Fig. 5. Structure of deconvolution matrix $\mathbf{F}$

Fig. 6. System $G_1(s)$ with feedforward FIR filter ($p = 500$)

step occurs. Hence, the FIR filter does exhibit proactive behavior. The proactive behavior makes following the desired output possible very well with a reasonably large control input. Since we are weighting the input, we can not observe steady state accuracy. To improve steady state behavior, the weighting of the input, $\mathbf{u}$, has to be replaced by the weighting of the input's deviation from its steady state value $\mathbf{u} - \mathbf{u}_{stat} = \mathbf{u} - \mathbf{y}_d/G(0)$, where $G(0)$ is the system's steady state gain. The derivation of the optimal $\mathbf{u}^*$ is straightforward and leads again to a deconvolution of the form $\mathbf{u}^* = \mathbf{F}\mathbf{y}_d$. It is furthermore easy to show that this extension does not affect the structure of $\mathbf{F}$.

5. CONCLUSION

A new method for designing a proactive optimal FIR filter for feedforward preview control of asymptotically stable SISO systems has been proposed. We introduced the necessary system representation, determined an optimal proactive deconvolution, and observed that we can always build an FIR filter from that. The FIR filter's effectiveness was then shown for a nonminimum phase system. Compared to other methods, this filter stands out by virtue of its easy implementation and the possibility it offers for taking future knowledge about the desired output into account. Furthermore, knowing a system's impulse response suffices for the filter design. The method can be used for all asymptotically stable SISO systems. The filter's behavior can be easily adjusted with a hand full of parameters all of which have a physical meaning. Using the weighting matrices, we can set the focus on the deviation of the output from

the desired output, the needed input or the rate of change of the input. The parameter M describes the length of the control horizon; the parameter p has to be chosen according to the available preview horizon. The FIR filter thus can be parametrized intuitively and independently of the original system dynamics, which makes it quite a universal tool. Furthermore, it is by definition always stable, which ensures stability for the overall system.

Future work will involve further extensions of the objective function as well as attempts to ease the current restrictions. Furthermore, the method will be implemented and tested for road-profile preview control of an active suspension of a quarter car.

REFERENCES

Cutler, C.R. and Ramaker, B.L. (1980). Dynamic matrix control - a computer control algorithm. *Joint Automatic Control Conference*, 17.

Devasia, S., Degang Chen, and Paden, B. (1996). Nonlinear inversion-based output tracking. *IEEE Transactions on Automatic Control*, 41(7), 930–942.

Dunne, F. and Pao, L.Y. (2016). Optimal blade pitch control with realistic preview wind measurements. *Wind Energy*.

Ford, N.J., Savostyanov, D.V., and Zamarashkin, N.L. (2014). On the decay of the elements of inverse triangular toeplitz matrices. *SIAM Journal on Matrix Analysis and Applications*, 35(4), 1288–1302.

Hunt, L.R., Meyer, G., and Su, R. (1996). Noncausal inverses for linear systems. *IEEE Transactions on Automatic Control*, 41(4), 608–611.

MacAdam, C.C. (1981). Application of an optimal preview control for simulation of closed-loop automobile driving. *IEEE Transactions on Systems, Man, and Cybernetics*, 11(6), 393–399.

Marro, G., Prattichizzo, D., and Zattoni, E. (2002). Convolution profiles for right inversion of multivariable nonminimum phase discrete-time systems. *Automatica*, 38(10), 1695–1703.

Schindler, A. (2009). *Neue Konzeption und erstmalige Realisierung eines aktiven Fahrwerks mit Preview-Strategie*, volume 31 of *Schriftenreihe des Instituts für Angewandte Informatik - Automatisierungstechnik, Universität Karlsruhe (TH)*. KIT Scientific Publ, Karlsruhe.

Takegaki, M. and Matsui, K. (1985). A design method of optimal feedforward compensator. *Transactions of the Society of Instrument and Control Engineers*, 21(4), 367–373.

Vosen, S. (1999). Hybrid energy storage systems for stand-alone electric power systems: Optimization of system performance and cost through control strategies. *International Journal of Hydrogen Energy*, 24(12), 1139–1156.

Wagner, B. (1999). *Analytische und iterative Verfahren zur Inversion linearer und nichtlinearer Abtastsysteme*, volume 763 of *Fortschritt-Berichte VDI Reihe 8, Meß-, Steuerungs- und Regelungstechnik*. VDI-Verl., Düsseldorf.

Zou, Q. and Devasia, S. (2004). Preview-based optimal inversion for output tracking: Application to scanning tunneling microscopy. *IEEE Transactions on Control Systems Technology*, 12(3), 375–386.

A.2 Proactive Disturbance Compensator for Vibration Damping of a Quarter-Car

Contributions: The derivation of the proactive disturbance compensator, implementation, simulations, analysis, experiments and writing have been conducted predominantly by the first author.

Anwendungen

Johannes N. Strohm* und Boris Lohmann

Vorausschauende Störgrößenaufschaltung für die Schwingungsdämpfung am Viertelfahrzeug

Proactive disturbance compensator for vibration damping of a quarter-car

Zusammenfassung: Dieser Beitrag zeigt eine neuartige Störgrößenaufschaltung und deren Anwendung zur Schwingungsdämpfung am Viertelfahrzeug. Dazu präsentieren wir zunächst die optimale vorausschauende Vorsteuerung. Diese basiert auf einem Impulsantwortmodell der Regelstrecke und kann analytisch berechnet werden. Der große Vorteil der Vorsteuerung liegt in der vorausschauenden Arbeitsweise und der einfachen Parametrierbarkeit über ein Gütemaß. Auf dieser Vorsteuerung aufbauend, wird eine Möglichkeit zum Entwurf einer Störgrößenaufschaltung dargestellt. Im zweiten Schritt wenden wir letztere zur Dämpfung der durch Straßenunebenheiten erregten Schwingungen am Viertelfahrzeug an. Dazu wird zunächst der Einfluss verschiedener Parameter auf die Leistungsfähigkeit der Aufschaltung untersucht. Abschließend zeigen wir, dass diese Störgrößenaufschaltung sowohl in der Simulation als auch im Versuch zu deutlich gedämpften Schwingungen führt.

Schlüsselwörter: Vorausschauende optimale Vorsteuerung, vorausschauende Störgrößenaufschaltung, FIR-Filter, Viertelfahrzeug, Schwingungsdämpfung.

Abstract: This article presents a new disturbance compensator and its application to vibration damping of a quarter car. First, we introduce an optimal feedforward preview controller. It is based on an impulse response model of the system dynamics and can be calculated analytically. The advantages of this feedforward controller are its simple parametrization via an objective function and its ability to use preview data. Then, we present how to design the disturbance compensator using the feedforward controller. In the second part, we apply the compensator to vibration damping of the quarter car. Therefore, we analyze the influence of some parameters on the performance of the compensator. Finally, we show that the disturbance compensator leads in simulation as well as in experiment to a remarkable damping of oscillations.

Keywords: Optimal feedforward preview control, preview disturbance compensator, quarter car, vibration damping.

1 Einleitung

Autonomes Fahren ist in aller Munde. Zumeist werden damit im regelungstechnischen Kontext die Herausforderungen bezüglich Trajektorienplanung und -folge assoziiert. Eine weitaus weniger berücksichtigte Problematik ist die der steigenden Komfortansprüche. Bisher versuchten Automobilhersteller bei der Fahrwerksauslegung einen Kompromiss zwischen komfortablem Fahren und sportlichem Fahrgefühl zu finden. Da autonome Fahrzeuge dem Fahrer jegliche Fahraufgaben abnehmen, wird letzteres in Zukunft kein vorrangiges Auslegungsziel mehr sein. Zusätzlich werden die Komfortansprüche steigen: Weil nicht mehr selbst gefahren werden muss, werden die Insassen sich während der Fahrt eine andere Beschäftigung suchen. Die meisten Tätigkeiten lassen sich jedoch nur dann sinnvoll ausführen, wenn der Fahrzeugaufbau sich nicht zu stark in vertikaler Richtung bewegt.

Bei klassischen passiven Fahrwerken, bestehend aus einer Feder und einem Dämpfer, gibt es immer einen Zielkonflikt zwischen Fahrkomfort und Fahrsicherheit. In Folge dessen lässt sich der Komfort nicht beliebig erhöhen, ohne dass die Fahrsicherheit abnimmt. Abhilfe können Aktuatoren im Federbein schaffen, die diesen Zielkonflikt mildern können. Dazu ist jedoch eine geeignete Steuerung oder Regelung notwendig.

*Korrespondenzautor: Johannes N. Strohm, Technische Universität München, Lehrstuhl für Regelungstechnik, Boltzmannstraße 15, 85748 Garching bei München, E-Mail: johannes.strohm@tum.de
Boris Lohmann: Technische Universität München, Lehrstuhl für Regelungstechnik, Boltzmannstraße 15, 85748 Garching bei München

Weiterhin erfassen autonome Fahrzeuge mit verschiedensten Sensoren große Mengen an Daten über ihre Umwelt. Aus diesen Daten können nicht nur Informationen über den Straßenverlauf oder andere Verkehrsteilnehmer gewonnen werden, sondern auch über die Oberflächenbeschaffenheit der Straße vor dem Fahrzeug. Diese stellt bezüglich des Komforts gerade die Störanregung dar.

Mit der Kenntnis der zukünftigen Störung lässt sich eine Störgrößenaufschaltung (SGA) entwerfen, welche die Aktuatoren im Federbein so ansteuert, dass die Störanregung bestmöglich kompensiert wird. Dadurch kann eine Steigerung des Fahrkomforts bei sichergestellter Fahrsicherheit erreicht werden. Dieser Beitrag stellt den Entwurf solch einer SGA vor und zeigt, dass diese sowohl in Simulation als auch im Experiment das angestrebte Ziel erreicht.

2 Methode

Dieser Abschnitt stellt zunächst die vorausschauende optimale Vorsteuerung über Finite Impulse Response (FIR) Filter dar. Darauf aufbauend wird im nächsten Schritt die vorausschauende SGA entworfen.

2.1 Optimale vorausschauende Vorsteuerung

Zu Beginn wird eine geeignete Systemdarstellung hergeleitet. Der Ausgangspunkt für den Entwurf ist ein lineares zeitinvariantes (LZI), asymptotisch stabiles System mit einem Eingang und einem Ausgang (Single-Input Single-Output (SISO)). Die diskret abgetastete Impulsantwort $g[n]$ sei als bekannt angenommen. Da für lineare Systeme das Superpositionsprinzip gilt, kann über diese Impulsantwort die Ausgangsfolge $y[n]$ des Systems für eine beliebige Eingangsfolge $u[n]$ berechnet werden. Dazu fassen wir $u[n]$ als eine Folge von Einzelimpulsen

$$u[n] = u_0\delta[n] + u_1\delta[n-1] + \cdots \qquad (1)$$

auf, welche jeweils eine skalierte Impulsantwort zeitversetzt im Ausgang erzeugen. Die Ausgangsfolge ergibt sich aus der Summe dieser Impulsantworten. Mathematisch ausgedrückt ist dies die Faltung

$$y[n] = \sum_{i=-\infty}^{\infty} g[i]u[n-i] = \sum_{i=0}^{\infty} g[i]u[n-i]. \qquad (2)$$

Die Einschränkung in (2) auf die Summe beginnend bei $i = 0$ ist darauf zurückzuführen, dass ein reales System eine kausale Impulsantwort besitzt. Das heißt, dass frühestens zu dem Zeitpunkt, an dem der Impuls auf das System wirkt, eine Änderung im Ausgang sichtbar ist. Deshalb gilt $g[n] = 0$ für $n < 0$ und jegliche Summanden in (2) mit $i < 0$ verschwinden. Außerdem benötigt die Faltung deshalb keine zukünftigen Werte der Stellgröße $u[j]$ mit $j > n$.

Auf Grund der asymptotischen Stabilität nähert eine auf $N + 1$ Zeitschritte begrenzte Impulsantwort

$$\tilde{g}[n] = g_0\delta[n] + g_1\delta[n-1] + \cdots + g_N\delta[n-N] \qquad (3)$$

die unendlich lange Impulsantwort $g[n]$ mit beliebig kleinem Fehler an. Für die Faltung dieser genäherten Impulsantwort mit dem Eingang $u[n]$ kann die obere Grenze der Summe in (2) auf $i = N$ abgesenkt werden. Dies stellt das FIR-Filter

$$G_z(z) = g_0 + g_1 z^{-1} + \cdots + g_N z^{-N} \qquad (4)$$

kompakt dar. Beschränken wir zusätzlich die Länge der Eingangsfolge $u[n]$ auf $M + 1$ Elemente, so lässt sich die Faltung ausdrücken als Matrix-Vektor-Produkt

$$\underbrace{\begin{bmatrix} y_0 \\ \vdots \\ y_{N+M} \end{bmatrix}}_{\mathbf{y}} = \underbrace{\begin{bmatrix} g_0 & & \\ \vdots & \ddots & \\ g_N & & g_0 \\ & \ddots & \vdots \\ & & g_N \end{bmatrix}}_{\text{Faltungsmatrix } \mathbf{G}} \underbrace{\begin{bmatrix} u_0 \\ \vdots \\ u_M \end{bmatrix}}_{\mathbf{u}}, \qquad (5)$$

wobei $\mathbf{G}$ Toeplitz-Struktur hat und die Einträge der Spalten den Koeffizienten der Impulsantwort $\tilde{g}[n]$ entsprechen. Im Kontext der modellprädiktiven Regelung (Model Predictive Control (MPC)) wird die Länge M des Eingangsvektors $\mathbf{u}$ als Stellhorizont und die Länge $N + M$ des Ausgangsvektors $\mathbf{y}$ als Vorhersagehorizont bezeichnet [8]. Die Systemdarstellung (5) nutzen wir im Folgenden für den Entwurf der optimalen vorausschauenden Steuerung. Um jedoch die Einschränkung der begrenzten Länge der Eingangs- und Ausgangsfolge aufzuheben, ist eine Rücktransformation der Matrix-Vektor-Form auf ein FIR-Filter wie in (4) notwendig. Dies ist möglich, wenn:

– die Matrix Toeplitz-Struktur aufweist und somit eine Faltung darstellt, und

– die Einträge der Spalten der Matrix, welche den Impulsantwortkoeffizienten entsprechen, abklingen. Dies ist gleichbedeutend mit einer asymptotisch stabilen Systemdynamik, weshalb eine Annäherung dieser durch ein FIR-Filter zulässig ist.

Ziel der Vorsteuerung ist die Berechnung der Stellgrößenfolge $u^*[n]$ so, dass der Ausgang des Systems möglichst

genau einer Wunschtrajektorie $y_w[n]$ folgt. Dafür wird zunächst die Abweichung zwischen Wunsch- und Istausgang definiert:

$$\mathbf{e} = \mathbf{y}_w - \mathbf{y} = \mathbf{y}_w - \mathbf{G}\mathbf{u}. \tag{6}$$

Die Abweichung soll zusammen mit dem Stellaufwand und der Stellgrößenänderung minimiert werden. Wir drücken dies über das quadratische Gütemaß

$$J = \mathbf{e}^T\mathbf{Q}\mathbf{e} + \mathbf{u}^T\mathbf{R}\mathbf{u} + \Delta\mathbf{u}^T\tilde{\mathbf{R}}\Delta\mathbf{u} \tag{7}$$

aus, das die Regelabweichung $\mathbf{e}$, den Stellgrößeneinsatz $\mathbf{u}$ und die zeitliche Änderung der Stellgröße $\Delta\mathbf{u}$ über die positiv definiten Gewichtungsmatrizen $\mathbf{Q}$, $\mathbf{R}$ und $\tilde{\mathbf{R}}$ gewichtet. Die Größe $\Delta\mathbf{u}$ wird über

$$\Delta\mathbf{u} = \begin{bmatrix} 1 & & & \\ -1 & 1 & & \\ & \ddots & \ddots & \\ & & -1 & 1 \end{bmatrix}\mathbf{u} = \mathbf{D}\mathbf{u} \tag{8}$$

gewonnen. Die optimale Steuerung ergibt sich durch Einsetzen von (6) in (7) und Nullsetzen der Ableitung des Gütemaßes bezüglich $\mathbf{u}$ zu:

$$\mathbf{u}^* = \left(\mathbf{G}^T\mathbf{Q}\mathbf{G} + \mathbf{R} + \mathbf{D}^T\tilde{\mathbf{R}}\mathbf{D}\right)^{-1}\mathbf{G}^T\mathbf{Q}\mathbf{y}_w = \mathbf{F}\mathbf{y}_w. \tag{9}$$

Mit (9) kann über die Entfaltungsmatrix $\mathbf{F}$ bereits eine Steuerfolge $\mathbf{u}^*$ zur im Sinne des Gütemaßes optimalen Umsetzung der Wunschtrajektorie $\mathbf{y}_w$ berechnet werden. Jedoch ist dies nur für eine Wunschtrajektorie begrenzter Länge möglich. Daher liegt es nahe zu untersuchen, ob wir (9) durch ein FIR-Filter darstellen können.

Zur besseren Veranschaulichung analysieren wir dies zunächst für ein Beispielsystem. Im Anschluss werden die Aussagen verallgemeinert. Ausgangspunkt ist das asymptotisch stabile LZI-System

$$G(s) = \frac{-3s + 2}{(s + 1)(s + 2)}, \tag{10}$$

welches eine Nullstelle bei $s = \frac{2}{3}$ aufweist. Abbildung 1 zeigt die Koeffizienten g_i der dazugehörigen Impulsantwort für das mit $T_s = 0{,}1$ s diskretisierte System. Diese wurde nach $N = 99$ Zeitschritten abgeschnitten. Für dieses System entwerfen wir nun eine optimale vorausschauende Steuerung mit den Gewichtungsmatrizen

$$\mathbf{Q} = \mathbf{I} \quad \mathbf{R} = 0{,}01\mathbf{I} \quad \tilde{\mathbf{R}} = 0{,}01\mathbf{I}, \tag{11}$$

wobei $\mathbf{I}$ der Einheitsmatrix entspricht. Über (9) lässt sich die Entfaltungsmatrix $\mathbf{F}$ berechnen. Abbildung 2 zeigt diese graphisch für einen Stellhorizont von $M = 99$. Zwischen der 30. und der 90. Spalte tritt eine Toeplitz-ähnliche Struktur auf. Das heißt, dass keine exakte Toeplitz-Struktur vorliegt, sondern geringfügige Abweichungen zwi-
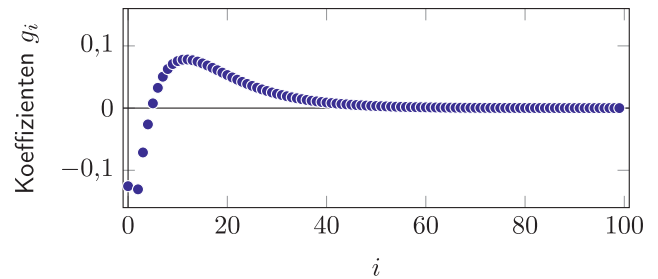

Abbildung 1: Impulsantwort des Beispielsystems.
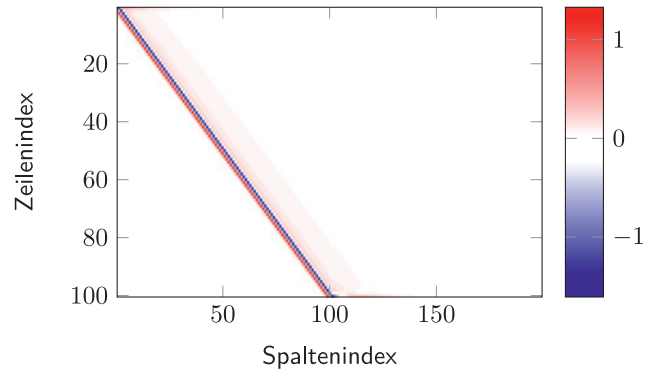
Abbildung 2: Entfaltungsmatrix $\mathbf{F}$.

schen den Einträgen zweier Spalten möglich sind. Außerdem klingen die Einträge der Spalten in diesem Bereich ab, sodass beide Bedingungen für eine Transformation auf einen FIR-Filter erfüllt sind. Im Gegensatz zur Faltungsmatrix $\mathbf{G}$ besitzt die Matrix $\mathbf{F}$ auch Einträge oberhalb der Diagonale. Diese sorgen dafür, dass zukünftige Werte der Wunschtrajektorie $\mathbf{y}_w$ bereits die jetzige Stellgröße beeinflussen. Werden die Spalten der Matrix als Impulsantwort des angenäherten inversen Systems betrachtet, so ist diese nicht kausal. Zum Beispiel löst ein Impuls zum 60. Zeitschritt eine Impulsantwort aus, wie sie durch die Einträge der 60. Spalte von $\mathbf{F}$

$$\tilde{f}_{60}[n] = f_{-59}\delta[n + 59] + f_{-58}\delta[n + 58] + \cdots$$
$$+ f_{-1}\delta[n + 1] + f_0\delta[n] + f_1\delta[n - 1] + \cdots$$
$$+ f_{40}\delta[n - 40] \tag{12}$$

dargestellt wird. Wird der Zeitpunkt des Impulses als Nullpunkt definiert, ergibt sich der in Abbildung 3 dargestellte Verlauf. Die Faltung berechnet mit Hilfe dieser Impulsantwort den Stellgrößenverlauf $\mathbf{u}^*$ für eine beliebig lange Wunschtrajektorie $y_w[n]$:

$$u^*[n] = \sum_{i=-\infty}^{\infty} \tilde{f}_{60}[i]\, y_w[n - i] = \sum_{i=-59}^{40} \tilde{f}_{60}[i]\, y_w[n - i]. \tag{13}$$

Im Gegensatz zur Faltung in (2) gehen nun auf Grund der nichtkausalen Impulsantwort zukünftige Werte der

Abbildung 3: 60. Spalte der Matrix $\mathbf{F}$.

Wunschtrajektorie $y_w[i]$, $0 < i < 60$ in die Berechnung ein. Dies erzeugt das gewünschte vorausschauende Verhalten. Di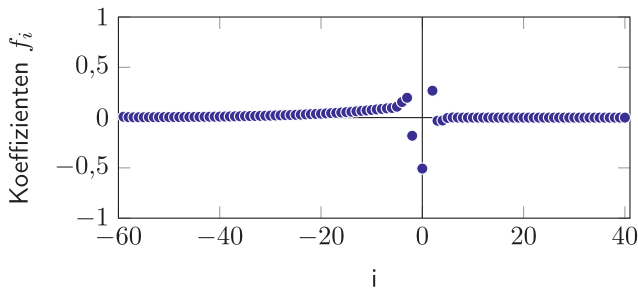e Wahl der Spalte beeinflusst dabei die benötigte Anzahl zukünftiger Werte der Wunschtrajektorie. Im Beispiel haben wir die 60. Spalte gewählt, weshalb die Faltung 59 zukünftige Werte von $y_w[n]$ benötigt.

Ganz allgemein führt die p-te Spalte zu einer Vorausschau von $p - 1$ Werten. Da die Faltung in (13) mit Hilfe einer endlich langen Impulsantwort $\tilde{f}_p$ berechnet wird, lässt sich dies in ein FIR-Filter transformieren:

$$F_z(z) = f_{-p+1}z^{p-1} + \cdots + f_{-1}z$$
$$+ f_0 + f_1 z^{-1} + \cdots + f_{M-p+1}z^{-(M-p+1)}. \quad (14)$$

Damit ist eine allgemeine Formulierung für das optimale vorausschauende FIR-Filter gefunden. Die Matrix $\mathbf{F}$ hat immer die in Abbildung 2 gezeigte Struktur, sofern der Stellhorizont M ausreichend groß ist und die Gewichtungsmatrizen der Form $k\mathbf{I}$ mit $\mathbb{R} \ni k > 0$ sind (siehe [15])[1]. Der Entwurf der optimalen vorausschauenden Vorsteuerung lässt sich daher in drei Schritte zusammenfassen:

1. Aufstellen der Matrix $\mathbf{G}$ und des Gütemaßes J.
2. Berechnen der Entfaltungsmatrix $\mathbf{F}$ und überprüfen der Struktur. Liegt im mittleren Bereich der Matrix keine Toeplitz-ähnliche Struktur vor, so ist M solange zu erhöhen, bis dies der Fall ist.
3. Die Spalte p von $\mathbf{F}$ muss gemäß der vorhandenen Anzahl an bekannten zukünftigen Werten der Wunschtrajektorie $y_w[n]$ gewählt werden. Die Einträge dieser Spalte stellen die Filterkoeffizienten für das FIR-Filter (14) dar.

---

1 Die Gewichtungsmatrizen gewichten den zeitlichen Verlauf einer Größe, sodass durch deren Diagonalform die Wechselwirkung zwischen zwei verschiedenen Zeitschritten nicht berücksichtigt wird. Außerdem werden durch die Form $k\mathbf{I}$ alle Zeitschritte mit dem gleichen Faktor gewichtet. Da solch eine Gewichtung für viele Problemstellungen ausreichend ist, ist die geforderte Form keine große Einschränkung.

2.2 Optimale vorausschauende Störgrößenaufschaltung

Eine SGA versucht den Einfluss einer gemessenen oder geschätzten Störgröße $z[n]$ auf den Ausgang zu kompensieren. Eine Form der SGA für lineare Systeme ist die „dynamische Störgrößenaufschaltung" (vgl. [7]). Abbildung 4 zeigt das zugehörige Blockschaltbild. Über die Störübertragungsfunktion $G_{zy}(z)$ wird die Wirkung der Störung auf den Ausgang berechnet und der Vorsteuerung negiert als Sollgröße vorgegeben. Die Vorsteuerung besteht im klassischen Fall aus der invertierten Systemdynamik G_{uy}^{-1}, weshalb diese nicht für nichtminimalphasige Systeme geeignet ist. Die Wirkung der so berechneten Stellgröße und die Wirkung der Störung löschen sich im Ausgang aus, sodass dieser von der Störung unbeeinflusst bleibt.

Die optimale vorausschauende SGA folgt dem selben Prinzip. Einziger Unterschied ist die Vorsteuerung. Diese wird durch die in Abschnitt 2.1 vorgestellte vorausschauende Vorsteuerung ersetzt. Essenziell ist, dass ein Teil der zukünftigen Störung bekannt sein muss, um die benötigte zukünftige Solltrajektorie $y_w[n]$ berechnen zu können. Der Vorteil der vorausschauenden SGA liegt im Ausnutzen des Wissens über die zukünftige Störung. So kann bereits auf die Störung reagiert werden, bevor diese tatsächlich auf das System wirkt. Dies wirkt sich nicht nur bei nichtminimalphasigen Systemen positiv aus, da durch das proaktive Handeln der Stellaufwand zur Unterdrückung der Störung verringert wird.

2.3 Alternative Ansätze für vorausschauende Steuerungen

Der hier gezeigte Ansatz zum Entwurf einer optimalen vorausschauenden Steuerung hat einige Parallelen zu bereits bekannten Methoden. Die Schritte zur Herleitung der Entfaltungsmatrix $\mathbf{F}$ entsprechen dem Vorgehen bei Dynamic Matrix Control (DMC) [1]. Bei dieser frühen Variante der MPC wird die erste Zeile der Matrix $\mathbf{F}$ genutzt, um
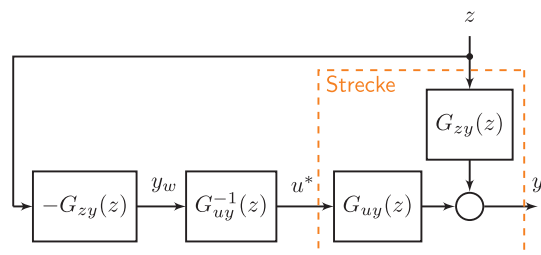

Abbildung 4: Dynamische Störgrößenaufschaltung.

die aktuelle Stellgröße zu berechnen. Da so jedoch keine Vergangenheitswerte der Wunschtrajektorie einfließen, muss der aktuelle Ausgangswert zurückgeführt werden, wodurch eine Regelung entsteht. Würde der aktuelle Ausgangswert z. B. über ein Parallelmodell geschätzt werden, so könnte auch über DMC eine vorausschauende optimale Steuerung entworfen werden. Im Vergleich zum per Definition stabilen FIR-Filter kann aber diese Variante der Vorsteuerung instabil werden.

Ebenso lässt sich zeigen, dass mit Methoden der linearen MPC für asymptotisch stabile SISO-Systeme ohne Eingangs- oder Zustandsbeschränkungen eine Vorsteuerung entworfen werden kann, welche auf ein Infinite Impulse Response (IIR) Filter führt. Hierzu wird ein MPC-Regler berechnet, der auf das Nominalmodell angewandt wird. Zur Steuerung der realen Strecke wird dann die Stellgröße für das Nominalmodell verwendet, weshalb keine Rückführung notwendig ist.

Ein zweiter Ansatz, der ebenfalls zu vorausschauenden Vorsteuerungen führt, ist der der nichtkausalen Inversion nichtminimalphasiger Systeme. Eine frühe Arbeit dazu für lineare Systeme stammt aus dem Jahr 1996 von Hunt et al. [3]. Devasia et al. führten im selben Jahr die nichtkausale Inversion für nichtlineare Systeme ein [2]. Beide Arbeiten zeigen für kontinuierliche Systeme, wie unter Berücksichtigung zukünftiger Werte der Wunschtrajektorie, eine stabile Systeminverse als Vorsteuerung gefunden werden kann. Jedoch ist es nicht möglich, die Amplitude der Stellgröße im Entwurf zu berücksichtigen. Dies ändert sich mit den Arbeiten von Zou [18] [17]. In diesen leitet er eine optimale nichtkausale Systeminverse für kontinuierliche lineare Systeme her. Für diskrete lineare Systeme entwerfen Marro et al. in [10] [9] ein FIR-Filter, das die Funktion einer nichtkausalen Systeminversen erfüllt. In seinem Ansatz findet jedoch im Gegensatz zu dem hier gezeigtem Vorgehen *keine* Optimierung statt.

Zuletzt stellt Wagner in seiner Arbeit [16] verschiedene Möglichkeiten zum Erstellen von FIR-Filtern als Vorsteuerungen vor. Zwar wird eine Optimierung dieser durchgeführt, jedoch ohne die Berücksichtigung der Stellgröße. Die so entworfenen FIR-Filter bleiben kausal und weisen kein vorausschauendes Verhalten auf. Wagner erwähnt jedoch in seiner Arbeit auch, dass eine Gewichtung der Stellgröße im Gütemaß zu einer Entfaltungsmatrix führt, welche zukünftige Informationen über die Wunschtrajektorie benötigt. Den Übergang von der Entfaltungsmatrix zu einem FIR-Filter vollzieht er jedoch nicht.

3 Anwendung zur Schwingungsdämpfung am Viertelfahrzeug

Der folgende Abschnitt zeigt die Anwendung der SGA auf das Problem der Schwingungsdämpfung am Viertelfahrzeug. Hierzu erläutern wir zunächst den Zielkonflikt zwischen Fahrkomfort und Fahrsicherheit und stellen den lehrstuhleigenen Viertelfahrzeugprüfstand vor, bevor verschiedene Modellierungsvarianten des Viertelfahrzeugs aufgezeigt werden. Basierend auf einem linearen Modell, führen wir daraufhin den SGA Entwurf durch und präsentieren anschließend die Ergebnisse aus Simulationen und Versuch.

3.1 Zielkonflikt

Ein passives Pkw-Fahrwerk besteht aus der Radaufhängung, einem Dämpfer und einer Feder. Es verbindet den Fahrzeugaufbau mit dem Rad. Über Feder und Dämpfer soll möglichst wenig der von der Straße auf das Rad übertragenen vertikalen Störanregung auf den Fahrzeugaufbau übertragen werden. Das gewünschte Fahrverhalten bezüglich der Vertikaldynamik wird über die Parametrierung der Federsteifigkeit und der Dämpfungskonstante eingestellt. Für ein möglichst komfortables Verhalten, wie z. B. in einem Rolls-Royce, sind sowohl Feder als auch Dämpfer weich auszuführen. Dies führt dazu, dass das Rad leicht einfedern kann und somit nur geringe Kräfte z. B. beim Überfahren einer Bodenwelle auf den Fahrzeugaufbau wirken. Gleichzeitig tendiert dadurch das Rad dazu, bei Störanregungen von der Straße abzuheben. Dies reduziert die Normalkraft des Reifens auf die Straße, wodurch die übertragbaren Antriebs-, Brems- und Querkräfte verringert werden: Die Fahrsicherheit nimmt ab. Umgekehrt führt eine harte Auslegung des Fahrwerks, wie z. B. in einem Sportwagen, zu einer hohen Fahrsicherheit, da das Rad besseren Kontakt zum Boden hat. Durch die harte Feder- und Dämpfereinstellung wird die Straßenanregung jedoch stärker auf den Fahrzeugaufbau übertragen, wodurch der Komfort sinkt. Ein Auflösen dieses Zielkonfliktes ist nur durch das Einbringen von aktiven Komponenten in die Radaufhängung möglich [12].

Zur Quantifizierung der Fahrsicherheit wird die dynamische Radlast F_{dyn} betrachtet. Diese stellt den Anteil der Normalkraft des Rades dar, der zusätzlich zur durch die Erdbeschleunigung entstehenden statischen Kraft F_{stat} wirkt. Um deren zeitlichen Verlauf auf eine skalare Größe abzubilden, wird das quadratische Mittel (Root Mean
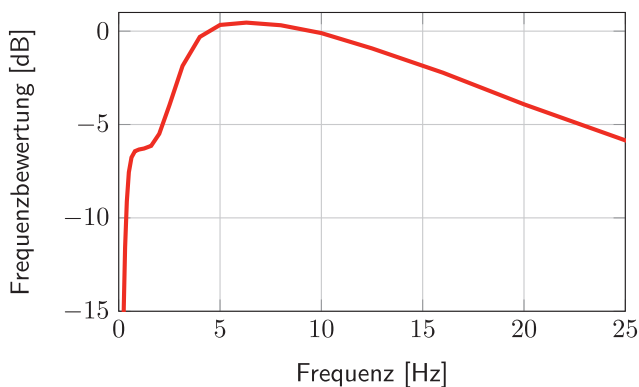
Abbildung 5: Frequenzgewichtung nach [4].

Abbildung 6: Viertelfahrzeugprüfstand.

Square (RMS)) $|F_{dyn}|_{RMS}$ genutzt. Je geringer dieses ist, desto gleichmäßiger wird der Reifen mit F_{stat} gegen die Fahrbahn gedrückt und desto höher ist die Fahrsicherheit. Zur Bemessung des Komforts verwenden wir den RMS-Wert der Aufbaubeschleunigung $|\ddot{z}_c|_{RMS}$. Auch hier gilt: Je geringer dieser ist, desto höher ist der Komfort. Um das subjektive Komfortempfinden besser beschreiben zu können, wird außerdem der RMS-Wert der frequenzgewichteten Aufbaubeschleunigung $|\ddot{z}_{c,comf}|_{RMS}$ betrachtet. Diese berechnet sich durch Filterung der Aufbaubeschleunigung mit einem Filter nach [4], welcher besonders die Frequenzen von 4–8 Hz (siehe Abbildung 5), in denen die Eigenfrequenzen der inneren Organe des Menschen liegen, betont.

Die Bewertung der Performance geschieht über das Kriterium

$$\Gamma(|\cdot|) = 1 - \frac{|\cdot|_{aktiv}}{|\cdot|_{passiv}}. \tag{15}$$

Dieses setzt den RMS-Wert einer Zielgröße eines aktiven, geregelten oder gesteuerten Fahrwerks in Bezug zu dem RMS-Wert des nicht aktuierten, passiven Fahrwerks bei gleicher Straßenanregung. Ein positiver Wert bedeutet dabei eine Verbesserung der Zielgröße, ein negativer Wert eine Verschlechterung.

3.2 Viertelfahrzeugprüfstand

Abbildung 6 zeigt den Viertelfahrzeugprüfstand, bestehend aus einem Rad, einer Aufhängung, einem Federbein und einem Viertel der Aufbaumasse (rot lackiert). Das Rad und die Doppelquerlenker-Aufhängung stammen aus einem 7er BMW (Modell Jahr 2009). Das Federbein beinhaltet eine hybride Aktuatorkonfiguration: Zum einen wurde ein kontinuierlich verstellbarer Dämpfer, ebenfalls aus einem 7er BMW, und zum anderen eine langsam aktive Federfußpunktverstellung aus dem Active Body Control-System (ABC) eines Mercedes SL Roadster verbaut. Durch die Kombination des schnellen Dämpfers (Bandbreite $\approx$ 16 Hz), der nur Energie dissipieren kann, und der langsamen (Bandbreite $\approx$ 5 Hz), aber aktiven Federfußpunktverstellung, lässt sich mit geringem Energieaufwand eine Performance ähnlich eines vollaktiven Fahrwerks (siehe Abschnitt 3.3) erreichen (vgl. [5]). Die Straßenanregung wird durch einen Hydraulikzylinder unterhalb des Rades umgesetzt.

3.3 Modellierung

Dieser Abschnitt stellt drei Modelle des Viertelfahrzeugs vor. Zunächst benötigt die in Abschnitt 2.1 vorgestellte Entwurfsmethode die Impulsantwort eines linearen SISO-Systems. Deshalb verwenden wir zur Auslegung das in Abbildung 7a gezeigte, vollaktive lineare Viertelfahrzeugmodell. Das Federbein zwischen der Aufbaumasse m_c und der Radmasse m_w ist als lineare Feder mit Steifigkeit c_c und linearer Dämpfer mit Dämpfung d_c modelliert. Der Reifen wird durch das Gehmannmodell dargestellt [12]. Bei diesem wird parallel zur Reifensteifigkeit c_w ein Dämpfer d_w mit einer weiteren Feder c_g in Serienschaltung angenommen. Die Koordinate z_h beschreibt die Position des Verbindungspunktes dieser beiden Elemente. Stelleingang u sei eine beliebig große, beliebig schnelle, ideal umgesetzte Kraft $F(t)$ zwischen der Aufbau- und Radmasse. Als Ausgang y kommen entweder die Aufbaubeschleunigung $\ddot{z}_c$ oder die dynamische Radlast F_{dyn} in Frage. Bei einem Entwurf der SGA mit ersterer als Ausgang ($y_1 = \ddot{z}_c$) wird die Vertikaldynamik bezüglich Fahrkomfort optimiert. Wird die dynamische Radlast als Ausgang gewählt ($y_2 = F_{dyn}$), so wird über die SGA die Fahrsicherheit maximiert.
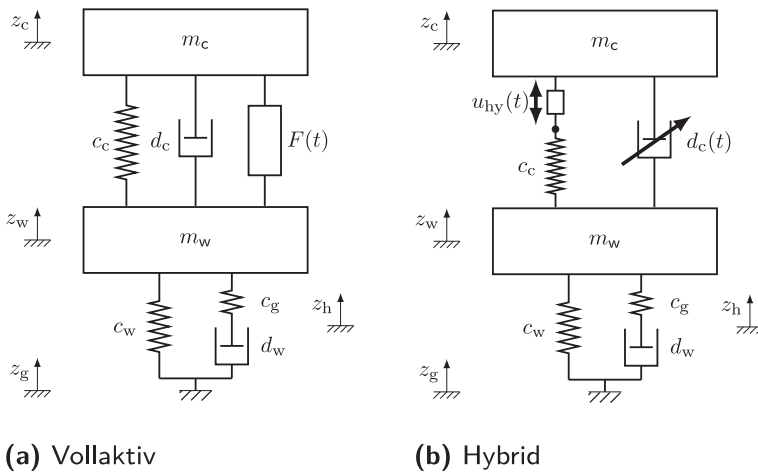
(a) Vollaktiv **(b)** Hybrid

Abbildung 7: Viertelfahrzeugmodelle.

Beide Ausgänge gleichzeitig zu betrachten ist auf Grund des vorausgesetzten SISO-Systems nicht möglich. Als Störung wirkt die Straßenanregungsgeschwindigkeit $\dot{z}_g$ auf das System. Über Impulsbilanzen an den beiden Massen erhalten wir das Zustandsraummodell:

$$\dot{\mathbf{x}} = \mathbf{A}\mathbf{x} + \mathbf{B}u + \mathbf{E}\dot{z}_g, \text{ wobei} \tag{16}$$

$$\mathbf{x} = \begin{bmatrix} z_c - z_w & \dot{z}_c & z_w - z_g & \dot{z}_w & z_h - z_g \end{bmatrix}^T \tag{17}$$

$$\mathbf{A} = \begin{bmatrix} 0 & 1 & 0 & -1 & 0 \\ -\frac{c_c}{m_c} & -\frac{d_c}{m_c} & 0 & \frac{d_c}{m_c} & 0 \\ 0 & 0 & 0 & 1 & 0 \\ \frac{c_c}{m_w} & \frac{d_c}{m_w} & \frac{-c_w-c_g}{m_w} & \frac{-d_c}{m_w} & \frac{c_g}{m_w} \\ 0 & 0 & \frac{c_g}{d_w} & 0 & -\frac{c_g}{d_w} \end{bmatrix} \tag{18}$$

$$\mathbf{B} = \begin{bmatrix} 0 & \frac{1}{m_c} & 0 & -\frac{1}{m_w} & 0 \end{bmatrix}^T \tag{19}$$

$$\mathbf{E} = \begin{bmatrix} 0 & 0 & -1 & 0 & 0 \end{bmatrix}^T \tag{20}$$

$$y_1 = \begin{bmatrix} -\frac{c_c}{m_c} & -\frac{d_c}{m_c} & 0 & \frac{d_c}{m_c} & 0 \end{bmatrix} \mathbf{x} + \frac{1}{m_c}u \tag{21}$$

$$y_2 = \begin{bmatrix} 0 & 0 & -c_w - c_g & 0 & c_g \end{bmatrix} \mathbf{x}. \tag{22}$$

Die Werte für die Parameter sind Tabelle 1 zu entnehmen. Dieses Modell wird neben der Berechnung der Impulsantwort für den Steuerungsentwurf auch noch zur Bestimmung des Übertragungsverhaltens G_{zy} vom Störeingang $\dot{z}_g$ auf den Ausgang $y_{1/2}$, welches für die SGA benötigt wird, genutzt.

Für die simulativen Studien zur Performance der SGA werden zwei weitere Modelle des Viertelfahrzeugs genutzt. Das zweite Modell hat eine Aktuatorkonfiguration wie das soeben vorgestellte lineare Entwurfsmodell (vollaktives Modell, idealer Aktor). Jedoch berücksichtigen wir für dieses die nichtlinearen Kennlinien des Dämpfers, der Aufbau- und der Radsteifigkeit. Außerdem wird das Abheben des Rades von der Straße modelliert. Weiterhin ge-

Tabelle 1: Parameter des linearen Viertelfahrzeugmodells.

Bezeichnung	Parameter	Wert
Aufbaumasse	m_c	507 kg
Radmasse	m_w	68 kg
Aufbausteifigkeit	c_c	24 000 N/m
Aufbaudämpfung	d_c	1400 Ns/m
Radsteifigkeit	c_w	378 000 N/m
Raddämpfung	d_w	130 Ns/m
Gehmannsteifigkeit	c_g	52 900 N/m

hen eine Coulomb-Reibung im Dämpfer und die dynamische Übersetzungsänderung ein [11]. Letztere wird durch das geneigte Federbein bedingt. Beim Ein- und Ausfedern tritt eine Winkeländerung des Federbeins auf, wodurch eine konstante Geschwindigkeit oder Kraft im Federbein zu einer veränderlichen Geschwindigkeit bzw. Kraft in vertikaler Richtung führen. Dieses Modell wird für die Untersuchung der Einflussfaktoren der SGA genutzt, da zum einen die nichtlineare Dynamik des Viertelfahrzeugs sehr genau abgebildet wird und zum anderen von einem idealen Aktor ausgegangen wird. So können wir bei den durchgeführten Studien den Einfluss verschiedener Parameter betrachten, ohne dass das reale Aktuatorverhalten das Ergebnis verfälscht.

Das in Abbildung 7b gezeigte dritte Modell berücksichtigt die selben Nichtlinearitäten wie das zweite, jedoch entspricht die Aktuatorkonfiguration der hybriden Anordnung des Prüfstands (vgl. Abschnitt 3.2). Zusätzlich wird die Aktuatordynamik der Federfußpunktverstellung einbezogen. Da die SGA nur eine umzusetzende Kraft zwischen Fahrzeugaufbau und Rad berechnet, muss für die Simulation mit diesem Modell und die Versuche am Prüfstand eine Stellgrößenverteilung eingesetzt werden. Die-

se teilt die ideale Kraft auf die beiden realen Stellgrößen Auslenkung der Federfußpunktverstellung u_{h_y} und Dämpfung d_c unter Berücksichtigung der Bandbreitenbeschränkung der Federfußpunktverstellung auf. Dabei wird versucht, möglichst viel der geforderten Kraft über die Federfußpunktverstellung zu realisieren und den Anteil, den diese nicht umsetzen kann, über den Verstelldämpfer zu stellen [14].

3.4 Entwurf der vorausschauenden SGA

Das Anwenden der vorausschauenden SGA setzt voraus, dass die zukünftige Störung, zumindest teilweise, bekannt ist. Eine Möglichkeit zum Erfassen der Störung am Fahrzeug ist ein Sensor, der an der Stoßstange vor dem Rad montiert ist. Dieser erfasst die Unebenheiten der Straße, bevor diese über den Reifen auf das System Viertelfahrzeug wirken. Wir nehmen für die folgenden Betrachtungen an, dass die Straßenanregungshöhe z_g für eine gewisse Strecke vor dem Fahrzeug exakt bekannt sei. So können wir auf Basis des vollaktiven linearen Viertelfahrzeugmodells die vorausschauende SGA entwerfen. Dazu wird das kontinuierliche LZI-System (16) mit Ausgang (21) oder (22) mit der Abtastzeit 3 ms diskretisiert und jeweils für y_1 und y_2 die Impulsantwort bestimmt. Mit diesen berechnen wir gemäß Abschnitt 2 für beide Ausgänge je eine SGA. Beim Entwurf müssen die folgenden Parameter festgelegt werden:

- die Gewichtungsmatrizen im Gütemaß (7),
- die Länge des Stellhorizontes M,
- die Spalte der Matrix $\mathbf{F}$, deren Einträge als Koeffizienten für das optimale vorausschauende FIR-Filter dienen.

Der Einfluss dieser Parameter auf die Performance bezüglich Fahrkomfort und Fahrsicherheit soll nun analysiert werden. Dazu wird als Straßenanregung ein berechnetes Profil einer Landstraße genutzt, über die mit 80 km/h gefahren wird. Die Gewichtungsmatrizen im Gütemaß J_1 für die SGA für y_1 und in J_2 für die SGA für y_2 wurden empirisch bestimmt zu:

$$J_1: \quad \mathbf{Q}_1 = 10^6\mathbf{I} \quad \mathbf{R}_1 = 0{,}05\mathbf{I} \quad \tilde{\mathbf{R}}_1 = 200\mathbf{I}, \quad (23)$$

$$J_2: \quad \mathbf{Q}_2 = \mathbf{I} \quad\quad \mathbf{R}_2 = 0{,}18\mathbf{I} \quad \tilde{\mathbf{R}}_2 = 90\mathbf{I}. \quad (24)$$

Weiterhin wird zunächst angenommen, dass die Störung beliebig weit im Vorhinein bekannt ist, sodass wir die Spalte p beliebig wählen können. Im ersten Schritt variieren wir die Länge des Stellhorizontes, womit sich auch die Größe der Matrizen $\mathbf{G}$ und $\mathbf{F}$ ändert. Als FIR-Filter Koeffizienten werden immer die Einträge der $(M + 1)/2$-ten
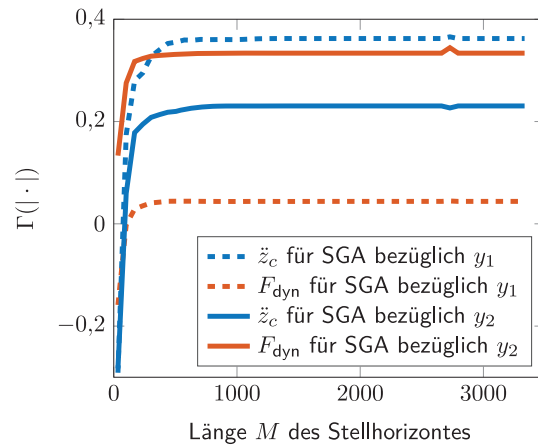

Abbildung 8: Analyse des Einflusses der Länge des Stellhorizontes.

Spalte (bei geradem M aufgerundet) verwendet. Die Simulationen führen wir mit dem vollaktiven, nichtlinearen Modell durch. Abbildung 8 zeigt die Performance bezüglich Fahrsicherheit und Fahrkomfort über die Länge des Stellhorizontes M aufgetragen. Die gestrichelten Verläufe stellen das Bewertungskriterium Γ für die SGA entworfen für den Ausgang Aufbaubeschleunigung dar, die durchgezogenen für die SGA für den Ausgang dynamische Radlast. Gut erkennbar ist, dass die Performance hinsichtlich des Ziels, für das die SGA entworfen wurde, besser ist, als für das jeweilige konfliktäre Ziel. Abbildung 8 verdeutlicht außerdem, dass die Performance mit größerer Länge M zunimmt und gegen eine obere Schranke konvergiert. Das schlechte Verhalten für sehr kurze Stellhorizonte kann mit der geringen Größe der Matrix $\mathbf{F}$ erklärt werden. Diese weist noch keine Toeplitz-ähnliche Struktur auf, weshalb die Implementierung als FIR-Filter unzulässig ist. Das Konvergenzverhalten lässt sich ebenfalls über die Struktur der Entfaltungsmatrix erklären. Ist der Stellhorizont ausreichend lang gewählt, so tritt die gewünschte Toeplitz-ähnliche Struktur auf. Wird M daraufhin vergrößert, ändert dies nichts an der Information, die in den Spalten enthalten ist. Die mittleren Einträge der Spalte bleiben identisch und lediglich am Anfang beziehungsweise am Ende entstehen neue Einträge die ungefähr gleich Null sind.

Die Peaks in den Verläufen bei einer Länge von $M = 2700$ sind auf die Wahl der Spalte für die FIR-Filterkoeffizienten zurückzuführen. Bei feinerer Rasterung von M lässt sich zeigen, dass die Verläufe mehrere dieser Maxima aufweisen. Weiterführende Analysen haben gezeigt, dass die $(M + 1)/2$-te Spalte nicht immer die beste Performance liefert. Teilweise kann durch die Wahl einer Spalte etwas neben der $(M + 1)/2$-ten Spalte eine geringfügig bessere Performance bezüglich des Auslegungsziels erreicht werden.
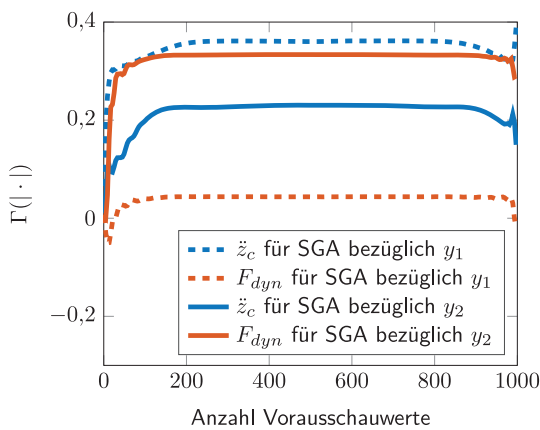
Abbildung 9: Analyse des Einflusses der Anzahl der Vorausschauwerte.

Abbildung 10: Paretofronten für das vollaktive und hybride Modell.

Für die weiteren Untersuchungen wird als Kompromiss zwischen benötigter Rechenleistung und erzielbarem Performancegewinn eine Länge des Stellhorizontes von $M = 1000$ gewählt.

Im zweiten Schritt analysieren wir die Vorausschaulänge. Es wurde hierfür eine SGA mit den gleichen Parametern wie zuvor entworfen. Einziger Unterschied ist, dass $M = 1000$ und die Spalte p für die FIR-Filterkoeffizienten variabel gewählt werden. Abbildung 9 zeigt die Ergebnisse der Simulation mit dem nichtlinearen, vollaktiven Modell. Die besten Ergebnisse werden für 200 bis 800 Vorausschauwerte erzielt. Dies entspricht den Spalten in der Matrix **F**, für die die Toeplitz-ähnliche Struktur am ausgeprägtesten ist und somit die Darstellung als FIR-Filter den geringsten Fehler hat.

Wird eine Spalte am Anfang der Matrix gewählt, was einer sehr geringen Anzahl an Vorausschauwerten entspricht, so ist die Performance zum einen wegen der mangelnden Toeplitz-ähnlichen Struktur zum anderen wegen der ungenügend langen Vorausschau schlechter. Ein ähnliches Verhalten zeigt sich bei sehr vielen Vorausschauwerten. Neben der schlechter ausgeprägten Toeplitz-ähnlichen Struktur ist die zu geringe Anzahl an berücksichtigten Vergangenheitswerten der Wunschtrajektorie Ursache für das schlechte Verhalten.

Zuletzt untersuchen wir den Einfluss der Gewichtungsmatrizen auf die Performance der SGA. Hierzu wählen wir die Gewichtung **Q** des Fehlers konstant und die der Stellgröße **R** und der Stellgrößenänderung **R̃** variabel. Als Straßenprofil dient wiederum das synthetische Profil einer Landstraße ($v = 80$ km/h) und die Länge des Stellhorizontes ist $M = 1000$. Die Anzahl der Vorausschauwerte wird auf $p = 500$ gesetzt, sodass gemäß Abbildung 9 eine bestmögliche Performance zu erwarten ist. Abbildung 10 zeigt in einem Konfliktdiagramm die Paretofronten der Simula-
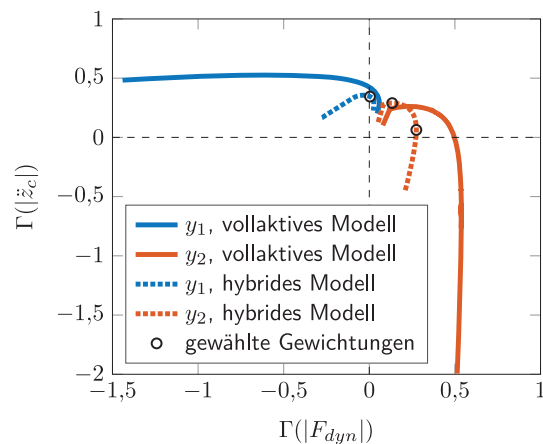
tionen mit dem vollaktiven und dem hybriden Modell, jeweils für die SGA für y_1 und y_2. Auf der Abszisse ist das Performancekriterium bezüglich der Fahrsicherheit und auf der Ordinate bezüglich des Fahrkomforts dargestellt. Ziel ist es, eine Gewichtung zu finden, bei der hinsichtlich beider Ziele eine Verbesserung ($\Gamma > 0$) erreicht wird.

Aus den Paretofronten geht hervor, dass bei idealer Kraftumsetzung eine Verbesserung von über 50% in beiden Zielen möglich ist. Jedoch nimmt bei diesen großen Verbesserungen die Performance des jeweiligen anderen Ziels, gemäß dem Zielkonflikt, deutlich ab. Ist die SGA damit noch sinnvoll einsetzbar? Ja, in einem Bereich, in dem die Verbesserung eines einzelnen Ziels nicht maximal ist und dadurch auch eine Verbesserung des entgegengesetzten Ziels möglich wird.

Bei Simulationen mit dem hybriden Modell stellt sich ein ähnliches Verhalten ein. Durch die begrenzte Bandbreite der Federfußpunktverstellung und den rein dissipierenden Dämpfer ist jedoch die maximal erreichbare Verbesserung halbiert worden. Anhand dieser Paretofronten wurden eine komfortoptimale, eine radlastoptimale und eine kompromissorientierte Gewichtung ausgewählt und damit weitere Simulationen und Versuche am Prüfstand durchgeführt.

3.5 Ergebnisse

Im vorangegangenen Abschnitt wurden alle Parameter der optimalen vorausschauenden SGA bestimmt und eine komfortoptimale (FIR-SGA KO), eine radlastoptimale (FIR-SGA RO) und eine kompromissorientierte (FIR-SGA Kompromiss) SGA entworfen. Dieser Abschnitt stellt die Ergebnisse aus Simulationen und Versuchen am Viertelfahrzeugprüfstand vor. Das verwendete Straßenprofil ist das

einer schlechten, realen Landstraße, über die mit 50 km/h gefahren wird. Die Straßenanregung $\dot{z}_g$ nehmen wir als exakt bekannt an. Um die Simulationsergebnisse besser mit denen aus dem Versuch vergleichen zu können, verwenden wir das hybride Viertelfahrzeugmodell. Analysiert wird das Performancekriterium Γ hinsichtlich dynamischer Radlast F_{dyn}, Aufbaubeschleunigung $\ddot{z}_c$, frequenzgewichteter Aufbaubeschleunigung $\ddot{z}_{c,comf}$, Einfederung z_{cw} und minimaler Einfederung $\min(z_{cw})$. Dargestellt wird dies in Spinnennetzdiagrammen, bei denen die 0% Linie die Performance des passiven Fahrwerks darstellt. Zum Vergleich ziehen wir zum einen den in der Industrie weit verbreiteten Skyhook-Regler (d_{sky} = 2000 Ns/m) (vgl. [6]) und zum anderen einen komfortorientiert ausgelegten LQR nach [13] heran.

Zunächst wird der Fall einer unbegrenzt langen Vorausschau angenommen, sodass wir erneut die Einträge der Spalte p = 500 der Matrix **F** als FIR-Filterkoeffizienten nutzen können. In die SGA gehen daher 499 zukünftige Werte der Störung $\dot{z}_g$ ein. Bei einer Abtastzeit von T_s = 3 ms und einer Fahrgeschwindigkeit von 50 km/h bedeutet dies, dass die Straßenanregung mindestens 20,8 m vor dem Rad bekannt sein muss. Abbildung 11 zeigt das Spinnennetzdiagramm für die Simulation. Die Performancewerte der Vergleichsregler sind gestrichelt dargestellt und die der drei SGAs durchgezogen. Es fällt auf, dass die
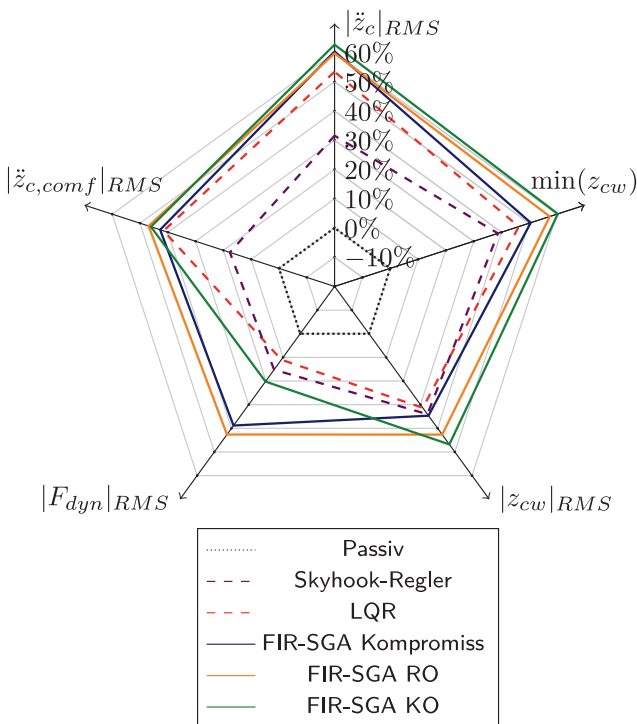
SGAs in allen Kriterien ein besseres Verhalten aufweisen als die Benchmarkregler. Bezüglich der Aufbaubeschleunigung $\ddot{z}_c$ und der dynamischen Radlast F_{dyn} entspricht die Performanceverbesserung den gewählten Gütemaßen der SGAs. Neben einer Komfort- und Fahrsicherheitsverbesserung kann außerdem eine Verringerung des benötigten Federweges festgestellt werden.

Abbildung 12 stellt die Versuchsergebnisse für die selben SGAs und Regler dar. Die Performance der SGAs ist weiterhin besser als die des LQR. Durch Modellungenauigkeiten entsteht jedoch eine um 10% geringere Performanceverbesserung bezüglich Komfort und Einfederung und die Verbesserung der dynamischen Radlast geht um etwa 30% zurück. Dies ist zum einen mit der nicht berücksichtigten Dämpferdynamik zu erklären und zum anderen mit dem schwer zu modellierenden Reifenverhalten. Insgesamt ist der mit der SGA erreichte Performancegewinn von 50% im Fahrkomfort bei gleichzeitiger Verbesserung von über 10% in der Fahrsicherheit erheblich.

Bisher ist von einer Vorausschau von über 20 Metern vor dem Rad ausgegangen worden. Dies lässt sich mit heutigen Mitteln nur schwer realisieren. Wird von dem in Abschnitt 3.4 beschriebenen Abstandssensor in der Stoßstange ausgegangen, verkürzt sich die vorhandene Vorausschau auf einen Meter. Im Folgenden werden die Ergebnisse für diese reale Vorausschau betrachtet.

Abbildung 13 zeigt die Performanceverbesserung aus der Simulation. Bei kurzer Vorausschau verliert die SGA je nach Ausprägung unterschiedlich an Performance. Die komfortorientierte SGA muss die größten Einbußen hinnehmen. Dies ist mit der kurzen Vorausschau zu erklären. Damit die für die Aufbaubeschleunigung kritischen
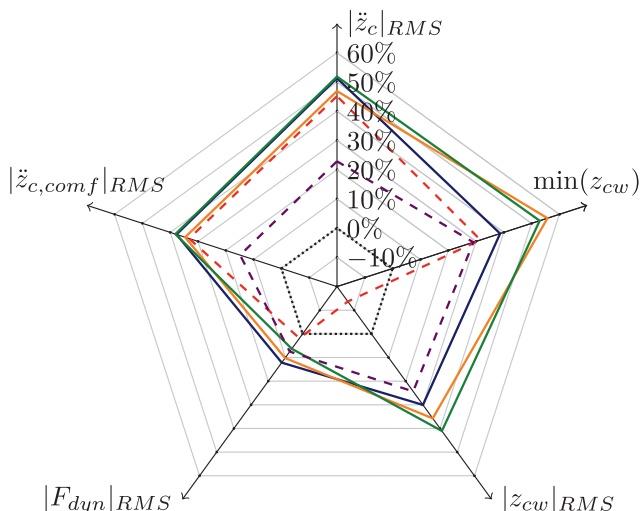

Abbildung 11: Spinnennetzdiagramm für die Simulation mit beliebiger Vorausschau.

Abbildung 12: Spinnennetzdiagramm für den Versuch mit beliebiger Vorausschau.

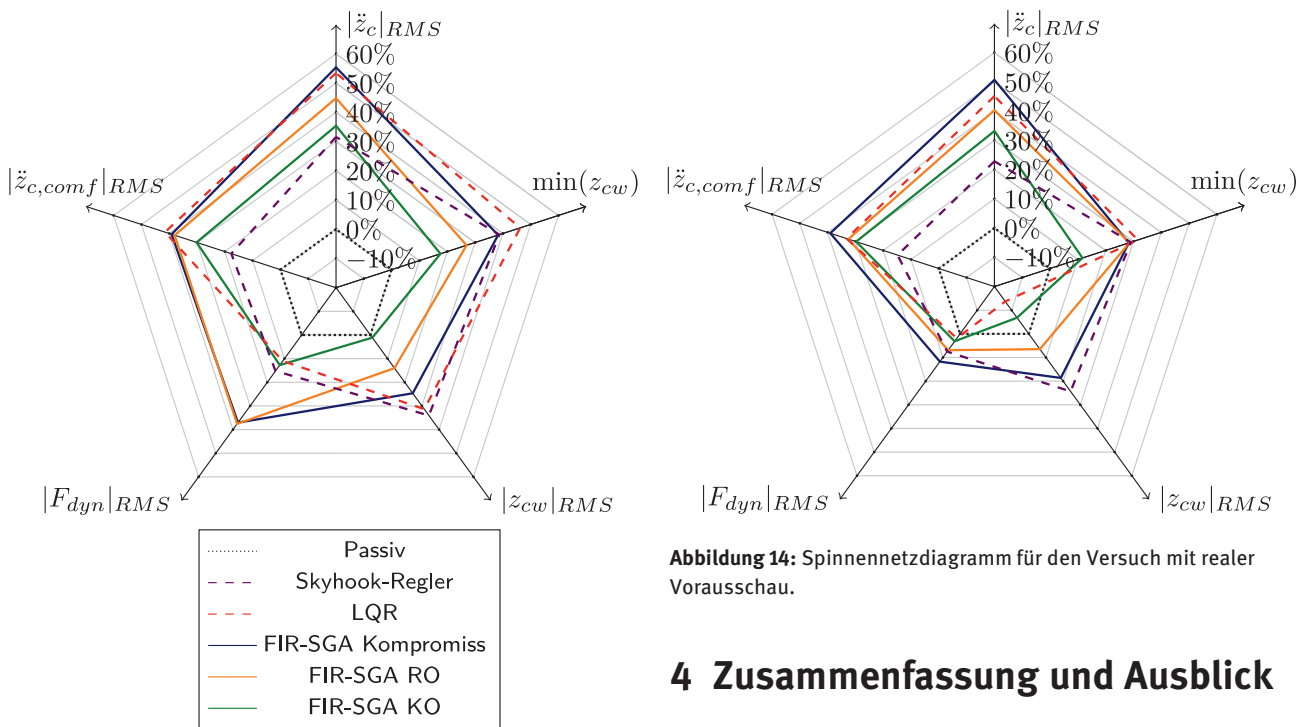**Abbildung 13:** Spinnennetzdiagramm für die Simulation mit realer Vorausschau.

Abbildung 14: Spinnennetzdiagramm für den Versuch mit realer Vorausschau.

Störungen im Bereich der Aufbaueigenfrequenz von 1 Hz durch die SGA effektiv kompensiert werden können, müssen diese ganz erfasst werden. Bei einer Fahrgeschwindigkeit von 50 km/h müsste daher eine Vorausschau von 13,9 m vorhanden sein, um Wellen dieser kritischen Frequenzen erfassen zu können.

Die radlastoptimale und die kompromissorientierte SGA wurden mit dem Auslegungsziel der Reduzierung der dynamischen Radlast entworfen. Deren Eigenfrequenz liegt bei ca. 12 Hz, sodass die verfügbare Vorausschau Störungen dieser Frequenz größtenteils erfassen kann. Durch das Bedämpfen dieser Frequenzen wird die Störung durch diese SGAs bereits kompensiert, bevor sie den Fahrzeugaufbau erreicht, wodurch sich auch der Komfort verbessert.

Abbildung 14 stellt die Ergebnisse zum dazugehörigen Versuch am Prüfstand dar. Auch hier können allgemeine Einbußen der Performance gegenüber der Simulation beobachtet werden. Jedoch fallen diese sehr unterschiedlich aus, sodass die kompromissorientierte SGA im Versuch einen deutlichen Vorteil gegenüber dem LQR aufweist. Es ist also auch bei einer geringen Vorausschau von nur einem Meter möglich, allein über das Wissen über die Störung $\dot{z}_g$ mit der hier gezeigten optimalen vorausschauenden SGA *ohne* jegliche Regelung eine Komfortverbesserung von 50% bei gleichzeitiger Verbesserung der dynamischen Radlast von über 10% zu erreichen.

4 Zusammenfassung und Ausblick

In diesem Beitrag haben wir eine neuartige Entwurfsmethode für eine optimale vorausschauende Vorsteuerung gezeigt. Außerdem haben wir ausgehend von dieser eine optimale vorausschauende Störgrößenaufschaltung entworfen. Diese wurde angewandt zur Schwingungsdämpfung am Viertelfahrzeug. Wir haben zusätzlich aufgezeigt, wie sich verschiedene Parameter auf die Performance der SGA bezüglich der Schwingungsdämpfung auswirken. Zuletzt konnten wir durch Simulationen und Versuche nachweisen, dass auch bei einer geringen Vorausschau allein auf Basis der hier eingeführten SGA eine deutliche Komfortverbesserung bei gleichzeitiger Verbesserung der Fahrsicherheit möglich ist.

Beim Entwurf der SGA wurden einige Annahmen gemacht, die bei der Anwendung im Vollfahrzeug so nicht haltbar sind. Zum einen wurde die Straßenanregung als exakt bekannt angenommen. Im Vollfahrzeug würde diese jedoch gemessen oder geschätzt werden und so fehlerbehaftet sein. Wie man die Straßenanregung z_g am besten schätzt und auch die Frage wie sich Fehler auf die Performance der SGA auswirken sind Gegenstand zukünftiger Forschung. Eine weitere Annahme war die konstante Fahrgeschwindigkeit. Im realen Fahrzeug wird diese in den wenigsten Fällen exakt konstant sein. Eine Änderung der Fahrgeschwindigkeit geht mit einer Änderung der Anzahl der Vorausschauwerte einher. Auch die Frage, wie die vorgestellte SGA anzupassen ist, um auf Systeme mit variabler Vorausschau angewendet werden zu können, wird in Zukunft untersucht werden. Bisher wurde die Performance der SGA ohne jegliche Regelung betrachtet. Wei-

tere Analysen sollen zeigen, inwieweit eine zusätzliche Regelung die Performance noch weiter verbessern kann. Außerdem wird momentan untersucht, ob sich die Methode auf Single-Input Multi-Output und Multi-Input Multi-Output Systeme übertragen lässt, sodass eine gleichzeitige Gewichtung von Aufbaubeschleunigung und dynamischer Radlast im Gütemaß möglich ist. Zuletzt ist geplant, den genauen Zusammenhang zwischen MPC und der hier gezeigten Vorsteuerung zu untersuchen und der Frage nachzugehen, ob beide Ansätze ineinander überführt werden können.

Literatur

1. C. R. Cutler and B. L. Ramaker. Dynamic matrix control – a computer control algorithm. *Joint Automatic Control Conference*, 17, 1980.
2. S. Devasia, D. Chen, and B. Paden. Nonlinear inversion-based output tracking. *IEEE Transactions on Automatic Control*, 41(7):930–942, 1996.
3. L. R. Hunt, G. Meyer, and R. Su. Noncausal inverses for linear systems. *IEEE Transactions on Automatic Control*, 41(4):608–611, 1996.
4. ISO 2631-1:1997: International Organization for Standardization. Mechanical vibration and shock – evaluation of human exposure to whole-body vibration, 1997-05.
5. G. Koch, O. Fritsch, and B. Lohmann. Potential of low bandwidth active suspension control with continuously variable damper. *Control Engineering Practice*, 18(11):1251–1262, 2010.
6. G. Koch, S. Spirk, E. Pellegrini, N. Pletschen, and B. Lohmann. Experimental validation of a new adaptive control approach for a hybrid suspension system. In *Proceedings of the 2011 American Control Conference*, pages 4580–4585, 2011.
7. G. Ludyk. *Theoretische Regelungstechnik 1: Grundlagen, Synthese linearer Regelungssysteme*. Springer-Lehrbuch. Springer, Berlin and Heidelberg, 1995.
8. J. M. Maciejowski. *Predictive control with constraints*. Prentice Hall, Harlow, 2002.
9. G. Marro, D. Prattichizzo, and E. Zattoni. Convolution profiles for noncausal inversion of multivariable discrete-time systems. In *Proceedings of the 8th IEEE Mediterranean Conference on Control & Automation (MED 2000)*, 2000.
10. G. Marro, D. Prattichizzo, and E. Zattoni. Convolution profiles for right inversion of multivariable non-minimum phase discrete-time systems. *Automatica*, 38(10):1695–1703, 2002.
11. W. Matschinsky. *Radführungen der Straßenfahrzeuge: Kinematik, Elasto-Kinematik und Konstruktion*. Springer-Verlag Berlin Heidelberg, 3., aktualisierte und erweiterte Auflage edition, 2007.
12. M. Mitschke and H. Wallentowitz. *Dynamik der Kraftfahrzeuge*. VDI-Buch. Springer Vieweg, Wiesbaden, 5., überarb. u. erg. Aufl. edition, 2014.
13. N. Pletschen. Nonlinear H2 control of a low-bandwidth active vehicle suspension system using Takagi-Sugeno methods. In *Proceedings of the 13th International Symposium on Advanced Vehicle Control (AVEC'16), Munich, Germany*, 2016.
14. S. Spirk. *Modulare vertikaldynamische Regelungskonzepte für ein hybrid aktuiertes Fahrwerk*. Dissertation, Technische Universität München, München, 2016.
15. J. N. Strohm and B. Lohmann. Optimal feedforward preview control by FIR filters. In *Proceedings of the 20th IFAC World Congress*, angenommen, 2017.
16. B. Wagner. *Analytische und iterative Verfahren zur Inversion linearer und nichtlinearer Abtastsysteme*, Volume 763 of *Fortschritt-Berichte VDI Reihe 8, Meß-, Steuerungs- und Regelungstechnik*. VDI-Verl., Düsseldorf, 1999.
17. Q. Zou. Optimal preview-based stable-inversion for output tracking of nonminimum-phase linear systems. *Automatica*, 45(1):230–237, 2009.
18. Q. Zou and S. Devasia. Preview-based optimal inversion for output tracking: Application to scanning tunneling microscopy. *IEEE Transactions on Control Systems Technology*, 12(3):375–386, 2004.

Autoreninformationen

Johannes N. Strohm, M. Sc.
Technische Universität München, Lehrstuhl für Regelungstechnik, Boltzmannstraße 15, 85748 Garching bei München
johannes.strohm@tum.de

Johannes Strohm ist wissenschaftlicher Mitarbeiter am Lehrstuhl für Regelungstechnik an der Technischen Universität München. Hauptarbeitsgebiete: aktive Fahrwerksdämpfung, vorausschauende Vorsteuerungen.

Prof. Dr.-Ing. habil. Boris Lohmann
Technische Universität München, Lehrstuhl für Regelungstechnik, Boltzmannstraße 15, 85748 Garching bei München

Prof. Dr.-Ing. habil. Boris Lohmann leitet den Lehrstuhl für Regelungstechnik an der Fakultät für Maschinenwesen der TU München. Seine Forschungsinteressen umfassen Methoden der Regelungstechnik für unterschiedliche Systemklassen, Modellbildung und -Reduktion sowie Anwendungen in der Mechatronik und im Automotive-Bereich.

A.3 A Fast Convergence FxLMS Algorithm for Vibration Damping of a Quarter Car

Contributions: The derivation of the fcFxLMS algorithm, its analysis, the application to the quarter car, implementation, simulations, and writing have been executed predominantly by the first author.

A Fast Convergence FxLMS Algorithm for Vibration Damping of a Quarter Car

Johannes N. Strohm[1] and Boris Lohmann[1]

Abstract— We present a new adaption rule for the filtered x least mean squares (FxLMS) algorithm and its application as a disturbance compensator for the quarter car. Therefore we combine an adaption rule, which is based on the normalized, leaky-ν FxLMS algorithm, with a novel method for the initialization of the filter coefficients. This leads to fast convergence, which is important in the case of sudden changes in the primary path's delay time.

Thereafter, the new algorithm is applied as a disturbance compensator for road irregularities. The goal is to improve driving comfort and safety by exploiting the knowledge of the road surface (i.e. disturbance). Assuming that it is known a certain time in advance, we show the improved performance of the developed algorithm and compare it to the standard FxLMS algorithm and to a static disturbance compensator.

I. INTRODUCTION

The automotive world is heading towards autonomous driving. Although the mass media usually set the focus on the lateral and longitudinal dynamics, there are, at a closer look, many more challenges connected to autonomous cars, e.g. learning from mistakes, interaction between cars and prediction of an agent's behavior [3]. The need for improved driving comfort is the challenge we are dealing with in this paper. As the driver becomes a passenger in the autonomous vehicle, having good driving experience is not of importance anymore. Instead, comfort will have a much higher priority, as the passenger usually wants to use the time during the ride to work or to relax. In passive car suspensions, the comfort can be increased by lowering the stiffness of the spring [14]. However, this always results in a loss in driving safety as the wheel tends to lose road contact. The solution to this conflict is (semi-)active components, e.g. variable dampers or hydraulic actuators in the suspension. Combined with a suitable control law, these achieve a high driving comfort (meaning low chassis acceleration) and simultaneously high driving safety (meaning low dynamic wheel loads).

Besides these challenges, autonomous driving brings new opportunities as well. One of them is the vast amount of data, which is recorded. Since a lot of information about the environment is required for autonomous driving, these cars are usually packed with sensors. With these sensors it is possible to detect the road surface ahead of the car, which is one source for vibration in the chassis. For example, in [6] it is shown how to extract the road profile from images from a camera, which is mounted behind the windshield.

The question is how to design a feedforward controller for a (semi-)active quarter car that uses this knowledge about the future road surface to increase the driving comfort without decreasing driving safety. Moreover, the preview of the road profile may suddenly change, for instance, if another car arrives in front of the autonomous car and hides parts of the street surface beneath it. Furthermore, the slowly varying dynamics of a vehicle, e.g. due to different loads or aging effects of the damper and the spring, have to be taken into account. The road profile characteristics, i.e. the waviness and roughness, depend on the type of street, e.g. country road, highway and urban streets [14]. To improve the performance for each road type, the controller has to adapt to these variations.

First approaches dealing with the problem of using preview data date back to 1968 [1], where Wiener filter theory was used to design a feedforward disturbance compensator for a quarter car. Later on, optimal control methods in the time domain are applied in [20] and [7] to get a feedback controller and a preview feedforward controller. Both discuss the influence of varying preview time. However, none of these approaches is adaptive.

A standard approach for adaptive disturbance compensators is Active Noise Control (ANC). This method adapts the coefficients of a Finite Impulse Response (FIR) filter in each timestep, so that the mean square error of the noise is minimized. We apply the Least Mean Square (LMS) algorithm, which can be interpreted as an stochastic gradient descent, to achieve the minimum [11]. It is well known that the variations to which the FIR filter should adapt have to be sufficiently slow [8].

There are few works regarding the LMS algorithm in the context of vibration damping in a quarter car. The LMS algorithm is applied to a fully active quarter car in [19], but without exploiting preview data. The FxLMS (see Section II-A) with preview of the road profile is used for semi-active suspensions in [10]. However, in [10] it is assumed that the preview time is always constant, which is not the case in a real world application. Thus, a sudden change results in a poor performance as the filter adapts more slowly to the new system behavior than the change in preview time appears. A good initial guess of the filter coefficients is therefore an effective way to improve the convergence speed. Nonetheless, a common approach is to initialize with random numbers or zeros, when the LMS algorithm is applied for ANC. A better initialization method is shown for example in [9]. In this work, a causal Wiener filter is determined beforehand and its coefficients are used as an initial guess

[1]All authors are with the Institute of Automatic Control, Faculty of Mechanical Engineering, Technical University of Munich, 85748 Garching, Germany johannes.strohm@tum.de

for the adaptive FIR filter.

In this paper we show how to design a fast converging adaptive feedforward controller for a hybrid quarter car configuration (see Sec. IV-B) that exploits the knowledge about the future road surface. Therefore we present a new method to determine an optimal, non-causal FIR filter, whose coefficients serve as an initial guess for the adaptive FIR filter. In combination with a new adaption law, the proposed method is able to compensate even sudden changes in preview time.

The remainder of the paper is organized as follows: Section II briefly introduces the FxLMS algorithm and the optimal, non-causal FIR filter. Based on these methods, the fast convergence FxLMS (fcFxLMS) algorithm is derived in Section III. The application of this new method to the problem of active vibration damping for a quarter car is presented in Section IV, before simulation results are shown in Section V. Concluding remarks and an outlook are given in Section VI.

II. PRELIMINARIES

A. FxLMS Algorithm

The LMS algorithm is the standard approach to ANC problems. In these problems, an undesired known noise or oscillation in the output is to be canceled out by adding the 180° phase shifted noise or oscillation signal, respectively. As a feedback controller can only determine the input based on the current state, the system's reaction is often too late to fully compensate the noise in the output. A more effective way to cancel out the undesired noise in the output are feedforward controllers, which calculate the required input based on the known noise signal right on time. These controllers can even influence a system proactively, if there is a delay between the measurement of the noise and its effect on the output. An improvement over a static feedforward controller is the adaptive one, which copes with slow changes in the noise characteristics or actuator behavior.

Such an adaptive feedforward controller can be designed using the FxLMS algorithm [2]. Its structure is shown in Fig. 1. The noise signal $x(n)$ at time step n disturbs the
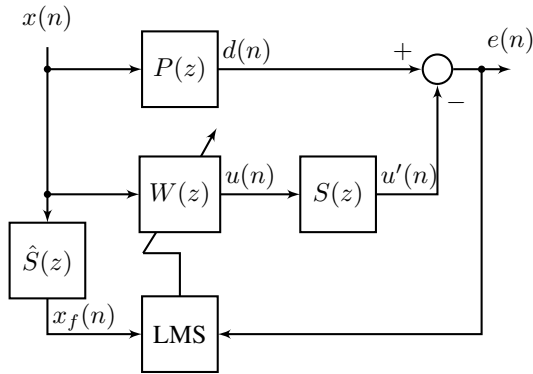

Fig. 1: ANC with LMS (adapted from [11])

primary path $P(z)$, represented in the frequency domain with

the complex variable z, and leads to an undesired behavior in the output $d(n)$. The adaptive feedforward controller $W(z)$ tries to determine an input $u(n)$ for the actuator $S(z)$ such that its output $u'(n)$ cancels out the disturbance $d(n)$. Usually, the adaptive filter $W(z)$ is assumed to be an FIR filter and thus, always stable. The LMS algorithm adapts the L coefficients $\mathbf{w}(n) = [w_0(n) \cdots w_{L-1}(n)]^T$ of the filter $W(z)$ using the error $e(n)$ and the signal $x_f(n)$ with $X_f(z) = \hat{S}(z)X(z)$. The filter $\hat{S}(z)$ approximates the actuator dynamics $S(z)$. For the derivation of the adaption law it is assumed that $\hat{S}(z) = S(z)$. Furthermore, the order of $W(z)$ and $S(z)$ is reversed, so that the error is

$$e(n) = d(n) - u(n) = d(n) - \mathbf{w}^T(n)\mathbf{x}_f(n), \qquad (1)$$

with $\mathbf{x}_f(n) = [x_f(n) \ x_f(n-1) \cdots x_f(n-L+1)]^T$. The adaption minimizes the expected value $E[\cdot]$ of the squared error

$$J(n) = E[e(n)^2]. \qquad (2)$$

For stationary signals with known cross-/autocorrelation matrices the optimal constant filter $W(z)$ can be calculated by solving a linear system of equations (for more details see [11] or [8]). Usually this is not the case, so we minimize (2) with the method of steepest descent using stochastic gradient descent. Therefore the filter coefficients are updated in each time step according to

$$\mathbf{w}(n+1) = \mathbf{w}(n) - \frac{1}{2}\mu\nabla\tilde{J}(n), \qquad (3)$$

where μ is the step size and $\nabla\tilde{J}(n)$ is the gradient of $\tilde{J}(n)$ with respect to the coefficients $\mathbf{w}(n)$. Here, the cost function $\tilde{J}(n) = e(n)^2$ is used, as we determine the instantaneous gradient of one error sample and not of the expected value of the error. It is easy to show that the gradient $\nabla\tilde{J}(n)$ is given by $\nabla\tilde{J}(n) = -2\mathbf{x}_f(n)e(n)$ [11]. The convergence of this method depends amongst others on the step size μ and the initial guess $\mathbf{w}(0)$.

There are many extensions to this FxLMS algorithm. In the following we use the normalized, leaky-ν FxLMS algorithm. To improve convergence, the step size μ is normalized with the signal power: $\mu(n) = \alpha/(\mathbf{x}^T\mathbf{x})$, where α is the new constant step size [15]. The leaky-ν extension is needed to avoid divergence [5]. The final update rule for the normalized, leaky-ν FxLMS algorithm is

$$\mathbf{w}(n+1) = \nu\mathbf{w}(n) + \alpha\frac{\mathbf{x}_f(n)e(n)}{\max(\mathbf{x}_f(n)^T\mathbf{x}_f(n), P_{\min}L)}, \quad (4)$$

where $P_{\min}$ the minimal signal power for avoiding division by zero.

B. Optimal Preview FIR-Filter

In [17] we showed how to design an optimal feedforward preview FIR filter. In [18] we applied this filter to active suspension control. We summarize here the basics of this design procedure, to aid understanding of the following sections. The starting point is the question of how to use the knowledge about a future disturbance in order to compensate for it. We assume that the disturbance at time step n is known

and impacts the plant, according to the delay τ at time step $n+\tau$. From the plant's point of view, this can be interpreted as knowing the disturbance in advance. Thus, the delay τ in Fig. 2 can also be seen as the available preview time. Fig. 2 shows the structure of a disturbance compensator. The ideal one is built using $\tilde{G}(z) = z^{-\tau}G_{uy}^{-1}$. Thus, the dynamics of the plant's transfer function $G_{uy}(z)$ is compensated and the time delay is taken into account by delaying the input u. To
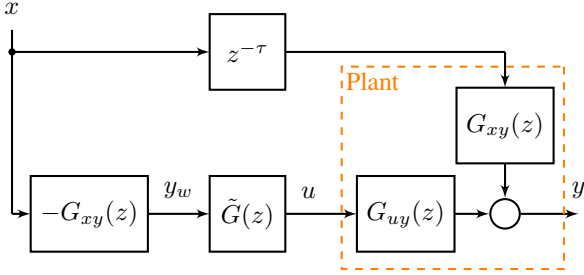

Fig. 2: Disturbance Compensation

keep the output y unaffected by the disturbance x, the desired trajectory y_w has to be chosen as $Y_w(z) = -G_{xy}(z)X(z)$. In theory, this cancels the disturbance completely. However, G_{uy}^{-1} will be unstable, if G_{uy} has zeros outside the unit disk. Furthermore, there is no possibility of benefiting from the knowledge about the future disturbance, as the delay in the upper path is compensated by delaying $\tilde{G}(z)$.

To solve both of the problems, we suggested in [17] a method for the design of a proactive FIR filter for $\tilde{G}(z)$ that is an optimized, non-causal inverse of G_{uy}. An alternative approach is given in [12], where a state-space structure of the system dynamics is used and only the error in the output is minimized. In contrast, we use an impulse response representation of the system dynamics as in dynamic matrix control (DMC) [4] and minimize the error and the required input. The system output $\mathbf{y}$ to an input sequence $\mathbf{u}$ is determined via a matrix product: $\mathbf{y} = \mathbf{G}\mathbf{u}$. The dynamic matrix $\mathbf{G}$ has a Toeplitz structure, such that each column consists of the shifted values g_i of the impulse response of the system

$$\mathbf{G} = \begin{bmatrix} g_0 & & \\ \vdots & \ddots & \\ g_N & & g_0 \\ & \ddots & \vdots \\ & & g_N \end{bmatrix}. \tag{5}$$

To build the stable, optimized inverse of G_{uy} it is necessary to minimize the error sequence between the desired output and actual output $\mathbf{e} = \mathbf{y}_w - \mathbf{y}$ while keeping the input $\mathbf{u}$ and the change of input $\Delta\mathbf{u}$ as small as possible. This leads to the cost function

$$J_{FIR} = \mathbf{e}^T\mathbf{Q}\mathbf{e} + \mathbf{u}^T\mathbf{R}\mathbf{u} + \Delta\mathbf{u}^T\tilde{\mathbf{R}}\Delta\mathbf{u}, \tag{6}$$

with positive definite weighting matrices $\mathbf{Q}$, $\mathbf{R}$ and $\tilde{\mathbf{R}}$. Under the condition of sufficient length of the input and output sequence (also called control and prediction horizon) and of

the weighting matrices of the form $k\mathbf{I}$ with a finite $k > 0$ and $\mathbf{I}$ identity, the optimal solution is found by deriving (6) with respect to $\mathbf{u}$ and solving for $\mathbf{u}$. The result

$$\mathbf{u}^* = (\mathbf{G}^T\mathbf{Q}\mathbf{G} + \mathbf{R} + \mathbf{D}^T\tilde{\mathbf{R}}\mathbf{D})^{-1}\mathbf{G}^T\mathbf{Q}\mathbf{y}_w = \mathbf{F}\mathbf{y}_w \tag{7}$$

is again a matrix product with the deconvolution matrix $\mathbf{F}$ and the finite difference matrix $\mathbf{D}$ (for details see [17]). The matrix $\mathbf{F}$ has a Toeplitz-like structure, meaning that there are some deviations from the true Toeplitz structure as in (5) in the first and last columns. Each column represents the required input sequence for an impulse in the desired output $\mathbf{y}_w$ at a certain time step τ. Thus, the values of each column can be seen as the coefficients of a FIR filter $F_{z,\tau}(z)$ which is the optimal inverse of G_{uy} for a specific preview time τ. If there is no preview, which means only the current value of the desired trajectory $y_w(n)$ is known, the optimal coefficients for the FIR filter will be the values of the first column of $\mathbf{F}$. If the desired trajectory is known τ time steps in advance, the best coefficients for the FIR filter $F_{z,\tau}(z)$ will be the values in the $(\tau + 1)$-th column of $\mathbf{F}$. The resulting, non-causal filter is

$$F_{z,\tau}(z) = f_0 z^\tau + f_1 z^{\tau-1} + \cdots + f_M z^{\tau-M}, f \tag{8}$$

where f_i is the i-th entry of the $\tau + 1$-th column of $\mathbf{F}$ and M is the length of the column. So once the deconvolution matrix $\mathbf{F}$ is determined, an optimal FIR filter is available for each preview time.

For application of this optimal preview FIR filter in the context of disturbance compensators, $\tilde{G}(z)$ (Fig. 2) has to be implemented as the delayed — and thus causal — static filter $z^{-\tau}F_{z,\tau}(z)$. Due to the non-causal behavior of $F_{z,\tau}(z)$ the time delay in $\tilde{G}(z)$ is 0, such that $\tilde{G}(z)$ influences the system before the disturbance has reached the plant.

III. FAST CONVERGENCE FXLMS

The main contribution of this paper is the combination of the two above presented methods. Comparing Fig. 1 with Fig. 2, the similar structure of both methods becomes obvious. The primary path $P(z)$ in Fig. 1 corresponds to the delayed transfer function $z^{-\tau}G_{xy}(z)$ in Fig. 2, $S(z)$ to $G_{uy}(z)$ and $W(z)$ to $-G_{xy}\tilde{G}(z)$. It is stated in [11] that a delay in the primary path $P(z)$ is necessary for the compensation of broadband noise. If the delay in $P(z)$ is not big enough, the effect of the noise $d(n)$ reaches the output faster than the effect of the reaction $u'(n)$. The only difference in the structure of the two methods is the "LMS" block. Whereas the disturbance compensator using the optimal preview FIR filter is static, the compensator using the FxLMS algorithm adapts to changes in disturbance or plant behavior. On the other hand, the static disturbance compensator exhibits high performance from the very beginning, while the adaptive one needs some time to converge towards an optimal solution (as illustrated in Section V). A combination of these two solves the latter problem.

As already stated in Section II-A, the convergence of the LMS algorithm can be accelerated by using an initial guess near the optimum for the filter coefficients $\mathbf{w}(0)$ and a

suitable step size α. Usually these coefficients are initialized with zeros or random numbers. If good performance is needed from the very first second, this initialization is not sufficient. To find a good starting vector $\mathbf{w}_0 = \mathbf{w}(0)$ that considers the time delay in $P(z)$ we design an optimal preview FIR filter with the above presented method. As seen in the figures, the filter $W(z)$ corresponds to $-G_{xy}\tilde{G}(z)$. Approximating $G_{xy}(z)$ by a FIR filter $\tilde{G}_{xy}(z)$ and multiplying it by $\tilde{G}(z) = z^{-\tau}F_{z,\tau}(z)$ leads to the optimal FIR filter whose coefficients $\mathbf{w}_{opt}$ are the initial guess $\mathbf{w}_0$. To prove that the LMS algorithm converges to $\mathbf{w}_{opt}$, we add the weighting of the input and of the input increment to the cost function

$$\tilde{J}(n) = \frac{1}{2}(e(n)^2 + Re_u(n)^2 + \tilde{R}e_{\Delta u}(n)^2), \quad (9)$$

with the difference in desired and actual value of the input $e_u(n) = u_d(n) - u(n)$ and the input increment $e_{\Delta u}(n) = \Delta u_d(n) - \Delta u(n)$. The FxLMS algorithm minimizes (9) iteratively, using the gradient

$$\nabla \tilde{J}(n) = -\mathbf{x}_f(n)e(n) - \mathbf{x}(n)e_u(n) - \Delta\mathbf{x}(n)e_{\Delta u}(n), \quad (10)$$

with $\Delta\mathbf{x}(n) = \mathbf{x}(n) - \mathbf{x}(n-1)$. If a series of measurement data is known, the optimal filter coefficients can be found through offline optimization using matrix and vector notation

$$\mathbf{e}(n) = \mathbf{d}(n) - \mathbf{X}_f(n)\mathbf{w}(n) \quad (11)$$

$$\mathbf{d}(n) = [d(0) \; d(1) \cdots \; d(n)]^T \quad (12)$$

$$\mathbf{X}_f(n) = \begin{bmatrix} x_f(0) & & & \\ x_f(1) & x_f(0) & & \\ \vdots & \vdots & & \\ x_f(n) & x_f(n-1) & \cdots & x_f(n-L) \end{bmatrix} \quad (13)$$

$$\mathbf{u}(n) = \mathbf{X}(n)\mathbf{w}(n) \quad (14)$$

$$\Delta\mathbf{u}(n) = \mathbf{D}\mathbf{X}(n)\mathbf{w}(n) \quad (15)$$

$$\mathbf{R} = R\mathbf{I}_n \qquad \tilde{\mathbf{R}} = \tilde{R}\mathbf{I}_n, \quad (16)$$

with the finite difference matrix $\mathbf{D}$ and the matrix $\mathbf{X}(n)$ as in (13). Setting $\Delta u_d(i) = u_d(i) = 0$ for $i = 0, 1, \cdots, n-1$ and inserting (11)–(16) in (9) the optimal filter coefficients $\mathbf{w}_{opt}$ are determined by $\partial\tilde{J}/\partial\mathbf{w}(n) = 0$. This results in

$$\mathbf{w}_{opt} = (\mathbf{X}_f^T(n)\mathbf{X}_f(n) + \mathbf{X}^T(n)\mathbf{R}\mathbf{X}(n) + \\ \mathbf{X}^T(n)\mathbf{D}^T\tilde{\mathbf{R}}\mathbf{D}\mathbf{X}(n))^{-1}\mathbf{X}_f(n)\mathbf{d}(n). \quad (17)$$

If we apply an impulse disturbance at time step 0, $\mathbf{X}$ becomes $\mathbf{I}_n$ and $\mathbf{X}_f$ represents the impulse response of $S(z)$ as in (5). With $\mathbf{Q} = \mathbf{I}_n$ and $\mathbf{d} = \mathbf{y}_w$ (7) leads to the same result as (17). As the impulse disturbance excites all frequencies, the LMS algorithm has the same optimum as the optimal preview FIR filter as long as $x(n)$ contains all frequencies as well.

Initialization of the FxLMS algorithm with $\mathbf{w}_{opt}$ is applied in the case of a constant time delay. If there is a sudden change in the time delay, the FxLMS algorithm needs some time to adapt to it. To avoid this, we suggest a new update rule for the filter coefficients $\mathbf{w}(n)$ (see (18)–(24)). It exploits the matrix $\mathbf{F}$, which provides in its columns the filter coefficients of $\tilde{G}(z) = z^{-\tau}F_{z,\tau}(z)$ for various time delays.

Combining $\tilde{G}(z)$ with $\tilde{G}_{xy}(z)$ we determine an initial guess $\mathbf{w}_{\tau,0}$ for each time delay. The new update rule uses these initial guesses in the case of a change in time delay τ

$$i(n) = \begin{cases} i(n-1) + 1 & \text{if } \tau(n) = \tau(n-1) \\ 1 & \text{if } \tau(n) \neq \tau(n-1) \end{cases}, \quad (18)$$

$$\alpha(n+1) = \begin{cases} \beta_1\alpha(n) + (1-\beta_1)\alpha_c & \text{if } \tau(n) = \tau(n-1) \\ 1 & \text{if } \tau(n) \neq \tau(n-1) \end{cases}, \quad (19)$$

$$P_x(n) = \max(\mathbf{x}_f(n)^T\mathbf{x}_f(n) + R\mathbf{x}^T(n)\mathbf{x}(n) + \\ \tilde{R}\Delta\mathbf{x}^T(n)\Delta\mathbf{x}(n), P_{\min}L), \quad (20)$$

$$\gamma(n+1) = \beta_2^{i(n)}(\mathbf{w}(n) - \mathbf{w}_{\tau,0}) + \frac{(1-\beta_2^{i(n)})\nabla\tilde{J}}{P_x(n)}, \quad (21)$$

$$\mathbf{w}(n+1) = \nu\mathbf{w}(n) - \alpha(n+1)\gamma(n+1), \quad (22)$$

$$\alpha(0) = 1, \qquad i(0) = 1, \quad (23)$$

$$0 < \beta_1 < 1, \qquad 0 < \beta_2 < 1. \quad (24)$$

The value of β_2 is usually set close to 1. For large n and constant τ our update rule converges towards the standard FxLMS algorithm (4). In this case i increases (see (18)), the variable step size $\alpha(n)$ approaches, according to (19), the constant value α_c and $\beta_2^{i(n)}$ in (21) tends to zero. Thus, the normalized gradient $\gamma(n)$ in (21) equals the normalized gradient in (4) with the additional weighting terms as in (10). This behavior ensures the desired beneficial properties of the standard FxLMS algorithm in the long term, i.e. adaption to slow changes in the plant or disturbance. To improve the short term performance of the standard FxLMS, the term $\mathbf{w}(n) - \mathbf{w}_{\tau,0}$ was added to the gradient (21). Each time there is a change in the time delay τ, $i(n)$ and $\alpha(n+1)$ are set to 1 according to (18) and (19). For the limit case of $\beta_2 = 1$ the gradient $\gamma(n+1)$ becomes the difference between the current filter weights $\mathbf{w}(n)$ and the offline calculated optimal filter weights $\mathbf{w}_{\tau,0}$ for the time delay $\tau(n)$. This results, with reference to (22), in new filter coefficients $\mathbf{w}(n+1)$ which are close to the optimal ones $\mathbf{w}_{\tau,0}$. After this reinitialization step, the values of $\alpha(n)$ and $\gamma(n)$ converge with growing n towards the constant step size α_c and the gradient of the FxLMS algorithm, respectively. Thus, an adaptive filter with fast convergence is achieved.

The parameters α_c, β_1, and β_2 are design parameters and have to be adjusted according to the system dynamics. The value β_1 represents the decay rate of the step size after a reinitialization and β_2 describes the decay rate of the influence of the static optimal filter coefficients $\mathbf{w}_{\tau,0}$ on the gradient γ.

IV. APPLICATION TO ACTIVE VEHICLE SUSPENSION

In the following we apply the fcFxLMS algorithm for disturbance compensation in a quarter car. If the heave dynamics alone (no pitch, no roll) are to be considered, the vehicle's dynamics can be modeled by a quarter car, consisting of a tire model, the suspension strut and a quarter vehicle mass. The disturbance is the road irregularities, which are assumed

to be known a certain distance in front of the car and which resemble a broadband noise. In fact, there are already cars in series production that have a camera mounted behind the rear-view mirror to detect the road surface (e.g. Mercedes S-Class). These sense irregularities up to 15 m in front of the cars, which, at a speed of 50 km/h, equals a preview time of $\tau_1 \approx 1.08/T_s$ time steps, with sample time T_s. We consider the following two scenarios:

1) The car drives with a constant speed of 50 km/h on a bad country road for ca. 60 s.
2) The car starts driving with a constant speed of 50 km/h on a bad country road. At 30 s another vehicle appears 3 m in front of the car, which reduces the available preview distance immediately and diminishes the preview time to $\tau_2 \approx 0.216/T_s$ time steps.

Thus, there is a jump in the preview time. This can be considered equivalent to a sudden change of car velocity with constant preview distance. Subsequently, we focus on the case of constant driving velocities and a jump in the preview distance. Before presenting the results, we introduce the quarter car models used for the compensator design and for simulation.

A. Design Model

The FxLMS algorithm, as well as the optimal preview FIR filter design method, are based on a linear system model. Therefore, we model the quarter car as a linear two mass oscillator as in [18] (Fig. 3a). The tire (mass m_w)
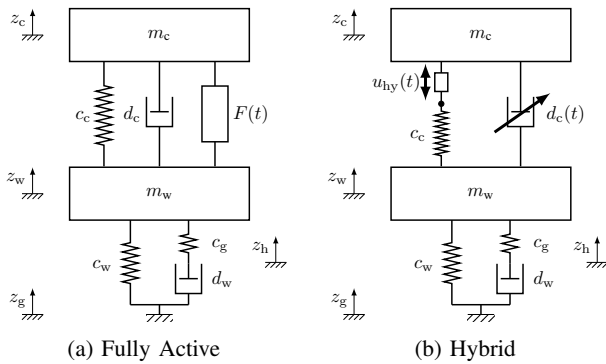

(a) Fully Active   (b) Hybrid

Fig. 3: Quarter car models [18]

is represented by a Gehmann model [14]. The suspension (spring with constant stiffness c_c, damper with constant damping coefficient d_c) is assumed to be fully active. That means an arbitrary force $F(t)$ can be applied as the input u between wheel and chassis mass m_c. The state variables are the disturbance z_g, the Gehmann position z_h, the wheel position z_w and the chassis position z_c. The output y of the system is either the chassis acceleration $y_1 = \ddot{z}_c$ (for maximizing the comfort) or the dynamic wheel load $y_2 = F_{dyn}$ (for maximizing driving safety). For the fcFxLMS algorithm, y_1 is chosen as output, as the focus is on high driving comfort. The final linear time-invariant model is of the form $\dot{x} = Ax + Bu + E\dot{z}_g$ with the state vector $x = [z_c - z_w \ \dot{z}_c \ z_w - z_g \ \dot{z}_w \ z_h - z_g]^T$. The matrix A, the

vectors B, E and the needed parameter values are assumed as in [18].

B. Simulation Model

The simulations are performed with a *nonlinear* hybrid quarter car model (see Fig. 3b), which represents the dynamics of the institute's quarter car test stand very accurately. It is called a "hybrid" configuration as there is no longer one ideal actuator as in Fig. 3a, but two non-ideal actuators. The first one is the semi-active damper, which can vary its damping in a certain range. Due to the damper's dissipative character, it is not possible to add energy to the system. This is done with the second actuator, the so-called Spring Mount Adjustment (SMA). The SMA is a slow hydraulic actuator (cutoff frequency of 5 Hz), which is mounted between the main suspension spring and the chassis. Although the actuators have different properties, the impact on the quarter car is the same: a force between chassis mass and wheel mass. The FxLMS algorithm is designed based on the fully active quarter car model. Thus, it calculates only one desired input $u = F(t)$. This force has to be distributed onto the two real actuators, which is done using a dynamic optimal division (see [16] for details). The principle is to assign as much force as possible to the SMA, while the damper takes over the remaining high-frequency portion.

To sufficiently reflect the test stand's behavior, the following nonlinearities are incorporated in the simulation model:

- Asymmetric and degressive force velocity characteristics of the damper d_c
- Nonlinear spring characteristics c_c with end stops
- Coulomb friction in the damper
- A quadratic stiffness of the spring c_w
- A kinematic transmission factor between forces in the suspension strut plane and the tire plane during spring compression (see [13]).

Furthermore, the cutoff frequency of the SMA is taken into account in the simulation model.

C. Design of the Fast Convergence FxLMS Algorithm

In the first design step, the matrix F with the optimal initial guesses for the FIR filter has to be calculated (see Section II-B). Therefore we exploit results from the parameter studies in [18]. The sample time T_s is set to 3 ms. It was shown that the length $M = 1000$ is sufficient, such that a larger M does not improve the performance. The dynamic matrix G is easily assembled using the impulse response of the discretized transfer function G_{uy}. Furthermore, we analyzed the performance of the static optimal preview feedforward controller depending on the weighting matrices $Q = k_Q I$, $R = k_R I$, and $\tilde{R} = k_{\tilde{R}} I$ and on the choice of the output y. Using $y_2 = F_{dyn}$ it is possible to maximize the driving safety whereas the choice of $y_1 = \ddot{z}_c$ as output leads to a maximization of driving comfort for certain matrices Q, R, and $\tilde{R}$. Considering ideal actuators, a high k_Q and a low k_R lead to low chassis acceleration but to high input forces and vice versa. As the eigenfrequency of the wheel differs from the eigenfrequency of the chassis, the

performance of the controller regarding the minimization of dynamic wheel load or chassis acceleration depends on the frequency spectrum of the input. The constant $k_{\tilde{\mathbf{R}}}$ weights the input increment and can therefore be used to modulate the amplitude of the high frequency portion of the input force. Thus, it influences the trade-off between driving safety and comfort. For computing the initial guesses for the fcFxLMS algorithm based on the matrix $\mathbf{F}$, we chose the output y_1. The constant multipliers $k_{\mathbf{Q}}, k_{\mathbf{R}}, k_{\tilde{\mathbf{R}}}$ for the weighting matrices are determined via an optimization as in [18] such that the driving comfort is maximized using the nonlinear model and a synthetic stochastic road profile.

After determination of $\mathbf{F}$, the fcFxLMS filter is built with the same weighting matrices. The filter $S(z)$ equals in this case G_{uy_1} as the goal is the minimization of the chassis acceleration $\ddot{z}_c$. The parameters are chosen as in Table I. The length L of the FIR filter was chosen according to the length M of the initial values. In the case of constant preview time, the parameters α_c and P_{min} influence the decay rate and are chosen to maximize it. The values of β_1 and β_2 have an impact on the behavior during a sudden change of the preview time. By choosing the values as in Table I we achieve on the one hand a fast decay in the step size α towards α_c and thus towards the standard FxLMS algorithm and on the other hand a fast convergence towards the optimal parameters, as the influence of the optimal filter coefficients on the gradient $\mathbf{w}_{\tau,0}$ is high after a change in preview time.

V. RESULTS

This section shows simulation results for the two scenarios. At first we regard the case of driving over a bad country road at 50 km/h with a constant preview time of 1.08 s (scenario 1). In the second step we present results for the scenario 2. To measure the performance of the disturbance compensation, the root mean square (RMS) value of the chassis acceleration $\ddot{z}_c$ and of the dynamic wheel load F_{dyn} is used. The convergence is compared via the sum of the absolute filter coefficients $\mathbf{w}(n)$

$$\Xi(n) = \sum_{i=0}^{L-1} |w_i(n)|. \tag{25}$$

In both scenarios, the controllers are designed based on the linear design model (Section IV-A) and simulated with the nonlinear simulation model (Section IV-B).

Table II presents the results for scenario 1. The static FIR filter with constant coefficients $\mathbf{w}_{\tau,0}$ improves comfort by more than 61% and the driving safety by more than 19% with respect to the passive suspension. The standard FxLMS algorithm (4), which was initialized with zeros, has a similar improvement in the comfort but a slightly better performance in terms of driving safety. Comparing this with

TABLE I: Parameters for the fcFxLMS algorithm

Parameter	L	P_{min}	ν	α_c	β_1	β_2
Value	1000	10^{-8}	0.99999	0.05	0.7	0.99

TABLE II: Performance for constant preview time

	Passive	Static	FxLMS	fcFxLMS
RMS($\ddot{z}_c$)	1.691	0.6468	0.6556	0.5933
$1 - \frac{\text{RMS}(\ddot{z}_c)}{\text{RMS}(\ddot{z}_{c,passive})}$	0	61.8%	61.2%	64.9%
RMS(F_{dyn})	1146	923.1	888.6	889.5
$1 - \frac{\text{RMS}(F_{dyn})}{\text{RMS}(F_{dyn,passive})}$	0	19.5%	22.5%	22.4%

TABLE III: Performance for varying preview time

	Passive	Static	FxLMS	fcFxLMS
RMS($\ddot{z}_c$)	1.691	1.277	0.8651	0.6929
$1 - \frac{\text{RMS}(\ddot{z}_c)}{\text{RMS}(\ddot{z}_{c,passive})}$	0	24.5%	48.8%	59.0%
RMS(F_{dyn})	1146	1029	923.5	909.9
$1 - \frac{\text{RMS}(F_{dyn})}{\text{RMS}(F_{dyn,passive})}$	0	10.2%	19.4%	20.6%

the fcFxLMS algorithm, we can state that, due to the fast convergence (as shown in Fig. 4), the fcFxLMS algorithm has the best performance. Fig. 4 shows the convergence of the FxLMS and fcFxLMS algorithm. As expected, the coefficients almost immediately converge using the fcFxLMS algorithm. Furthermore, the change in the coefficients' value during the simulation between 0 s and 20 s is low compared to the continuous change of the values adapted with the FxLMS algorithm. The standard FxLMS algorithm needs 5 s at the beginning to adapt the coefficients to the same level as the fcFxLMS algorithm. Moreover, it takes the FxLMS algorithm 30 s to achieve similar filter coefficients.
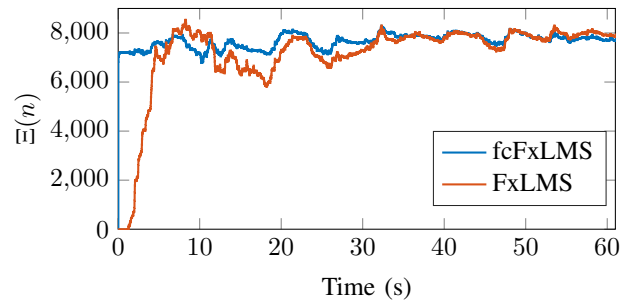
Fig. 4: Convergence of FxLMS and fcFxLMS

The second scenario is even more useful for showing the benefit of the fcFxLMS algorithm presented here. Again at first, we take a look at the RMS values for the three different compensator types (see Table III). The static compensator has the biggest losses compared to the constant preview case, as it assumes, at all times, a preview time of 1.08 s. The FxLMS algorithm still improves the comfort by almost 50%. The fcFxLMS algorithm again has the best performance for both driving comfort and safety, as it converges almost immediately after the change in preview time to the new optimum.

This is also seen in the trend in chassis acceleration $\ddot{z}_c$ (Fig. 5). The dashed black line shows the acceleration of an non-actuated passive suspension. Both adaptive disturbance compensators (FxLMS-red line and fcFxLMS-blue line) lead to significantly lower acceleration and thus, to better comfort.

Due to the sudden variation in preview time at 30 seconds, an increase in acceleration for the FxLMS algorithm occurs, while the fcFxLMS algorithm maintains the same level of amplitudes. After the adaption period of approx. 15 seconds, the FxLMS algorithm leads again to a similar comfort as the fcFxLMS. Although 15 seconds seem to be a tolerably short time span, this short increase of chassis acceleration is crucial. Each time another vehicle appears, for instance, after a lane change in front of the car, the car equipped with the standard FxLMS algorithm switches its behavior from a smooth ride to shaking and oscillating. This change is sensed by the car's passengers, which decreases driving comfort, even if the total chassis acceleration is lower than that of a passive car. Especially in autonomous cars, passengers do not want to perceive that something has appeared in front of their cars and has thus reduced the preview time.
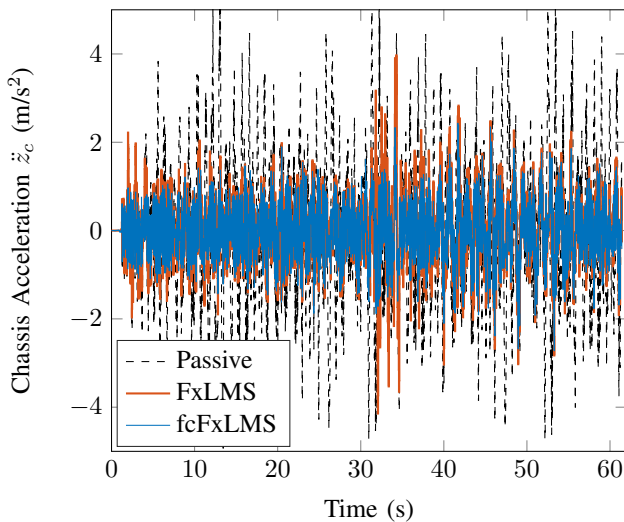

Fig. 5: Chassis acceleration during scenario 2

VI. CONCLUSIONS

We presented a new adaption rule for the FxLMS algorithm and its application to quarter car damping. The results show the high potential of this approach. However, there are some further investigations to be made.

Throughout the paper we assumed perfect knowledge about the road disturbance. In a real world application the values of z_g have some noise and drift. First tests showed that this approach is quite robust against such errors, but this has to be examined systematically. Furthermore, we are planning to test the algorithm on a quarter car test stand, to investigate the influence of noisy measurements of $\ddot{z}_c$. In addition, this algorithm can also be used to cope with varying vehicle velocities. A variation in velocity changes the preview time. Normally this change is not as abrupt as in the scenario considered here, but further research will be done into whether the fcFxLMS is also beneficial in such a scenario.

REFERENCES

[1] E. K. Bender. Optimum linear preview control with application to vehicle suspension. *Journal of Basic Engineering*, 90(2):213–221, 1968.

[2] J. C. Burgess. Active adaptive sound control in a duct: A computer simulation. *The Journal of the Acoustical Society of America*, 70(3):715–726, 1981.

[3] M. Campbell, M. Egerstedt, J. P. How, and R. M. Murray. Autonomous driving in urban environments: Approaches, lessons and challenges. *Philosophical transactions. Series A, Mathematical, physical, and engineering sciences*, 368(1928):4649–4672, 2010.

[4] C. R. Cutler and B. L. Ramaker. Dynamic matrix control - a computer control algorithm. *Joint Automatic Control Conference*, 17, 1980.

[5] R. D. Gitlin, H. C. Meadors, and S. B. Weinstein. The tap-leakage algorithm: An algorithm for the stable operation of a digitally implemented, fractionally spaced adaptive equalizer. *Bell System Technical Journal*, 61(8):1817–1839, 1982.

[6] C. Göhrle, A. Schindler, A. Wagner, and O. Sawodny. Road profile estimation and preview control for low-bandwidth active suspension systems. *IEEE/ASME Transactions on Mechatronics*, 20(5):2299–2310, 2015.

[7] A. Hać. Optimal linear preview control of active vehicle suspension. *Vehicle System Dynamics*, 21(1):167–195, 1992.

[8] S. S. Haykin. *Adaptive filter theory*. Always learning. Pearson, Upper Saddle River, NJ, 5. ed. edition, 2014.

[9] G. Kannan, A. A. Milani, I. M. S. Panahi, and N. Kehtarnavaz. Performance enhancement of adaptive active noise control systems for fMRI machines. *Conference proceedings: 32nd Annual International Conference of the IEEE Engineering in Medicine and Biology Society. IEEE Engineering in Medicine and Biology Society. Annual Conference*, 2010:4327–4330, 2010.

[10] P. Krauze and J. Kasprzyk. Vibration control in quarter-car model with magnetorheological dampers using FxLMS algorithm with preview. In *2014 European Control Conference (ECC)*, pages 1005–1010. IEEE, 2014.

[11] S.-M. Kuo and D. R. Morgan. *Active noise control systems: Algorithms and DSP implementations*. A Wiley-Interscience publication. Wiley, New York, NY, 1996.

[12] Y. Levinson and L. Mirkin. L^2 optimization in discrete FIR estimation: Exploiting state-space structure. *SIAM Journal on Control and Optimization*, 51(1):419–441, 2013.

[13] W. Matschinsky. *Radführungen der Straßenfahrzeuge: Kinematik, Elasto-Kinematik und Konstruktion*. Springer-Verlag Berlin Heidelberg, Berlin, Heidelberg, 3. edition, 2007.

[14] M. Mitschke and H. Wallentowitz. *Dynamik der Kraftfahrzeuge*. VDI-Buch. Springer Vieweg, Wiesbaden, 5. edition, 2014.

[15] J. Nagumo and A. Noda. A learning method for system identification. *IEEE Transactions on Automatic Control*, 12(3):282–287, 1967.

[16] S. Spirk. *Modulare vertikaldynamische Regelungskonzepte für ein hybrid aktuiertes Fahrwerk*. Fahrzeugtechnik. Dr. Hut, München, 2016.

[17] J. N. Strohm and B. Lohmann. Optimal feedforward preview control by FIR filters. *IFAC-PapersOnLine*, 50(1):5115–5120, 2017.

[18] J. N. Strohm and B. Lohmann. Vorausschauende Störgrößenaufschaltung für die Schwingungsdämpfung am Viertelfahrzeug. *at - Automatisierungstechnik*, 65(8), 2017.

[19] J. Sun and Q. Yang. Research on least means squares adaptive control for automotive active suspension. In *2008 IEEE International Conference on Industrial Technology*, pages 1–4. IEEE, 2008.

[20] A. G. Thompson, B. R. Davis, and C. E. M. Pearce. An optimal linear active suspension with finite road preview. SAE Technical Paper Series. SAE International, Warrendale, PA, United States, 1980.

A.4 A Proactive Nonlinear Disturbance Compensator for the Quarter Car

Contributions: The idea of applying the flatness based disturbance compensator to the quarter car has been developed by the first author. Preliminary analyses and implementations of the flatness based disturbance compensator, the construction of a flat output, and preliminary simulations have been conducted by the second author. The combination with the linear proactive disturbance compensator, theoretical considerations, final implementation, thorough simulation studies, experiments, and writing have been done predominantly by the first author.

A Proactive Nonlinear Disturbance Compensator for the Quarter Car

Johannes N. Strohm* ⓘ , Dominik Pech, and Boris Lohmann

Abstract: A new Proactive Nonlinear Disturbance Compensator (PNDC) for vibration damping in a quarter car is presented. A Flatness Based Disturbance Compensator (FBDC) for a nonlinear quarter car model is derived that decouples the chassis acceleration completely from the known road disturbance. This leads to a high level of driving comfort but to a loss in driving safety. Therefore a Proactive Linear Disturbance Compensator (PLDC) is added. This controller uses knowledge of the future road disturbance to reach a compromise between driving safety and driving comfort. The sensitivity of the nonlinear, proactive disturbance compensator to varying parameters or measurement noise is examined in simulations, and the tuning of the design parameters is shown. Furthermore, results from experiments on the institute's quarter car test stand are discussed. These have shown that the performance of the proposed method exceeds a linear quadratic regulator in simulations and experiments and that the driving comfort can be increased by more than fifty percent without a decrease in driving safety.

Keywords: Active suspension, flatness based disturbance compensation, nonlinear disturbance compensator, preview control, proactive disturbance compensation, quarter car.

1. INTRODUCTION

The media is heralding the advent of autonomous driving, and this brings with it a number of new ideas, use cases, and challenges. At the moment, the focus of developers is mainly set on environmental perception and trajectory planing, but as soon as vehicles prove sufficiently reliable in these areas, other requirements will come to the fore, such as the driving comfort. Until now, cars have been designed to give the driver good feedback about the vehicle dynamics and current driving state. As there is no need for a human driver in an autonomous car, this goal will be neglected. Moreover, the former driver will then be able to use the journey time to relax or work. Both are far more effective in a calm and comfortable vehicle. Thus, the driving comfort needs to be increased.

Comfort is mainly influenced by the suspension, which usually consists of a damper and a spring between the chassis and the tire and is supposed to decouple the chassis from road disturbances, e.g., bumps or potholes. When stiffness and damping are reduced, the driving comfort is improved. However, a soft spring and a soft damper lead to significant vertical movement of the tire. If the tire loses contact with the road, steering, braking or accelerating forces cannot be applied, resulting in a loss of driving safety [1–3]. Hence, designing a suspension explicitly involves making a compromise between driving comfort and driving safety. To further increase comfort without losing safety, semi-active, active or hybrid suspension systems have to be used, e.g., [4]. Whereas semi-active suspensions vary their damping coefficients and thus the damping force while driving [2], active suspension systems can apply a force in and against the direction of the relative movement between wheel and chassis [5]. As active suspension systems need to work throughout the entire relevant frequency range up to 25 Hz [1], the power demand is high. To lower the demand while maintaining a high performance level, the slow-active and hybrid suspension systems were introduced in [3, 6, 7]. The former use a slow actuator (cut-off frequency up to 5 Hz), which is connected in series with a spring. In hybrid systems, a semi-active damper is added to this configuration.

All these configurations share the common property that a control law is required to determine the actuators' inputs. The most broadly used is the skyhook controller, which emulates an imaginary damper between the chassis and the sky [8]. With growing computational power, and especially in research, methods from various fields of automatic control are applied to the problem of oscillation damping in a car. The Linear Quadratic Regulator (LQR) (e.g., [9–11]) and linear H∞ approaches, such as [2,12–14] are well known. Furthermore, adaptive (e.g., [15–18]) and nonlinear concepts, such as in [19, 20], have proven to successfully increase comfort. Also, the currently popu-

lar methods of artificial intelligence have been applied to controlling suspension systems for quite a long time (e.g., [21–24]). However, none of these controller designs takes knowledge about the road surface into account.

The road surface can be easily detected in autonomous cars, as autonomous driving requires a significant number of environment sensors. These can also be used for scanning the road surface in front of the car. In [25], a camera next to the rear-view mirror is used to extract the road profile from the data recorded. In [26] it is shown that a resolution of the detected road surface in millimeter range can be achieved with light detection and ranging (LIDAR) sensors mounted next to the headlights. Radar sensors also fulfill the same purpose as demonstrated in [27]. The methods used to determine the road profile based on the sensor data are discussed in [25, 26, 28]. Hence, it can be assumed that the road profile not only at the wheel but also in front of the car is known in autonomous cars. If there are not any preview sensors available, it is still possible to use a wheel-based preview approach. This means that the road disturbance is estimated when it affects the front wheel (e.g., with the method proposed in [29]) and then used as preview information for the controller of the rear wheel.

A far greater number of publications is available on how to use the preview information about road surface disturbances in control. The first one to consider this question was Bender in [30]. He designed an optimal linear preview controller based on Wiener Filter theory for a simplified linear one degree of freedom (DOF) model. Later on, a discrete optimal preview controller for a 1 DOF model and linear optimal preview controllers for a 2 DOF model were designed in [31–33]. All are a combination of a state feedback controller and a feedforward controller, and thus, require the whole state vector to be measured or estimated. Further schemes to deal with the dead time between the measurement and the effect of the disturbance in the quarter car model are the Padé approximation in continuous time and the augmentation of the state-space model in discrete-time. Based on these models, standard control approaches like LQR [34, 35] and H∞ control (e.g., [36, 37]) can be applied to design preview controllers. Due to increasing computational power, methods of model predictive control (MPC) have become popular in recent years. These are well suited for proactive vibration damping, as information about a future trajectory or disturbance can be easily included in the prediction of the system behavior [38–40]. However, the applicability of MPC in today's cars is limited, since the standard, series production control units are not yet powerful enough. Nevertheless, there are approaches for fast real-time capable MPC for vibration damping without road preview [41–43]. The real-time application of these to road preview control is still an open field with first promising results presented e.g., in [44].

Other approaches also exist that lead to a feedforward controller without a feedback portion. In [45] we proposed an optimal proactive Finite Impulse Response (FIR) filter, which is designed using an impulse response representation of the system dynamics and an optimization procedure. We applied this FIR filter as an PLDC on active vibration damping in [46], which led to very promising results. The effectiveness of adaptive FIR filters as feedforward controllers using the Filtered-x Least Mean Squares (FxLMS) algorithm was studied in [47]. To improve the convergence speed of the FxLMS algorithm we proposed a fast converging version in [48], which is based on the proactive disturbance compensator we introduced in [46]. These proactive feedforward controllers significantly enhance driving comfort by only using the knowledge about the future disturbance. However, they require a linear controller design model, so that the inherent nonlinearities of a suspension cannot be considered.

There are only a few approaches to preview feedforward control that exploit the nonlinear dynamics of a suspension. In [49], for instance, the dynamics and the inverse dynamics of the suspension are first identified using two neural networks before a third one is trained to track a reference suspension model. The results seem to be promising. However, there is no possibility of using existing knowledge about the suspension dynamics and nonlinear characteristics. Furthermore, there are many parameters that are not easy to determine.

The goal of this paper is to build a nonlinear proactive feedforward controller that can be intuitively tuned to maximize driving comfort while preserving driving safety and avoiding the suspension deflection limits. Furthermore this controller should exploit the knowledge about the future road disturbance, be applicable for different road types, and be insensitive to model mismatch and errors in the detected road profile, e.g. deviations in the preview time.

The main contribution is the design and the validation of such a controller. For this, we propose in this paper a model-based PNDC for a hybrid suspension system. It is determined based on an existing nonlinear model of the institute's quarter car test stand and has few parameters. The flatness based approach is chosen as the quarter car model is, as shown later, flat and as the FBDC has the capability to completely decouple the output from the disturbance which is assumed to be known. Moreover, the flatness based scheme allows the extension of the FBDC with the PLDC to tune the performance and include the road preview. The presented simulation results show that the proposed controller works proactively, can be intuitively tuned to realize an arbitrary performance regarding driving comfort, is insensitive to changes in the quarter car mass, and outperforms a standard feedback controller. The given results of experiments at the institute's quarter car test stand corroborate the superior performance.

The rest is organized as follows: Section 2 introduces

the theoretical background of both the FBDC and the proactive FIR filter. Section 3 formulates the problem and the goal based on the derived models and performance criteria. Section 4 contains the main results: The structure of the PNDC is explained, and its performance is examined in simulations and experiments. In Section 5, conclusions are drawn and an outlook for future work is given.

2. PRELIMINARIES

First, the theoretical background of the methods to subsequently be applied is briefly presented.

2.1. Flatness-based disturbance compensator

The FBDC was first published in [50] and [51]. The idea is to exploit the flatness property of a system to find a feedforward controller which decouples, under certain conditions, the output from a known disturbance. The design is as follows: The nonlinear system

$$\dot{\mathbf{x}} = \mathbf{f}(\mathbf{x}, u, z), \tag{1}$$
$$y = c(\mathbf{x}, u), \tag{2}$$

with input $u \in \mathbb{R}$, disturbance $z \in \mathbb{R}$, state $\mathbf{x} \in \mathbb{R}^n$, and output $y \in \mathbb{R}$ is considered. Assuming that $\mathrm{rank}(\frac{\partial \mathbf{f}(\mathbf{x}, u, z)}{\partial [u, z]}) = 2 \leq n$ and that the system with u and z as inputs is flat, a flat output

$$\mathbf{y}_f = [y_{f,1}, y_{f,2}]^T = \psi(\mathbf{x}, u, z, \dot{u}, \dot{z}, \cdots, \overset{(\alpha)}{u}, \overset{(\alpha)}{z}) \tag{3}$$

exists, such that

$$\mathbf{x} = \Phi_x(\mathbf{y}_f, \dot{\mathbf{y}}_f, \cdots, \overset{(\beta)}{\mathbf{y}}_f), \tag{4}$$
$$u = \Phi_u(\mathbf{y}_f, \dot{\mathbf{y}}_f, \cdots, \overset{(\beta+1)}{\mathbf{y}}_f), \tag{5}$$
$$z = \Phi_z(\mathbf{y}_f, \dot{\mathbf{y}}_f, \cdots, \overset{(\beta+1)}{\mathbf{y}}_f), \tag{6}$$

$\alpha > 0$, $\beta > 0$ (see e.g., [52]). Substituting (4) and (5) in (2), the output is expressed in terms of the flat output $\mathbf{y}_f$

$$y = c(\mathbf{y}_f, \dot{\mathbf{y}}_f, \cdots, \overset{(\beta+1)}{\mathbf{y}}_f). \tag{7}$$

The FBDC decouples the output y completely from the known disturbance z and tracks exactly the desired output trajectory y_d. This is achieved by finding a desired flat output trajectory $\mathbf{y}_{f,d}$ such that

$$c(\mathbf{y}_{f,d}, \dot{\mathbf{y}}_{f,d}, \cdots, \overset{(\beta+1)}{\mathbf{y}}_{f,d}) = y_d, \tag{8}$$
$$\Phi_z(\mathbf{y}_{f,d}, \dot{\mathbf{y}}_{f,d}, \cdots, \overset{(\beta+1)}{\mathbf{y}}_{f,d}) = z. \tag{9}$$

The required control input results then with (5) in

$$u = \Phi_u(\mathbf{y}_{f,d}, \dot{\mathbf{y}}_{f,d}, \cdots, \overset{(\beta+1)}{\mathbf{y}}_{f,d}). \tag{10}$$

To find the desired flat output trajectory, the implicit differential equations (8) and (9) have to be solved. Exact tracking and disturbance decoupling will only be achieved at any time t if the initial state satisfies

$$\mathbf{x}(0) = \Phi_x(\mathbf{y}_{f,d}(0), \dot{\mathbf{y}}_{f,d}(0), \cdots, \overset{(\beta)}{\mathbf{y}}_{f,d}(0)). \tag{11}$$

As (11) is a possibly nonlinear mapping, it is not assured that there is a solution for a given initial state $\mathbf{x}(0)$. In such a case, it is still possible to achieve asymptotic disturbance decoupling as presented in [51].

Furthermore, the following two challenges may arise when designing the FBDC:

1) As the FBDC contains the inverted system dynamics, the input u can become unbounded in the case of unstable internal dynamics of (1) with respect to the output (2). The internal dynamics describes a portion of the dynamics that remains unobservable in the input-output behavior of a plant. For a formal definition see [53].

2) The calculation of the control input (10) and the solution of the differential equations (8), (9) may require to derive the flat desired output with respect to time: $\overset{(\delta)}{\mathbf{y}}_{f,d}$. If the flat desired output to be derived depends directly on the desired trajectory y_d or the road disturbance z the derivative of these will be needed to calculate the input u. If y_d and z are not smooth enough, the required derivatives of y_d and z can become unbounded and thus, an unbounded input u can occur.

2.2. Proactive FIR filter

If the input-output behavior of a Single-Input Single-Output (SISO) system is to be inverted, e.g. for the design of a feedforward controller, several drawbacks may arise. Assuming, that the input-output behavior is described with a discrete-time transfer function

$$G_d(z) = \frac{Y_d(z)}{U_d(z)} = \frac{b_{d,0}z^q + b_{d,1}z^{q-1} + \cdots + b_{d,q}}{z^n + a_{d,1}z^{n-1} + \cdots + a_{d,n}}, \tag{12}$$

with coefficients $a_{d,i}, b_{d,i}$, the inverted dynamics is determined by inverting the transfer function (12). However, in the case of zeros outside the unit disk, the simple inversion leads to unstable dynamics of the feedforward controller and thus to infinitely increasing inputs. Furthermore, the inversion of the transfer function (12) does theoretically lead to exact tracking, but often there are further requirements, for example, the minimization of the required input. This cannot be considered in a classical system inversion. To overcome these drawbacks we proposed a method to design the proactive FIR filter in [45]. This FIR filter is an optimized inverse of the system dynamics taking several requirements, e.g., output tracking, input minimization and input increment minimization, into account. Furthermore the FIR filter is capable of using preview information to act proactively. The design method is applicable

for all Linear Time-Invariant (LTI), asymptotically stable systems. As an FIR filter is inherently stable it is very convenient to use it as feedforward controller for asymptotically stable systems.

This approach, which can be seen as a variant of dynamic matrix control [54], uses an impulse response representation of the system dynamics to determine an optimal, non-causal–and thus proactive–inverse of the system. The transfer function from input u to output y of the time-discrete, LTI system (12) can be approximated by an FIR filter

$$G_{FIR}(z) = \frac{g_0 z^N + g_1 z^{N-1} + \cdots + g_N}{z^N}. \tag{13}$$

To facilitate the calculations, the convolution that the FIR filter performs can be expressed under the restriction of a finite length input sequence $u[n]$ and output sequence $y[n]$ as a matrix product

$$\mathbf{y} = \begin{bmatrix} y_0 \\ \vdots \\ y_{N+M} \end{bmatrix} = \begin{bmatrix} g_0 & & \\ \vdots & \ddots & \\ g_N & & g_0 \\ & \ddots & \vdots \\ & & g_N \end{bmatrix} \begin{bmatrix} u_0 \\ \vdots \\ u_M \end{bmatrix} = \mathbf{Gu}, \tag{14}$$

with the Toeplitz matrix $\mathbf{G}$ called "dynamic matrix" [54]. In each column, the matrix $\mathbf{G}$ contains the coefficients of the FIR filter and, thus, the impulse response of the system. The optimal proactive FIR filter is found by minimizing the cost function

$$J = \mathbf{e}^T \mathbf{Q} \mathbf{e} + \mathbf{u}^T \mathbf{R} \mathbf{u} + \Delta \mathbf{u}^T \tilde{\mathbf{R}} \Delta \mathbf{u}, \tag{15}$$

with $\mathbf{e} = \mathbf{y}_d - \mathbf{y} = \mathbf{y}_d - \mathbf{Gu}$ and

$$\Delta \mathbf{u} = \begin{bmatrix} 1 & & & \\ -1 & 1 & & \\ & \ddots & \ddots & \\ & & -1 & 1 \end{bmatrix} \mathbf{u} = \mathbf{Du}. \tag{16}$$

The matrices $\mathbf{Q}, \mathbf{R}$ and $\tilde{\mathbf{R}}$ are of the form $k_{\{Q,R,\tilde{R}\}} \mathbf{I}$ with $k > 0$ and weight the deviation $\mathbf{e}$ from the desired trajectory $\mathbf{y}_d$, the input amplitudes, and the input increment, respectively. The minimization of (15) with respect to $\mathbf{u}$ yields the optimal control sequence $\mathbf{u}^*$

$$\mathbf{u}^* = (\mathbf{G}^T \mathbf{Q} \mathbf{G} + \mathbf{R} + \mathbf{D}^T \tilde{\mathbf{R}} \mathbf{D})^{-1} \mathbf{G}^T \mathbf{Q} \mathbf{y}_d = \mathbf{F} \mathbf{y}_d. \tag{17}$$

As stated in [45], the matrix $\mathbf{F}$ has a Toeplitz-like structure, such that the entries f_i of the p-th column of $\mathbf{F}$ can be used as the coefficients of an FIR filter

$$F_z(z) = \frac{f_0 z^M + f_1 z^{M-1} + \cdots + f_M}{z^{M-(p-1)}}. \tag{18}$$

Thus, the restriction of a finite length input and output sequence becomes obsolete. The choice of the column p,

whose entries are used as filter coefficients, depends on the available number of preview values of the desired trajectory. For $N_{pre} < M$ preview values, the entries in the $p = 1 + N_{pre}$-th column are to be used. As shown in [45], this FIR filter (18) behaves proactively.

3. PROBLEM AND GOAL FORMULATION

The main goal of vibration damping in a quarter car is to increase the comfort without decreasing the driving safety while meeting the suspension deflection limits. However, there are further requirements and assumptions that will be derived in the following subsections.

3.1. Quarter car dynamics and challenges

For the controller design and the simulations, various dynamic models will be used. As only the heave dynamics are to be considered (no pitching or rolling), it is sufficient to model only the quarter of a car. At first the fully active nonlinear quarter car (see Fig. 1(a)) is introduced, on which the controller design is based. The hybrid quarter car model with non-ideal actuators (see Fig. 1(b)) that is used for simulation purposes is then presented.

The equations of motion of the fully active quarter car can be derived via Newton's law regarding a two mass oscillator. The suspension is modeled to include effects such as nonlinear damper and spring characteristics, whereas the tire is modeled using the linear Gehmann model [1]. To present the dynamics in state-space, the state $\mathbf{x} = [z_c - z_w, \ \dot{z}_c, \ z_w - z_g, \ \dot{z}_w, \ z_h - z_g]^T$ is defined, which includes the suspension deflection, chassis mass (m_c) velocity, tire deflection, wheel mass (m_w) velocity, and deflection of the Gehmann damper (d_w), respectively.

The state-space model is as follows:

$$\dot{\mathbf{x}} = \mathbf{f}_c(\mathbf{x}) + \mathbf{G}_c[u \ z]^T, \tag{19}$$

$$\mathbf{f}_c = \begin{bmatrix} x_2 - x_4 \\ \frac{1}{m_c}\left(-\frac{i_x}{i_0} m_c g x_1 - F_d(\mathbf{x}) - F_c(\mathbf{x}) - F_r(\mathbf{x})\right) \\ x_4 \\ \frac{\frac{i_x}{i_0} m_c g x_1 + F_d(\mathbf{x}) + F_c(\mathbf{x}) + F_r(\mathbf{x}) + F_{dyn}(\mathbf{x})}{m_w} \\ \frac{c_g}{d_w}(x_3 - x_5) \end{bmatrix},$$
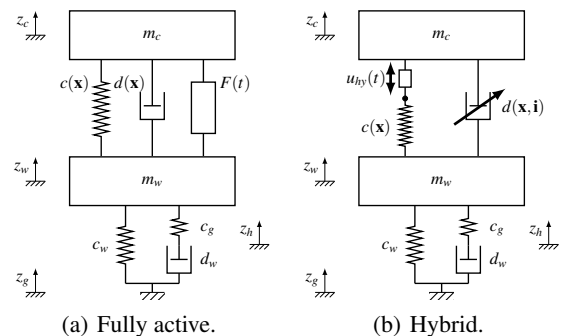

(a) Fully active. (b) Hybrid.
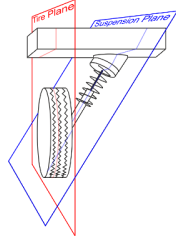
Fig. 1. Quarter car models [46].

Fig. 2. Suspension and tire plane.

$$\mathbf{G}_c = \begin{bmatrix} 0 & \frac{1}{m_c} & 0 & -\frac{1}{m_w} & 0 \\ 0 & 0 & -1 & 0 & 0 \end{bmatrix}^T,$$

$$y = \ddot{z}_c = \frac{-\frac{i_x}{i_0} m_c g x_1 - F_d(\mathbf{x}) - F_c(\mathbf{x}) - F_r(\mathbf{x}) + u}{m_c},$$
(20)

with the arbitrary input force u, the controlled output y and the time derivative of the road elevation z_g as disturbance input $z = \dot{z}_g$. All coordinates and forces are assumed to be in the tire plane (see Fig. 2). However, the actual damper and spring force are in the suspension plane, due to the inclined position of the suspension (see Fig. 2).

As the inclination depends on the suspension deflection, a dynamic kinematic transmission ratio i_{dyn} is introduced to convert forces, velocities, and deflections from one plane to the other

$$i_{dyn} = \frac{\dot{z}_c^{SP} - \dot{z}_w^{SP}}{\dot{z}_c - \dot{z}_w} = \frac{F}{F^{SP}} = i_0 - i_x(z_c - z_w) = i_0 - i_x x_1,$$
(21)

where the superscript SP denotes quantities in the suspension plane, i_0 is the constant transmission factor in the equilibrium, and i_x the deflection-dependent transmission ratio (for details see [55]).

Modeling was performed at the equilibrium point of the quarter car. Thus, gravitational forces are compensated by the springs and do not have to be taken into account. However, the changes in the gravitational force of the chassis mass in the tire plane, which arise due to the kinematic transmission, do have to be considered. This is achieved using the correction term $\frac{i_x}{i_0} m_c g x_1$. The forces F_d, F_c, and F_r are the nonlinear damper, spring, and friction force, respectively:

$$F_d(\mathbf{x}) = i_{dyn}(x_1) \cdot d(i_{dyn} \cdot (x_2 - x_4)),$$
(22)

$$F_c(\mathbf{x}) = i_{dyn}(x_1) \cdot (c_{MS} i_0 x_1 - c_{AS}(-i_0 x_1)),$$
(23)

$$F_r(\mathbf{x}) = F_{r,max} \tanh(c_r \cdot (x_2 - x_4)).$$
(24)

The nonlinear function $d(i_{dyn} \cdot (x_2 - x_4))$ represents the damping characteristics as depicted in Fig. 3 for the damper valve current of 1.2 A. The damper valve current is chosen to 1.2 A as the damping ratio of the linearized system is approximately 0.21, which resembles the ratio
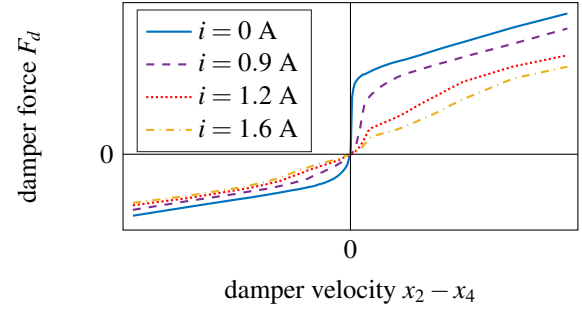
Fig. 3. Damping characteristics.
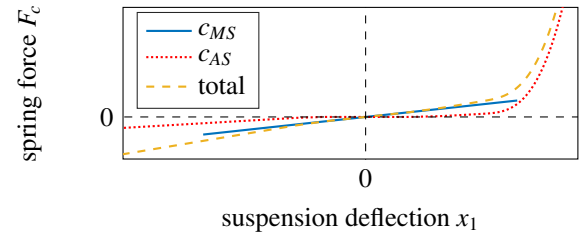
Fig. 4. Nonlinear spring characteristics.

of a typical, comfort oriented upperclass vehicle [15]. The spring force is composed of the main spring's linear stiffness c_{MS} and a nonlinear additional stiffness c_{AS} as shown in Fig. 4. The damper and spring characteristics are both implemented as look-up tables with linear interpolation. Furthermore, the dynamic transmission ratio for the displacement

$$z_c^{SP} - z_w^{SP} = i_0(z_c - z_w) - \frac{1}{2} i_x(z_c - z_w)^2$$
(25)

was linearized around the equilibrium

$$z_c^{SP} - z_w^{SP} \approx i_0(z_c - z_w)$$
(26)

as the maximum relative error arising at maximum suspension deflection is less than 4%. The wheel mass is additionally affected by the dynamic wheel force

$$F_{dyn} = -c_w x_3 - c_g \cdot (x_3 - x_5).$$
(27)

This force results from the interaction between tire and road. The tire is modeled using the linear Gehmann model, which consists of a main spring (stiffness c_w) parallel to a spring (stiffness c_g) and a damper (damping d_w) in series (see Fig. 1(a)).

The parameters for the nonlinear suspension model can be found in Table 1. The FBDC design is based on the presented model ("controller design model").

Two different models are used for the simulations. The first is almost identical to the controller design model. The only difference is the quadratic dynamic transmission ratio

Table 1. Nominal parameters.

Description	Parameter	Value
Chassis mass	m_c	507 kg
Wheel mass	m_w	68 kg
Tire stiffness	c_w	378 000 N/m
Tire damping	d_w	130 Ns/m
Gehmann stiffness	c_g	52 900 N/m
Const. transm. factor	i_0	0.685
Vari. transm. factor	i_x	0.309 1/m
Gravitational acceleration	g	9.81 m/s^2
Max. Coulomb-friction	$F_{r,max}$	65 N
Friction coefficient	c_r	0.04

(25) for the suspension displacement. As one ideal actuator is assumed for this model (see Fig. 1(a)) it is referred to as the "fully active model".

The second simulation model, called the "hybrid model," has the same dynamics as the fully active model. The only difference here is that the ideal actuator is replaced by a slow, hydraulic actuator between the spring and chassis (the so-called Spring Mount Adjustment (SMA), cut-off frequency ≈ 5 Hz) and a damper with variable damping (see Fig. 1(b)). The damping characteristics for various damper valve currents are shown in Fig. 3. To apply the feedforward controller to the hybrid model, the input force determined has to be split into two portions: one for the SMA and one for the damper. This is done in a dynamic optimal way [55]. This Dynamic Optimal Allocation (DOA) is also used for the experiments at the quarter car test stand at the authors' institute.

There are three challenges for the controller design that can be deduced from the modeling of the quarter car. The first one is the nonlinear dynamic, especially the spring and damper characteristics, which have to be taken into account. The second problem is that of the non ideal actuators in the hybrid model which represent the institute's test stand's configuration. The feedforward controller has to be insensitive to the actuator model mismatch between the controller design model and the more realistic hybrid model. The third challenging aspect is the parameter variation of the quarter car models. While damping and stiffness parameters usually vary very slowly over the lifespan of a car, the chassis mass experiences sudden remarkable changes, e.g. due to different number of persons traveling in the car.

3.2. Road profiles

Two different road profiles are used for simulations and tests. The first one is the profile of a highway traveled at a speed of 80 km/h (see Fig. 5). It is a synthetic profile generated by filtering a Gaussian white noise. The filter's amplitude characteristic ensures that the power spectral den-
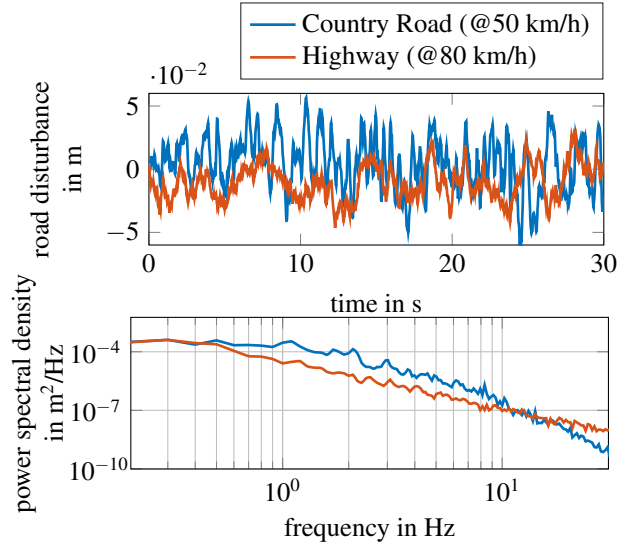

Fig. 5. Road profiles.

sity Φ of the generated road obeys the relation

$$\Phi(\Omega) = \Phi(\Omega_0) \left[\frac{\Omega}{\Omega_0} \right]^{-w}, \tag{28}$$

with angular spatial velocity Ω, waviness $w = 2.4$, roughness $\Phi(\Omega_0) = 5.3 \, \text{cm}^3$ and the reference wave number $\Omega_0 = 1 \, \text{m}^{-1}$ (for details see [1, 56]). The smaller the waviness w, the bigger is the portion of waves with high amplitudes and small wave lengths in the road profile [1]. This profile is used for choosing suitable disturbance compensator parameters and testing the compensator's sensitivity to model parameter variations and measurement errors in the road profile. Besides the road profile model in (28), there exist also models which describe the road profile as a superposition of M harmonics (for details see [57]).

As the disturbance compensator has to work for different types of roads, the road profile of a bad country road traveled at a speed of 50 km/h is introduced (see Fig. 5). This is a measured profile of a real country road, which has in the range from 0.5 Hz to 10 Hz considerably higher amplitudes. It is used for examining the overall performance of the compensator in simulations and experiments.

For all simulations and experiments it is assumed that the road profiles do not contain any low frequency parts, which would occur when, for example, driving up a hill. This is a valid assumption, as the preview sensors mounted in the car body change their orientation simultaneously with the car. Thus, the detected road surface is automatically high pass filtered.

3.3. Performance criteria

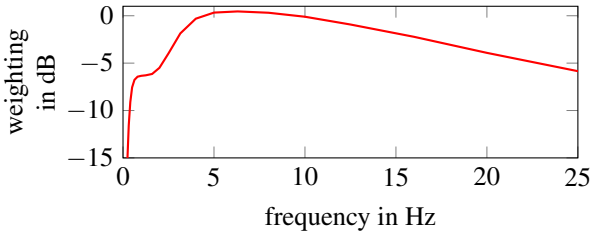Below, the performance criteria and the performance measure are presented.

Fig. 6. Frequency weighting filter according to [59].

3.3.1 Driving comfort

The quantity that is the most difficult to determine is comfort, since this is usually perceived quite subjectively. The ISO standard 2631-1 [58] and VDI guideline 2057 [59] state that the influence of vibrations on the human body can be measured via the acceleration. Thus, the chassis acceleration $\ddot{z}_c$ is used to evaluate comfort. High driving comfort is achieved with low acceleration $\ddot{z}_c$. Since the human body perceives vibrations depending on their frequency, a comfort filter for whole-body vibration in a vertical direction is proposed in [59] (see Fig. 6). The frequency-weighted chassis acceleration is denoted as $\ddot{z}_{c,comf}$.

3.3.2 Driving safety

Driving safety can be measured via the dynamic wheel load $F_{dyn} = -c_w x_3 - c_g(x_3 - x_5)$. To avoid contact loss between road and tire, the dynamic wheel load has to be smaller than the negative force of gravity of the quarter car: $F_{dyn} < -(m_c + m_w)g$ with acceleration of gravity g. Thus, the aim is to minimize F_{dyn} to guarantee driving safety.

3.3.3 Suspension deflection

The third quantity under evaluation is the suspension deflection $z_{cw} = z_c - z_w$. As the suspension is designed to move, a minimization of z_{cw} is not necessary. Instead, the deflection limits must be met. Since exceeding the compression limit leads to shocks in the chassis and thus to low comfort, it is particularly important for the minimum suspension deflection $\min(z_{cw})$ to be taken into account.

3.3.4 Performance measure

All these quantities are varying in time. To compare them, their root mean square (RMS) value (denoted as $|\cdot|$) is used. As the absolute RMS values depend on the road disturbances, general conclusions are difficult to draw. Therefore, these values are viewed in relation to the corresponding values from a passive quarter car that traveled on the same road:

$$\Gamma(\cdot) = 1 - \frac{|\cdot|_{controlled}}{|\cdot|_{passive}}. \tag{29}$$

Fig. 7. Hybrid suspension.

A positive Γ represents an improvement, a negative one a decrease in performance. The passive quarter car is modeled for simulation purposes identically to the "fully active model" but without an input force (damper current $i = 1.2\,\text{A}$). In experiments, the passive quarter car is realized by keeping the damper current at $i = 1.2\,\text{A}$ and the SMA at a fixed position.

3.4. Quarter car test stand

The controller is supposed to be applied to a real car. To test whether simulation results represent the real world behavior, experiments at the authors' institute's quarter car test stand are conducted. The test stand has a hybrid double wishbone suspension comprising a variable damper (Fig. 7, red frame) and a wheel from a BMW 7 Series car (model year 2009) and additionally an SMA from a Mercedes SL Roadster (Fig. 7, blue frame). The damper has a cutoff frequency of approx. 16 Hz and the bandwidth of the SMA is 0 to 5 Hz.

The measured quantities used for the feedback controllers are chassis acceleration, suspension deflection and wheel acceleration. The wheel mass and the chassis mass equal the values in table 1. The spring and damper characteristics presented in Section 3.1 are the recorded values of the test stand for constant deflection and constant damper velocities, respectively. The road disturbance is realized via a hydraulic cylinder. The controllers are implemented in Simulink and executed on a dSpace DS1103 PPC Controller Board with a sample time of 1 ms. For further details see [60]. The challenges for applying the proposed approach to the test stand are unmodeled effects like damper hysteresis, friction, and tire behavior.

3.5. Goal formulation

As previously stated, the objective of vibration control of a quarter car is threefold: maximization of driving comfort, preservation of driving safety, and avoidance of reaching the suspension deflection limits.

The aim of this paper is to design a disturbance compensator with the best possible performance regarding the above three objectives while considering the following challenges: nonlinear dynamics, proactive behavior, model mismatch, erroneous road profile data, different road types, and tunability.

4. MAIN RESULTS

Fig. 8 shows the general structure of the PNDC developed in this paper. It consists of the two feedforward
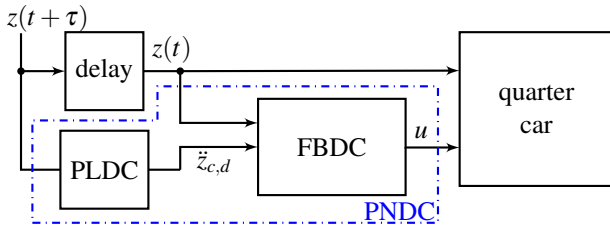
Fig. 8. Structure of the PNDC.

controllers FBDC and PLDC. The former determines the quarter car's input u based on the current road disturbance $z(t)$ at the wheel and on the desired chassis acceleration $\ddot{z}_{c,d}$. The PLDC computes the desired chassis acceleration $\ddot{z}_{c,d}$ based on the future road disturbance $z(t+\tau)$ in front of the car, in order to ensure that the PNDC acts proactively.

In this section, the design of the FBDC for the nonlinear quarter car and the extension with the PLDC are presented, as well as simulation and experimental results.

4.1. Nonlinear proactive disturbance compensator

The design of the FBDC is based on a flat output of the system (19) with u and z as inputs. It is found by constructing an output, for which the state space exact linearization problem is solvable (for details see [53, 61]). According to [61] and [62] such outputs are always flat outputs. The constructed flat output for the controller design model (19) is

$$\begin{bmatrix} y_{f,1} \\ y_{f,2} \end{bmatrix} = \begin{bmatrix} m_c x_2 + m_w x_4 + \frac{d_w}{c_g}(c_g + c_w)x_5 \\ x_1 \end{bmatrix}, \quad (30)$$

since (4),(5), and (6) are fulfilled:

$$x_1 = y_{f,2}, \quad (31)$$

$$x_2 = \frac{c_g c_w y_{f,1} + (c_g d_w + c_w d_w)\dot{y}_{f,1} + c_g c_w m_w \ddot{y}_{f,2}}{c_g c_w (m_c + m_w)}, \quad (32)$$

$$x_3 = -\frac{c_g \ddot{y}_{f,1} + d_w \dddot{y}_{f,1}}{c_g c_w}, \quad (33)$$

$$x_4 = \frac{c_g c_w y_{f,1} + (c_g d_w + c_w d_w)\dot{y}_{f,1} - c_g c_w m_c \ddot{y}_{f,2}}{c_g c_w (m_c + m_w)}, \quad (34)$$

$$x_5 = -\frac{\dot{y}_{f,1}}{c_w}, \quad (35)$$

$$z = \frac{d_w \dddot{y}_{f,1}}{c_g c_w} + \frac{y_{f,1} - m_c \ddot{y}_{f,2}}{m_c + m_w}$$
$$+ \frac{(c_g + c_w)d_w \dot{y}_{f,1} + (c_g m_c + c_w m_w)\ddot{y}_{f,1}}{(m_c + m_w)c_g c_w}$$
$$= \Phi_z(\mathbf{y}_f, \dot{\mathbf{y}}_f, \ddot{\mathbf{y}}_f, \dddot{\mathbf{y}}_f), \quad (36)$$

$$u = \frac{m_c m_w}{m_c + m_w}\left(\frac{(c_g d_w + c_w d_w)\ddot{y}_{f,1}}{c_g c_w m_w} + \ddot{y}_{f,2} + \frac{\dot{y}_{f,1}}{m_w}\right.$$

$$\left. + \frac{F_c(y_{f,2}) + F_r(\dot{y}_{f,2}) + F_d(\mathbf{y}_f, \dot{\mathbf{y}}_f) + \frac{1}{i_0}i_x g m_c y_{f,2}}{m_w} \right.$$

$$\left. + \frac{F_d(\mathbf{y}_f, \dot{\mathbf{y}}_f) + F_r(\dot{y}_{f,2}) + \frac{1}{i_0}i_x g m_c y_{f,2} + F_c(y_{f,2})}{m_c} \right)$$

$$= h(\mathbf{y}_f, \dot{\mathbf{y}}_f, \ddot{\mathbf{y}}_f). \quad (37)$$

The output to be controlled is the chassis acceleration, as the goal is to maximize comfort

$$y = \ddot{z}_c = \dot{x}_2$$
$$= \frac{c_g c_w \dot{y}_{f,1} + (c_g + c_w)d_w \ddot{y}_{f,1} + c_g c_w m_w \dddot{y}_{f,2}}{c_g c_w (m_c + m_w)}$$
$$= c(\dot{\mathbf{y}}_f, \ddot{\mathbf{y}}_f). \quad (38)$$

The desired flat output trajectory $\mathbf{y}_{f,d}$ is found by solving $c(\dot{\mathbf{y}}_{f,d}, \ddot{\mathbf{y}}_{f,d}) = y_d$ and $\Phi_z(\mathbf{y}_{f,d}, \dot{\mathbf{y}}_{f,d}, \ddot{\mathbf{y}}_{f,d}, \dddot{\mathbf{y}}_{f,d}) = z$ with the trajectories $y_d = \ddot{z}_{c,d}$ and z assumed to be known. Inserting $\mathbf{y}_{f,d}$ in (37) yields the input force u. As (36) and (38) are linear differential equations in $\mathbf{y}_f$, a linear time-invariant state-space system with linear output y_2 and nonlinear output mapping y_1 can be built

$$\dot{\mathbf{x}}_f = \mathbf{A}\mathbf{x}_f + \mathbf{b}w + \mathbf{e}z \quad (39)$$
$$\text{with } \mathbf{x}_f = [y_{f,d,1} \ \dot{y}_{f,d,1} \ \ddot{y}_{f,d,1} \ y_{f,d,2} \ \dot{y}_{f,d,2}]^T$$
$$\text{with } w = y_d + u_c,$$
$$y_1 = u = h(\mathbf{y}_{f,d}, \dot{\mathbf{y}}_{f,d}, \ddot{\mathbf{y}}_{f,d}), \quad (40)$$
$$y_2 = F_{dyn} = \mathbf{c}\mathbf{x}_f = [0 \ 1 \ \frac{c_g d_w + c_w d_w}{c_g c_w} \ 0 \ 0]\mathbf{x}_f \quad (41)$$

to determine the solution $\mathbf{y}_{f,d}$ and calculate the required input force $y_1 = u$. The matrices $\mathbf{A}, \mathbf{b}$ and $\mathbf{e}$ are shown in Appendix A. The solution of (39) yields the trajectories for the desired flat outputs $\mathbf{y}_{f,d}$ and their derivatives. Choosing $\mathbf{x}_f(0) = \mathbf{0}$ leads with (31)-(35) to $\mathbf{x}(0) = \mathbf{0}$. The quarter car is indeed in this state at time $t = 0$, as we assume that the disturbance compensator will start to work, when the car is started, which is in the equilibrium point. Thus, the condition (11) holds and exact disturbance rejection is possible.

The output $y_1 = h(\mathbf{y}_f, \dot{\mathbf{y}}_f, \ddot{\mathbf{y}}_f)$ is a sum of in $\mathbb{R}$ continuous functions $f_i(a)$ with the properties

$$f_i(0) = 0, \text{ and } f_i(a)a \geq 0 \ \forall a. \quad (42)$$

As the sum of continuous functions is again a continuous function, $h(\mathbf{y}_f, \dot{\mathbf{y}}_f, \ddot{\mathbf{y}}_f)$ is also continuous. Hence, the input $u = y_1 = h(\mathbf{y}_{f,d}, \dot{\mathbf{y}}_{f,d}, \ddot{\mathbf{y}}_{f,d})$ remains bounded, if its arguments are bounded. The arguments of h are the state $\mathbf{x}_f$ and the derivative of the state $\dot{\mathbf{x}}_f$ of the system (39). These are bounded, if the system is asymptotically stable and the disturbance z and the desired trajectory y_d are bounded. However, the linear system (39) has two zero eigenvalues, which cause instability. Therefore, a state feedback controller $u_c = \mathbf{K}\mathbf{x}_f$, which shifts the zero eigenvalues to the
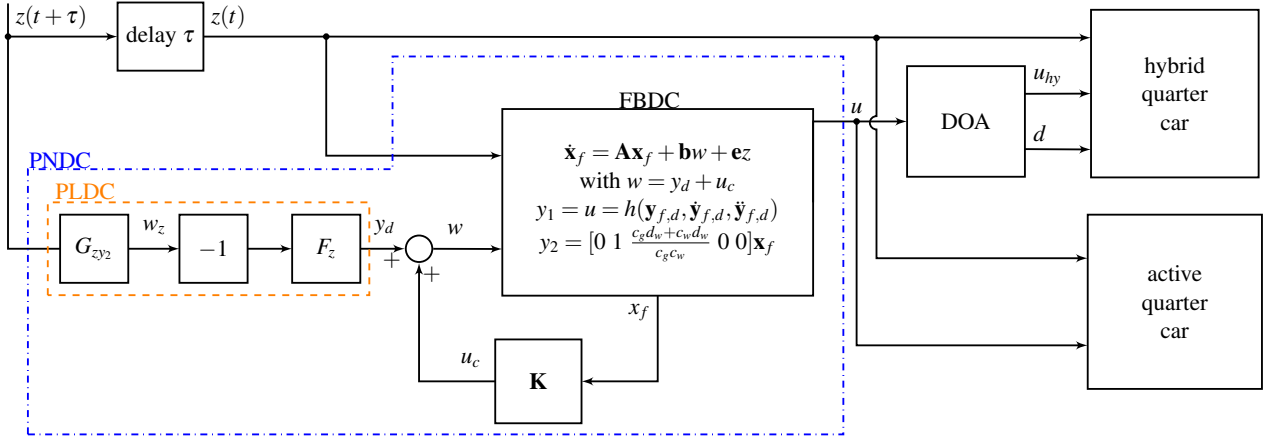
Fig. 9. Detailed structure of the PNDC.

negative complex half plane, is added. Thus, the input w of the system (39) consists of the sum of the desired chassis acceleration y_d and the control input u_c. The influence of the controller will be examined in Section 4.2 As the controlled system (43) is asymptotically stable, the calculated input u is bounded, as long as the disturbance w and the desired chassis acceleration $\ddot{z}_{c,d} = y_d$ remain bounded.

If the desired chassis acceleration is set to $\ddot{z}_{c,d} = y_d = 0$, the FBDC fully compensates–in the case of ideal actuators and the controller design model as simulation model–the disturbance so that $\ddot{z}_c$ equals 0. However, this causes high dynamic wheel loads and thus, a loss of driving safety (see Section 4.2). To find a compromise, the desired trajectory for the chassis acceleration y_d has to be modified.

This is done via the proactive FIR filter presented in Section 2.2 The idea is to consider the FBDC as a dynamic system with input $y_d = \ddot{z}_{c,d}$, disturbance z, and output $y_2 = F_{dyn}$ (see (41)). For this system a PLDC is designed that determines proactively the input y_d based on the future disturbance z such that the influence of the disturbance on the output y_2 is reduced. This is done by minimizing a cost function comprising the input y_d and the output y_2. Depending on the weighting of these two objectives the focus is set more on the minimization of the input y_d or more on the reduction of the output y_2, which corresponds to a maximization of the driving comfort and the driving safety, respectively. Thus, an arbitrary trade-off between comfort and safety can be set by changing the weighting in the cost function. The design of the PLDC is based on the with $u_c = \mathbf{K}\mathbf{x}_f$ controlled system (39):

$$\dot{\mathbf{x}}_f = (\mathbf{A} - \mathbf{b}\mathbf{K})\mathbf{x}_f + \mathbf{b}y_d + \mathbf{e}z. \quad (43)$$

As the system (39) is the feedforward controller and thus a virtual system, there are not any input constraints. Hence, the additional input $u_c = \mathbf{K}\mathbf{x}_f$ does not violate any saturation limits. However, it is important to consider the input saturation of the quarter car plant. The input of the quarter car is the output of the FBDC. The controller u_c

stabilizes the FBDC (39) to keep this output in an admissible range. The system (43) with the output (41) is a linear, time-invariant, asymptotically stable system. For this, a PLDC can be built as in [46]. The first step is to determine the transfer function

$$G_{zy_2} = \mathbf{c}(s\mathbf{I} - (\mathbf{A} - \mathbf{b}\mathbf{K}))^{-1}\mathbf{e} \quad (44)$$

representing the effect w_z of the disturbance z on the output $y_2 = F_{dyn}$. To reduce this effect, the inverted effect $-w_z$ has to be realized at the output y_2 through a suitable input trajectory y_d, which is determined with a feedforward controller (see Fig. 9). To exploit the disturbance preview, the proactive FIR filter F_z presented in Section 2.2 is used for this. Thus, $-w_z$ is the input for the FIR filter F_z. As it is assumed that the road disturbance is known in advance ($z(t + \tau)$), the FIR filter uses $-w_z(t + \tau)$ as input to act proactively. To determine the proactive FIR filter F_z, the transfer function $G_{y_d y_2}$ from input y_d to output $y_2 = F_{dyn}$ is discretized (sampling time 1 ms - according to the test stand's sampling time) and approximated with a dynamic matrix ($M = 1000$, $N = 1999$) and the steps presented in Section 2.2 are followed. The input increment Δu in (15) is neglected and the weighting factor k_Q of the output error in $y_2 = F_{dyn}$ is set to 10^{-3}. As the input of the linear closed-loop system (43) is the desired chassis acceleration y_d, the focus can be arbitrarily shifted from driving safety to driving comfort by adjusting just one parameter: the input weighting k_R.

4.2. Simulation results

In this section, the simulation results regarding parameter variations and sensitivity to measurement noise are analyzed. These simulations are all performed with the highway profile as disturbance (see Section 3.2). To examine the performance dependency on the road profile, further simulations are carried out with the measured road profile of the bad country road presented in Section 3.2 Furthermore, the simulation results based on this real world road
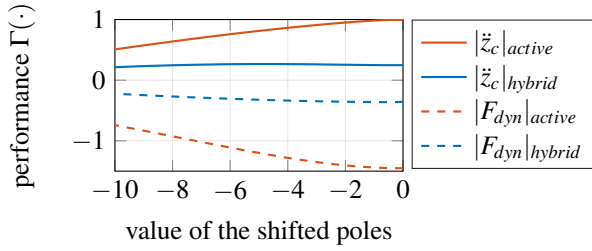
Fig. 10. Influence of the eigenvalues of the controlled system (39).

Fig. 11. Influence of the weighting factor k_R (top left $k_R = 10^5$ to bottom right $k_R = 10^{-4}$).

profile will be compared with the experimental results in Section 4.3 It is assumed that the road profile is exactly known in all simulations and experiments except the simulations for testing the sensitivity to errors in the disturbance signal.

4.2.1 Influence of the pole placement on the FBDC

First, the FBDC is examined. Fig. 10 shows the influence of the pole placement via the controller $\mathbf{K}$ on both comfort and safety performance. The controller shifts only the two zero eigenvalues, whereas the other three remain at their position. The results are presented for the fully active and hybrid models.

The fully active model completely compensates chassis acceleration for eigenvalues in zero or close to zero ($\Gamma(\ddot{z}_c) = 1$). The price of the perfect compensation is the loss of driving safety. When the eigenvalues decrease, the performance $\Gamma(\ddot{z}_c)$ of the active system degrades, while driving safety increases. However, driving safety is always worse than the passive suspension. Therefore, the PLDC is introduced in the next step. Generally spoken, the closer the poles are to zero, the better low frequencies can be compensated. The smaller the two eigenvalues are chosen, the bigger is the influence of the controller $u_c = \mathbf{K}\mathbf{x}_f$ compared to the desired trajectory $w = y_d$. For further investigations concerning the active model, the eigenvalues are set to -0.1. The simulations show that the hybrid model cannot achieve the performance of the active models due to the non-ideal actuators. The best performance in terms of comfort is achieved with eigenvalues in -4.7, which will be used in the rest of the paper for simulations with the hybrid model.

4.2.2 Influence of the weighting factor of the PNDC

To achieve a comfort improvement without a decrease in driving safety, the PLDC is added. As driving comfort and safety are two conflicting goals, the PLDC will increase the safety at the cost of the driving comfort, at least in the fully active case. The preview time τ is set to 0.5 s, which is, as will be shown later, long enough to obtain a good performance. Fig. 11 presents the performance of the PNDC depending on the weighting factor k_R.
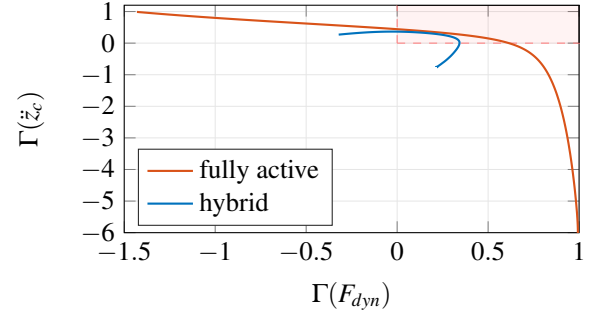
For the active model, arbitrary performance in one objective category can be chosen by varying k_R: from perfect road holding ($\Gamma(F_{dyn}) = 1$) to perfect comfort ($\Gamma(\ddot{z}_c) = 1$). This is enabled by the minimization of the PLDC's objective function (15). The parameter k_R weights the chassis acceleration $\ddot{z}_c$ in (15). The bigger k_R the bigger is the influence of $\ddot{z}_c$ on the costs and the smaller has to be $\ddot{z}_{c,d}$ to minimize (15). Thus, the comfort is improved when k_R is increased.

The maximum performance for the hybrid model is, again, much lower. However in the interesting region in Fig. 11 (red shaded), both objectives are better than or equal to the passive quarter car, but never worse. The performance of the hybrid model in this area is almost as good as that of the fully active model. The maximum achievable comfort for the hybrid model is greater with the PNDC ($\Gamma(\ddot{z}_c)_{max} = 0.365$) than with the FBDC only ($\Gamma(\ddot{z}_c)_{max} = 0.267$, see Fig. 10). As the goal is to improve comfort as much as possible without decreasing safety, the weighting factor k_R is chosen so that $\Gamma(F_{dyn}) = 0$ ($k_R = 447.3$ for the fully active model, $k_R = 687.1$ for the hybrid one).

4.2.3 Influence of the preview time

Next, the PNDCs with those comfort optimal weighting factors are used to investigate the influence of the preview length. For this, the quarter car disturbed with the highway profile is simulated with various constant preview
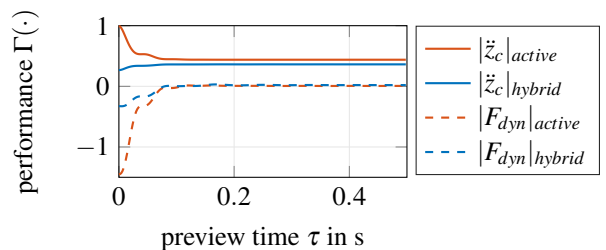

Fig. 12. Influence of preview time τ.

times. The PNDCs applied are also designed for these preview times. Fig. 12 shows the simulation results. Starting at 0.1 s, the performance does not change any more and stays at the desired level: no decrease in driving safety while improving the comfort as much as possible. From 0 s to 0.1 s, the behavior of the active model and the hybrid model differ. The comfort of the active simulation rises with decreasing preview time. If the preview time for the FIR filter F_z is too short, the possible reduction of the dynamic wheel load decreases. Thus, the minimum of the cost function (15) is shifted so that a smaller input leads to lower costs. As the input of the closed-loop system (39) represents the desired chassis acceleration y_d, a short preview time leads to small amplitudes in y_d. If there is no preview, y_d is almost zero and the PNDC resembles the FBDC. Thus, the PLDC becomes ineffective and the quarter car has maximum driving comfort but a loss of driving safety. Therefore, a shorter preview time leads to increased driving comfort and decreased safety in the case of the fully active simulation. The effect of smaller amplitudes in y_d for short preview times also occurs in the simulation with the hybrid model. As the extension of the FBDC with the PLDC increased the maximum achievable comfort, the smaller amplitudes in y_d result in a decrease in driving comfort.

The following sensitivity analyses of the proposed concept are carried out with the hybrid model only, since this model represents a real-world suspension configuration. Unless otherwise stated a preview time of 0.5 s is assumed.

4.2.4   Influence of deviations in the preview time

A big challenge for the design of preview controllers is presented by variations in the preview time. As soon as the car accelerates or brakes, the preview time changes. To test how sensitive to these changes the PNDC is, several simulation runs are performed, each with the highway profile and different constant preview time. However, this time the PNDC, which was designed for a nominal preview time $\tau_{nom} = 0.25$ s, stays unmodified. Fig. 13 shows the resulting performance.

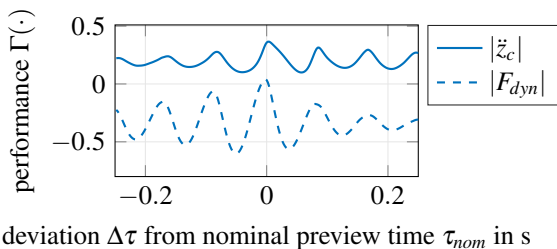The comfort always increases, independently of the preview time. However, the best comfort can be reached without a deviation $\Delta\tau$. Furthermore, the driving safety decreases for all deviations except for $\Delta\tau = 0$, as the compensating force is applied too early or too late. To achieve a high performance for various preview times, a weighting factor k_R could be chosen that increases both $\Gamma(\ddot{z}_c)$ and $\Gamma(F_{dyn})$ in the nominal case. If some deviations occur, the performance decreases, but will not be worse than that of the passive quarter car.
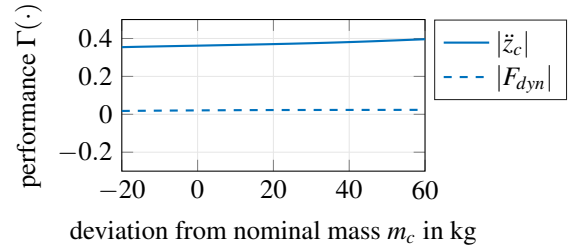
4.2.5   Influence of model parameter variations

In the real-world application, the mass of the chassis m_c varies under different load. To investigate the influence of load, the PNDC designed for the nominal mass m_c is applied to the hybrid model with a chassis mass that varies from run to run. The RMS values of the chassis acceleration and the dynamic wheel load are plotted in relation to values of passive quarter cars with correspondingly altered chassis masses. The results are depicted in Fig. 14.

A change in chassis mass has little influence on comfort and may even increase it slightly. Driving safety stays the same for all deviations. Thus, the performance of the PNDC is not affected by variations in the chassis mass.

4.2.6   Influence of errors in the road profile signal

As the disturbance compensating force u is determined solely based on the known road disturbance z_g, the performance depends on the quality of the signal z_g. The above simulations were all performed with exact knowledge of the road disturbance to examine the maximum possible performance. This is clearly an unrealistic assumption. Therefore the road disturbance signal is divided into the real profile $z_{g,r}$ and a measurement or estimation error Δz_g: $z_g = z_{g,r} + \Delta z_g$ and effects of Δz_g on the performance are discussed.

A simplifying frequency analysis of the linearized PNDC provides the hint that especially frequencies in the range of the eigenfrequency of the wheel (approx. 12 Hz) effect the PNDC's output. Low (<1 Hz) and high frequencies (>40 Hz) are considerably less amplified. This behavior leads to the assumption that a slow drift $\Delta z_g = kt$ in z_g, which occurs for example in front of a change in the road slope, has little influence on the performance. Moreover,
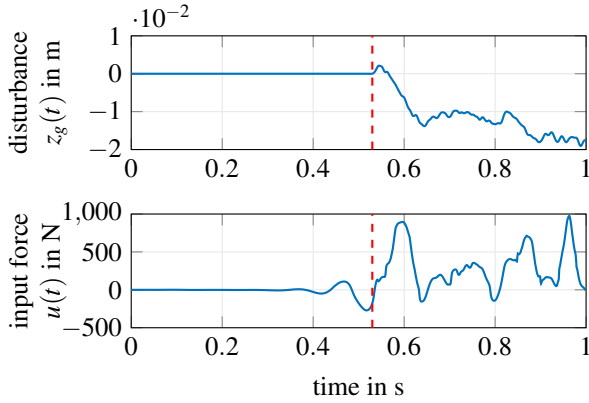

Fig. 14. Performance with regard to deviation in chassis mass, hybrid model.

Fig. 13. Performance with regard to deviation in preview time, hybrid model.

Fig. 15. Time plot for the disturbance compensator on the highway with $\tau = 0.5$ s.

Fig. 16. Performance in simulations with the real street profile, hybrid model.

high frequent measurement errors $\Delta z_g = w_g(t)$ also have little impact.

These properties are confirmed in simulations with the PNDC, the hybrid quarter car, and the highway profile as $z_{g,r}$ (standard deviation 0.019 m). Using the road profile with drift $\Delta z_g = kt$, $k = 0.1$ m/s still leads to a performance improvement of $\Gamma(\ddot{z}_c) = 28.5\%$ and $\Gamma(F_{dyn}) = 21.4\%$. To investigate the performance under errors in the whole frequency spectrum we choose $\Delta z_g = w_g(t)$ as zero-mean band-limited (cut-off frequency 360 Hz) white noise. The standard deviation of the noise is chosen to 0.01 m as experiments in [29, 63] show that road estimation with errors smaller than 0.01 m is possible. The results ($\Gamma(\ddot{z}_c) = 30.7\%$, $\Gamma(F_{dyn}) = 2.8\%$) confirm that the PNDC can also be used when such a challenging measurement error occurs.

However, to apply the PNDC to a car further analyses regarding the robustness have to be conducted, e.g. errors Δz_g in specific frequency ranges. This is not a trivial task and current field of research at the author's institute.

4.2.7 Proactive behavior

Fig. 15 shows the time plots of the road disturbance $z_g(t)$ and the input force $u(t)$ for the PNDC with 0.5 s preview. During the first 0.53 s, there is no road irregularity. Nevertheless, the input force starts to vary after 0.33 s. This is the desired proactive behavior: The system is preparing itself for the future disturbance.

4.2.8 Performance on the real road profile

In the last step, the hybrid quarter car is simulated with the comfort optimal weighting ($k_R = 687.1$) and the real measured street profile for preview times $\tau = 0$ s, $\tau = 0.072$ s, and $\tau = 0.5$ s. As the maximum achievable performance is to be examined, deviations or noise in the chassis mass, preview time and road profile are excluded. This different road profile is used to investigate whether the parametrization of the PNDC optimized with the highway
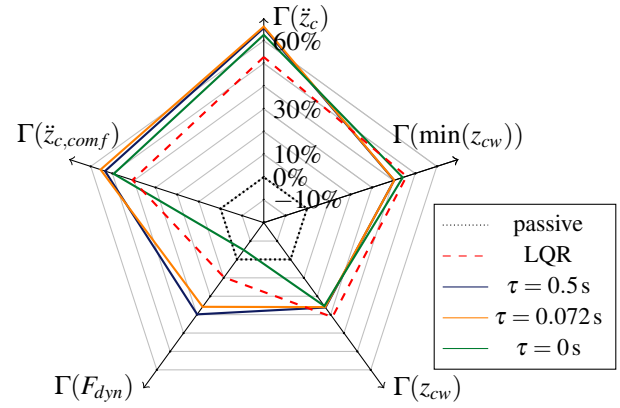
profile is also valid for other profiles and vehicle velocities.

Fig. 16 shows the performance of the PNDC for the three preview times. The dotted line represents the performance of the passive quarter car. As a benchmark controller, a comfort-oriented LQR (dashed red line) as designed in [19] is used. The PNDCs' improvement of comfort and safety is greater than that for the highway profile, although the parameters were optimized for the highway profile. Thus, the parametrization found is suitable for various road profiles. The PNDCs with preview (blue, orange) exceed the LQR in safety and comfort by more than 10 pp, and the improvement in suspension deflection is similar. All PNDCs achieve better performance in terms of suspension deflection than that achieved by the passive quarter car. This ensures that the deflection limits are met. The PNDC without preview (green) also achieves better comfort performance than the LQR. However, its driving safety is slightly worse than that of the passive system, which corresponds to the behavior for short preview times seen in Fig. 12.
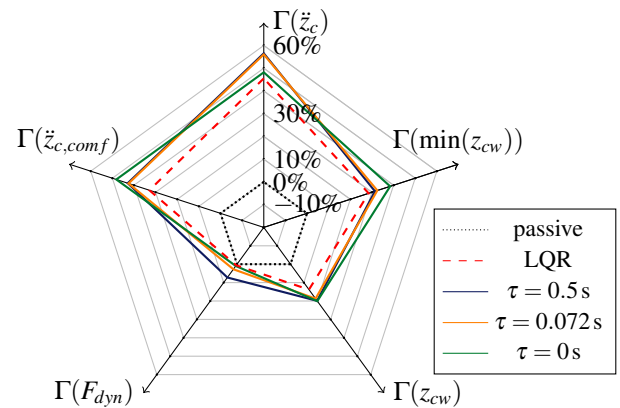
Fig. 17. Performance in experiments with the real street profile.

4.3. Experimental results

To validate these results, experiments are conducted on the quarter car test stand at the authors' institute (see Section 3.4). The parameters of the quarter car models in table 1 are chosen to be as close as possible to the test stand's parameters. Exactly the same PNDCs are used for the experiments as were applied to the earlier simulations. The results are shown in Fig. 17.

The comparison between experiments (Fig. 17) and simulations (Fig. 16) shows that the general behavior of the controllers remains the same: The PNDCs with preview exceed the LQR in comfort and safety while retaining the same level of suspension deflection. However, the comfort performance achieved in experiments is 10 pp lower than in simulations. Furthermore, the improvement in driving safety of the disturbance compensators with preview drops by 20 pp, but is still greater than zero. These differences are due to modeling errors, for instance in the tire and actuator behavior. The preview time of $\tau = 0.5\,\mathrm{s}$ is only beneficial in comparison to $\tau = 0.072\,\mathrm{s}$ in terms of driving safety. Thus, $0.072\,\mathrm{s}$ preview time, which equals $1\,\mathrm{m}$ preview length at a speed of $50\,\mathrm{km/h}$, is enough to improve $\Gamma(\ddot{z}_c)$ as much as possible.

5.　CONCLUSION AND OUTLOOK

This paper presents a flatness-based nonlinear disturbance compensator that completely decouples the chassis from road disturbances. As this approach led to a reduction in driving safety, a proactive FIR filter-based feedforward controller was added. Under the premise of an ideal actuator, it was shown that an arbitrary comfort or arbitrary safety can be set by means of one tuning parameter. For real actuators, the performance of the proposed proactive nonlinear disturbance compensator is restricted. However, parameterizations for an improvement in both comfort and safety, result in a quite similar performance to that with ideal actuators.

It was shown in simulations that the PNDC improves comfort in all considered cases, even if deviations from nominal mass and nominal preview time do occur. Furthermore the PNDC performed quite well on different road profiles and different vehicle velocities. It outperforms a standard LQR in simulations as well as in experiments at the quarter car test stand.

However, the PNDC still has to be tested in combination with a road profile observer, which could introduce further errors such as offset and drift. To further decrease the sensitivity to these errors, we intend to replace the proactive FIR filter with an adaptive FIR filter as in the fast convergence FxLMS in [48]. The incorporation should lead to improved performance in the case of deviations in preview time or chassis mass.

APPENDIX A

The matrices of the linear system (39) are:

$$\mathbf{A} = \begin{bmatrix} 0 & 1 & 0 & 0 & 0 \\ 0 & 0 & 1 & 0 & 0 \\ \frac{-c_g c_w}{d_w(m_c+m_w)} & \frac{-c_g-c_w}{m_c+m_w} & \frac{-c_g m_c-c_w m_w}{(m_c+m_w)d_w} & 0 & \frac{c_g c_w m_c}{d_w(m_c+m_w)} \\ 0 & 0 & 0 & 0 & 1 \\ 0 & -\frac{1}{m_w} & \frac{-(c_g+c_w)d_w}{c_g c_w m_w} & 0 & 0 \end{bmatrix},$$

$$\text{(A.1)}$$

$$\mathbf{b} = \begin{bmatrix} 0 & 0 & 0 & 0 & \frac{m_c+m_w}{m_w} \end{bmatrix}^T, \tag{A.2}$$

$$\mathbf{e} = \begin{bmatrix} 0 & 0 & \frac{c_g c_w}{d_w} & 0 & 0 \end{bmatrix}^T. \tag{A.3}$$

REFERENCES

[1] M. Mitschke and H. Wallentowitz, *Dynamik der Kraftfahrzeuge*, 5th ed., Springer Vieweg, Wiesbaden, 2014.

[2] S. M. Savaresi, C. Poussot-Vassal, and C. Spelta, *Semi-Active Suspension Control Design for Vehicles*, 1st ed., Elsevier professional, 2010.

[3] H. E. Tseng and D. Hrovat, "State of the art survey: Active and semi-active suspension control," *Veh. Syst. Dyn.*, vol. 53, no. 7, pp. 1034-1062, 2015.

[4] R. S. Sharp and D. A. Crolla, "Road vehicle suspension system design - a review," *Veh. Syst. Dyn.*, vol. 16, no. 3, pp. 167-192, 1987.

[5] W. D. Jones, "Easy ride - Bose Corp. uses speaker technology to give cars adaptive suspension," *IEEE Spectrum*, vol. 42, no. 3, pp. 12-14, 2005.

[6] G. Koch, O. Fritsch, and B. Lohmann, "Potential of low bandwidth active suspension control with continuously variable damper," *Control Eng. Pract.*, vol. 18, no. 11, pp. 1251-1262, 2010.

[7] R. S. Sharp and S. A. Hassan, "On the performance capabilities of active automobile suspension systems of limited bandwidth," *Veh. Syst. Dyn.*, vol. 16, no. 4, pp. 213-225, 1987.

[8] D. Karnopp, M. J. Crosby, and R. A. Harwood, "Vibration control using semi-active force generators," *J. Eng. Ind.*, vol. 96, no. 2, p. 619, 1974.

[9] S. Chen, Y. Cai, J. Wang, and M. Yao, "A novel lqg controller of active suspension system for vehicle roll safety," *Int. J. Control Autom. Syst.*, vol. 16, no. 5, pp. 2203-2213, 2018.

[10] D. Hrovat, "Survey of advanced suspension developments and related optimal control applications," *Automatica*, vol. 33, no. 10, pp. 1781-1817, 1997.

[11] C. Yue, T. Butsuen, and J. K. Hedrick, "Alternative control laws for automotive active suspensions," *J. Dyn. Syst.–T ASME*, vol. 111, no. 2, p. 286, 1989.

[12] C. Lauwerys, J. Swevers, and P. Sas, "Robust linear control of an active suspension on a quarter car test-rig," *Control Eng. Pract.*, vol. 13, no. 5, pp. 577-586, 2005.

[13] M. Yamashita, K. Fujimori, C. Uhlik, R. Kawatani, and H. Kimura, "H∞ control of an automotive active suspension," *Proc. of 29th IEEE Conference on Decision and Control*, pp. 2244-2250 vol. 4, IEEE, 1990.

[14] D. Sammier, O. Sename, and L. Dugard, "Skyhook and H∞ control of semi-active suspensions: Some practical aspects," *Veh. Syst. Dyn.*, vol. 39, no. 4, pp. 279-308, 2003.

[15] G. Koch, *Adaptive control of mechatronic vehicle suspension systems*, PhD thesis, Technische Universität München, München, 2011.

[16] H. Le Nguyen, K.-S. Hong, and S. Park, "Road-frequency adaptive control for semi-active suspension systems," *Int. J. Control Autom. Syst.*, vol. 8, no. 5, pp. 1029-1038, 2010.

[17] A. Alleyne and J. K. Hedrick, "Nonlinear adaptive control of active suspensions," *IEEE Trans. Control Syst. Technol.*, vol. 3, no. 1, pp. 94-101, 1995.

[18] A. Hać, "Adaptive control of vehicle suspension," *Veh. Syst. Dyn.*, vol. 16, no. 2, pp. 57-74, 1987.

[19] N. Pletschen, "Nonlinear H2 control of a low-bandwidth active vehicle suspension system using Takagi-Sugeno methods," in *Advanced Vehicle Control AVEC'16* (J. Edelmann, M. Plöchl, and P. E. Pfeffer, eds.), pp. 663-672, Crc Press, 2016.

[20] A. Alleyne and J. K. Hedrick, "Nonlinear control of a quarter car active suspension," *Proc. of American Control Conference*, pp. 21-25, 1992.

[21] R. J. Hampo and K. A. Marko, "Investigation of the application of neural networks to fault tolerant control of an active suspension system," *Proc. of American Control Conference*, pp. 11-15, IEEE, 1992.

[22] Ş. Yildirim, "Vibration control of suspension systems using a proposed neural network," *Journal of Sound and Vibration*, vol. 277, no. 4-5, pp. 1059-1069, 2004.

[23] A. Moran and M. Nagai, "Optimal active control of nonlinear vehicle suspensions using neural networks," *JSME International Journal. Ser. C, Dynamics, Control, Robotics, Design and Manufacturing*, vol. 37, no. 4, pp. 707-718, 1994.

[24] İ. Bucak and H. R. Öz, "Vibration control of a nonlinear quarter-car active suspension system by reinforcement learning," *Int. J. Syst. Sci.*, vol. 43, no. 6, pp. 1177-1190, 2012.

[25] S. Barton-Zeipert, *Fahrbahnprofilerfassung für ein aktives Fahrwerk*, PhD thesis, Helmut-Schmidt-Universität, Hamburg, 01.01.2014.

[26] A. Schindler, *Neue Konzeption und erstmalige Realisierung eines aktiven Fahrwerks mit Preview-Strategie, Ph.D. thesis*, vol. 31 of *Schriftenreihe des Instituts für Angewandte Informatik - Automatisierungstechnik, Universität Karlsruhe*, KIT Scientific Publ, Karlsruhe, 2009.

[27] M. Donahue and J. K. Hedrick, *Implementation of an Active Suspension Preview Controller for Improved Ride Comfort*, Diploma Thesis, Department of Mechanical Engineering, University of California at Berkely, 2001.

[28] C. Göhrle, A. Schindler, A. Wagner, and O. Sawodny, "Road profile estimation and preview control for low-bandwidth active suspension systems," *IEEE/ASME Trans. Mechatronics*, vol. 20, no. 5, pp. 2299-2310, 2015.

[29] J. C. Tudon-Martinez, S. Fergani, O. Sename, J. J. Martinez, R. Morales-Menendez, and L. Dugard, "Adaptive road profile estimation in semiactive car suspensions," *IEEE Trans. Control Syst. Technol.*, vol. 23, no. 6, pp. 2293-2305, 2015.

[30] E. K. Bender, "Optimum linear preview control with application to vehicle suspension," *J. Basic Eng.*, vol. 90, no. 2, pp. 213-221, 1968.

[31] M. Tomizuka, "'Optimum linear preview control with application to vehicle suspension'–revisited," *J. Dyn. Syst.–T ASME*, vol. 98, no. 3, p. 309, 1976.

[32] A. G. Thompson, B. R. Davis, and C. E. M. Pearce, "An optimal linear active suspension with finite road preview," *SAE Technical Paper Series, SAE International*, 1980.

[33] A. Hać, "Optimal linear preview control of active vehicle suspension," *Veh. Syst. Dyn.*, vol. 21, no. 1, pp. 167-195, 1992.

[34] R. S. Sharp and C. Pilbeam, "On the ride comfort benefits available from road preview with slow-active car suspensions," *Veh. Syst. Dyn.*, vol. 23, no. sup1, pp. 437-448, 1994.

[35] N. Louam, D. A. Wilson, and R. S. Sharp, "Optimal control of a vehicle suspension incorporating the time delay between front and rear wheel inputs," *Veh. Syst. Dyn.*, vol. 17, no. 6, pp. 317-336, 1988.

[36] A. Akbari and B. Lohmann, "Output feedback H∞ /GH2 preview control of active vehicle suspensions: A comparison study of LQG preview," *Veh. Syst. Dyn.*, vol. 48, no. 12, pp. 1475-1494, 2010.

[37] H. D. Choi, C. J. Lee, and M. T. Lim, "Fuzzy preview control for half-vehicle electro-hydraulic suspension system," *Int. J. Control Autom. Syst.*, vol. 16, no. 5, pp. 2489-2500, 2018.

[38] C. Göhrle, A. Schindler, A. Wagner, and O. Sawodny, "Design and vehicle implementation of preview active suspension controllers," *IEEE Trans. Control Syst. Technol.*, vol. 22, no. 3, pp. 1135-1142, 2014.

[39] R. K. Mehra, J. N. Amin, K. J. Hedrick, C. Osorio, and S. Gopalasamy, "Active suspension using preview information and model predictive control," *Proceedings of the 1997 IEEE International Conference on Control Applications*, pp. 860-865, Oct 1997.

[40] C. Poussot-Vassal, S. M. Savaresi, C. Spelta, O. Sename, and L. Dugard, "A methodology for optimal semi-active suspension systems performance evaluation," *Proc. of 49th IEEE Conference on Decision and Control (CDC)*, pp. 2892-2897, IEEE, 2010.

[41] M. Canale, M. Milanese, and C. Novara, "Semi-active suspension control using "fast" model-predictive techniques," *IEEE Trans. Control Syst. Technol.*, vol. 14, no. 6, pp. 1034-1046, 2006.

[42] K. M. Madhavan Rathai, M. Alamir, O. Sename, and R. Tang, "A parameterized nmpc scheme for embedded control of semi-active suspension system," *IFAC-PapersOnLine*, vol. 51, no. 20, pp. 301-306, 2018.

[43] K. M. Madhavan Rathai, M. Alamir, and O. Sename, "Experimental implementation of model predictive control scheme for control of semi-active suspension system," *IFAC-PapersOnLine*, vol. 52, no. 5, pp. 261-266, 2019.

[44] M. M. Morato, M. Q. Nguyen, O. Sename, and L. Dugard, "Design of a fast real-time LPV model predictive control system for semi-active suspension control of a full vehicle," *J. Franklin Inst.*, vol. 356, no. 3, pp. 1196-1224, 2019.

[45] J. N. Strohm and B. Lohmann, "Optimal feedforward preview control by FIR filters," *IFAC-PapersOnLine*, vol. 50, no. 1, pp. 5115-5120, 2017.

[46] J. N. Strohm and B. Lohmann, "Vorausschauende Störgrößenaufschaltung für die Schwingungsdämpfung am Viertelfahrzeug," *at - Automatisierungstechnik*, vol. 65, no. 8, 2017.

[47] P. Krauze and J. Kasprzyk, "Vibration control in quarter-car model with magnetorheological dampers using FxLMS algorithm with preview," *Proc. of European Control Conference (ECC)*, pp. 1005-1010, IEEE, 2014.

[48] J. N. Strohm and B. Lohmann, "A fast convergence fxlms algorithm for vibration damping of a quarter car," *Proc. of IEEE Conference on Decision and Control (CDC)*, pp. 6094-6100, Dec 2018.

[49] A. Moran and M. Nagai, "Optimal preview control of rear suspension using nonlinear neural networks," *Veh. Syst. Dyn.*, vol. 22, no. 5-6, pp. 321-334, 1993.

[50] B. Lohmann, "Flatness based disturbance compensation," *Scientific Report, Institute of Automation, University of Bremen*, 2002.

[51] J. Deutscher and B. Lohmann, "Flatness based asymptotic disturbance rejection for linear and nonlinear systems," *Proc. of European Control Conference (ECC)*, pp. 3183-3188, 2003.

[52] P. Rouchon, M. Fliess, J. L. Évine, and P. Martin, "Flatness and motion planning: the car with n trailers," *Proc. European Control Conference*, pp. 1518-1522, 1993.

[53] A. Isidori, *Nonlinear Control Systems*, Communications and Control Engineering Series, Springer, 3rd ed., Berlin, 2002.

[54] C. R. Cutler and B. L. Ramaker, "Dynamic matrix control - a computer control algorithm," *Proc. of Joint Automatic Control Conference*, vol. 1980, 1980.

[55] S. Spirk, *Modulare vertikaldynamische Regelungskonzepte für ein hybrid aktuiertes Fahrwerk*, Fahrzeugtechnik, München, Dr. Hut, 2016.

[56] F. Tyan, Y.-F. Hong, S.-H. Tu, and W. S. Jeng, "Generation of random road profiles," *CSME*, vol. 4, no. 2, pp. 151-156, 2009.

[57] J. Wu, Z. Liu, and W. Chen, "Design of a piecewise affine H_∞ controller for MR semiactive suspensions with nonlinear constraints," *IEEE Trans. Control Syst. Technol.*, vol. 27, no. 4, pp. 1762-1771, 2019.

[58] International Organization for Standardization, "Mechanical vibration and shock - evaluation of human exposure to whole-body vibration," 1997-05.

[59] VDI-Fachbereich Schwingungstechnik, "Human exposure to mechanical vibrations - whole-body vibration," 2012.

[60] G. Koch, E. Pellegrini, S. Spirk, N. Pletschen, and B. Lohmann, "Actuator control for a hybrid suspension system," *Technical Reports on Automatic Control*, Chair of Automatic Control, Technical University of Munich, 2011.

[61] J. Adamy, *Nichtlineare Systeme und Regelungen*, Springer, Berlin, Heidelberg, 2014.

[62] J. Lévine, *Analysis and Control of Nonlinear Systems: A Flatness-based Approach*, Mathematical Engineering, Springer-Verlag, Berlin, Heidelberg, 2009.

[63] R. Streiter, "ABC pre-scan im F700," *ATZ - Automobiltechnische Zeitschrift*, vol. 110, no. 5, pp. 388-397, 2008.

Johannes N. Strohm received his M.S. degree in Mechanical Engineering from Technical University of Munich, Germany in 2015. Afterwards, he started to work at the Chair of Automatic Control, Technical University of Munich, as a research assistant. His research interests include preview control, adaptive control and nonlinear control for active suspension systems.

Dominik Pech received his M.S. degree in Mechanical Engineering from Technical University of Munich, Germany in 2017. His research interests are in the field of automotive control.

Boris Lohmann is the head of the Chair of Automatic Control of the Mechanical Engineering department of the Technical Univeristy of Munich, Germany. His research interests include control methods for different system classes, modelling and model reduction as well as application of control methods in the field of mechatronic systems and automotive engineering.

A.5 Preview H∞ Control of a Hybrid Suspension System

Contributions: The main idea of modeling the quarter car as a time delay model and using controller design methods for time delay systems has been developed by the first author. The implementation, selection of the controller and preliminary simulations and analyses have been performed by the second author. Some further improvements, final simulations, analyses, and writing have been done predominantly by the first author.

Preview H∞ Control of a Hybrid Suspension System

Johannes N. Strohm * Fabian Christ *

* *Chair of Automatic Control, Department of Mechanical Engineering,
Technische Universität München, 85748 Garching, Germany (e-mail:
johannes.strohm@tum.de)*

Abstract: In this paper we compare various H∞ controllers, which differ in the way they exploit preview information about road irregularities. To this end, we introduce several linear models of the quarter car that incorporate the delay between sensing the road disturbance in front of the car and the arrival of the disturbance at the wheel in different ways. Based on these models, we design and compare feedforward controllers and feedback controllers coupled with a feedforward portion. For this, we use standard H∞ control methodology as well as an H∞ method for time delay systems. The latter is capable of coping with a varying time delay. We investigate the controller performance in simulations and discuss the influence of varying time delay on the performance.

1. INTRODUCTION

Car manufacturers and tech companies compete for the best algorithms for autonomous cars. For the most part, their focus is set on the driving task, i.e., autonomous accelerating, braking, and steering. However, the development of autonomous cars provides many more challenges, which are often less obvious. The one that will be tackled in this paper is the increased comfort demand. Comfort is mainly influenced by the car suspension, which usually consists of a spring and a damper. The stiffness and damping have to be set in the design process of a car. Depending on the choice of the parameters, the car behaves either more like an uncomfortable sports car with good road holding abilities, or like a less sporty but more comfortable sedan. In conventional suspension systems, conflict always arises between driving safety (road holding) and passenger comfort (Mitschke and Wallentowitz (2014)), with the result that the tuning of suspensions means making a compromise. Furthermore, comfort cannot be arbitrarily increased, as a specific level of safety has to be guaranteed. Since in the autonomous car the driver becomes a passenger, who wants to work or relax, an increased level of comfort is required. This improvement has to be higher than what is possible with conventional suspension systems.

To increase comfort without losing driving safety, semi-active or active components have to be included in the suspension. These are able to vary or insert forces between the wheel and the chassis to compensate for road-induced vibrations. A well-known example of an active system in series production is Mercedes' Magic Body Control system, which incorporates a hydraulic cylinder between the spring and the chassis (Schindler (2009)). To use such a system for comfort maximization, a control law is required, which determines the actuator force based on measurements of chassis acceleration, suspension deflection, and wheel acceleration, for example.

A commonly used approach is the so-called Skyhook controller. It connects a virtual damper between the chassis and the sky. Its force is applied through the active component between chassis and wheel, so that the movements of the body of a car are damped (Savaresi et al. (2010)). To enlarge the number of design parameters, a Linear Quadratic Regulator (LQR) can be used. This controller minimizes a cost function, which can include, for instance, the chassis acceleration (the measure of comfort), dynamic wheel load (measure of driving safety), suspension deflection, and the required input force (Unger (2012), Hrovat (1997)). Another approach is the H∞ controller, which minimizes the influence of unknown disturbances on the output based on the measured input data (Lauwerys et al. (2005)). All these regulators have in common that they are pure feedback controllers. They can only react to disturbances that have already impacted the car. If a road irregularity were known in advance, it would be much more reasonable to counteract before it reaches the tire.

Autonomous cars need many sensors to observe the environment. Some of these can also be used to detect the road surface in front of the car. As the driving comfort is supposed to be increased as much as possible, knowledge about future road disturbance has to be included in the control law via feedforward control. The first approach was made in Bender (1968), where a preview controller was designed for a one degree of freedom (DOF) quarter car based on Wiener filter theory. Later on, an H2-optimal linear preview controller with feedforward portion for a 2 DOF quarter car was developed in Hać (1992). Furthermore, methods of model predictive control, which can easily incorporate preview information into the prediction, have been developed for active suspension systems (Mehra

et al. (1997), Göhrle et al. (2014)). Also, methods of H∞ control can be used for the design of a preview controller. Therefore, the time delay between the measurement and the effect of the road irregularity is modeled by augmenting the discrete time state space model (see, for example, Akbari and Lohmann (2010)) so that a conventional H∞ design method can be applied. The disadvantage of this approach is that the controller is designed for a fixed time delay. As the time between the measurement and the effect of the disturbance varies with changing vehicle velocity, this approach is of limited suitability in real cars.

The novelty of this paper is the treatment of the problem from the perspective of time delay systems. To this end, we model the quarter car with preview information as a linear, continuous time system with time delay in its states. We apply the H∞ observer-based feedback controller design method presented in Sename (2007), which results in a controller that is independent of the delay length and thus applicable for varying vehicle velocities. We compare its performance with a pure feedforward variant of this controller, H∞ controllers designed using a Padé approximation of the time delay, and with H∞ controllers without preview. Furthermore, we examine the influence of a varying time delay on the controller performance.

The paper is organized as follows: Section 2 introduces the models used for the controller design and simulations, and the theoretical background of the H∞ controllers. In Section 3, the application of the controllers to the quarter car is shown. We present the simulation results in Section 4, before we close the paper in Section 5 with a conclusion and an outlook.

2. PRELIMINARIES

First, we present two linear quarter car models used for the different controller designs and a nonlinear one for simulation purposes. Afterwards, we introduce the two control design methods used in this paper.

2.1 Quarter car models

We model the quarter car as the linear two mass oscillator shown in figure 1a).

The delay between the measurement and the effect of the road irregularities z_g is neglected for now and added in the second modeling step. The application of Newton's second law for the chassis mass m_c and the wheel mass m_w yields the equations of motion
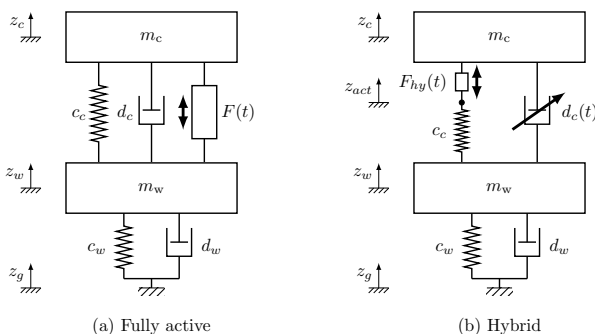

(a) Fully active   (b) Hybrid

Fig. 1. Quarter car models

$$m_c \ddot{z}_c + c_c(z_c - z_w) + d_c(\dot{z}_c - \dot{z}_w) = F \qquad (1)$$

$$m_w \ddot{z}_w + c_c(z_w - z_c) + d_c(\dot{z}_w - \dot{z}_c) + c_w(z_w - z_g) \\ + d_w(\dot{z}_w - \dot{z}_g) = -F. \qquad (2)$$

The coordinates and parameters are as shown in figure 1: chassis position z_c, wheel position z_w, main suspension spring stiffness c_c, suspension damping d_c, wheel stiffness c_w, wheel damping d_w, and actuator force $u = F$. Choosing the state vector as $\mathbf{x} = [z_c - z_w \ \dot{z}_c \ z_w - z_g \ \dot{z}_w]^T$ we build the state space representation of (1) and (2)

$$\dot{\mathbf{x}} = \mathbf{A}\mathbf{x} + \mathbf{B}_2 u + \mathbf{B}_1 \dot{z}_g \qquad \text{with} \qquad (3)$$

$$\mathbf{A} = \begin{bmatrix} 0 & 1 & 0 & -1 \\ -\frac{c_c}{m_c} & -\frac{d_c}{m_c} & 0 & \frac{d_c}{m_c} \\ 0 & 0 & 0 & 1 \\ \frac{c_c}{m_w} & \frac{d_c}{m_w} & -\frac{c_w}{m_w} & -\frac{d_c+d_w}{m_w} \end{bmatrix}$$

$$\mathbf{B}_2 = \begin{bmatrix} 0 & \frac{1}{m_c} & 0 & -\frac{1}{m_w} \end{bmatrix}^T \qquad \mathbf{B}_1 = \begin{bmatrix} 0 & 0 & -1 & \frac{d_w}{m_w} \end{bmatrix}^T.$$

The measured output $\mathbf{y}_m$ is chassis acceleration, suspension deflection, and wheel acceleration:

$$\mathbf{y}_m = [\ddot{z}_c \ (z_c - z_w) \ \ddot{z}_w]^T = \mathbf{C}_2 \mathbf{x} + \mathbf{D}_{22} u + \mathbf{D}_{21} \dot{z}_g$$
$$\text{with} \qquad (4)$$

$$\mathbf{C}_2 = \begin{bmatrix} -\frac{c_c}{m_c} & -\frac{d_c}{m_c} & 0 & \frac{d_c}{m_c} \\ 1 & 0 & 0 & 0 \\ \frac{c_c}{m_w} & \frac{d_c}{m_w} & -\frac{c_w}{m_w} & -\frac{d_c+d_w}{m_w} \end{bmatrix}$$

$$\mathbf{D}_{22} = \begin{bmatrix} \frac{1}{m_c} & 0 & -\frac{1}{m_w} \end{bmatrix}^T \qquad \mathbf{D}_{21} = \begin{bmatrix} 0 & 0 & \frac{d_w}{m_w} \end{bmatrix}^T.$$

The output to be controlled $\mathbf{z}$ is the chassis acceleration (the lower $\ddot{z}_c$, the higher the driving comfort), the suspension deflection, and the wheel compression (the lower $z_w - z_g$, the higher the driving safety). This model is used for the design of the H∞ controllers without preview. The parameter values for the model can be found in table 1.

Table 1. Model parameters

m_c	m_w	c_c	d_c	c_w	d_w
507 kg	68 kg	24.1 kN/m	1.4 kNs/m	378 kN/m	130 Ns/m

For the preview controller design with constant time delay τ between measurement and effect of the road profile velocity $\dot{z}_g$, the system (3) is augmented with the Padé approximation (5) so that the new disturbance input is the future value of the road profile velocity $\dot{z}_g(t + \tau)$. We use a Padé approximation

$$e^{-\tau s} \approx \frac{1 - k_1 s + k_2 s^2 + \cdots + (-1)^n k_n s^n}{1 + k_1 s + k_2 s^2 + \cdots + k_n s^n} \qquad (5)$$

of the order $n = 10$, where s is the complex variable and k_i are coefficients to be determined (Bequette (2010)).

As the Padé approximation of the time delay is only valid for one fixed delay, the augmented model can only be used for the controller design in the case of a constant preview time. To avoid this restriction, we build a time delay model, which represents the system dynamics for all possible time delays. Choosing the state vector as $\tilde{\mathbf{x}} = [z_c \ \dot{z}_c \ z_w \ \dot{z}_w \ z_g]^T$ and neglecting the wheel damping d_w, the equations of motion (1), (2) can be transformed into a time delay state space system considering the preview measurement of z_g:

$$\dot{\tilde{\mathbf{x}}}(t) = \mathbf{A}_0\tilde{\mathbf{x}}(t) + \mathbf{A}_1\tilde{\mathbf{x}}(t-\tau) + \mathbf{b}u(t) + \mathbf{e}\dot{z}_g(t) \qquad (6)$$

$$\text{with} \quad \mathbf{A}_0 = \begin{bmatrix} 0 & 1 & 0 & 0 & 0 \\ -\frac{c_c}{m_c} & -\frac{d_c}{m_c} & \frac{c_c}{m_c} & \frac{d_c}{m_c} & 0 \\ 0 & 0 & 0 & 1 & 0 \\ \frac{c_c}{m_w} & \frac{d_c}{m_w} & -\frac{c_c+c_w}{m_w} & -\frac{d_c}{m_w} & 0 \\ 0 & 0 & 0 & 0 & \dagger \end{bmatrix}$$

$$\mathbf{A}_1 = \begin{bmatrix} 0 & 0 & 0 & 0 & 0 \\ 0 & 0 & 0 & 0 & 0 \\ 0 & 0 & 0 & 0 & 0 \\ 0 & 0 & 0 & 0 & \frac{c_w}{m_w} \\ 0 & 0 & 0 & 0 & 0 \end{bmatrix} \quad \mathbf{b} = \begin{bmatrix} 0 & \frac{1}{m_c} & 0 & -\frac{1}{m_w} & 0 \end{bmatrix}^T$$

$$\mathbf{e} = [0\ 0\ 0\ 0\ 1]^T.$$

The entry $\dagger$ in $\mathbf{A}_0$ is actually 0, meaning that the road profile velocity $\dot{z}_g$ is integrated. For the controller design after Sename (2007), the system has to be stabilizable according to rank$[\mathbf{A}_0 + e^{-s\tau}\mathbf{A}_1; \mathbf{b}] = n \; \forall s \in \mathbb{C}$ with $\Re(s) \geq \beta \in \mathbb{R}_0^-$ and observable. The stabilizability is not given with an ideal integrator. To avoid this problem, $\dagger$ is set to -0.1. Thus, the integrator is extended to include an integrator and a high-pass filter. Although this seems to be an improper modification at first sight, from a practical point of view, the high-pass filtering of the road profile is beneficial. As the low frequency portion of the profile z_g, such as mountains, hills, and valleys, should not and cannot be compensated by the active suspension, it has to be removed from the signal beforehand. The *strong observability* can be proven for the case of the measured road profile using the criteria presented in Sename (2001).

The controllers are designed based on the linear fully active quarter car models presented before. However, the hybrid quarter car test stand at the authors' institute exhibits nonlinear behavior. To model the system dynamics as closely as possible to the test stand behavior, a nonlinear system model is built. It includes the following nonlinearities (for details see Pellegrini (2012)):

- Nonlinear damper and spring characteristics
- Nonlinear Gehmann model (Mitschke and Wallentowitz (2014)) with quadratic stiffness as tire model
- Dynamic kinematic transmission factor for the transformation of forces and velocities in suspension strut plane into the wheel plane, and vice versa

Furthermore, the ideal actuator of the fully active model (see fig. 1a)) is replaced by a slow hydraulic Spring Mount Adjustment (SMA) (cutoff frequency $\approx$ 5Hz) and a variable damper (see fig. 1b)). These actuators are also modeled in the nonlinear test stand model. To apply the controllers designed with the fully active linear models to the nonlinear hybrid simulation model, the input force has to be split into a portion F_{hy} for the SMA and one for the variable damper $d_c(t)$. This is done in a dynamic optimal manner. Therefore, we try to realize as much force as possible with the SMA, and apply the remaining high frequency portion to the dissipative variable damper.

2.2 H∞ control design methods

The H∞ controllers are built to minimize the effect of a disturbance $\mathbf{w}$ on an output $\mathbf{z}$. Mathematically, this is expressed by the minimization of the H∞ norm of the transfer function from disturbance to controlled output

$||\mathbf{T_{zw}}||_\infty$. The minimum value of this norm is denoted by γ_0. The standard H∞ control problem for a linear time-invariant state-space system was solved in Doyle et al. (1989). They use the system description

$$\dot{\mathbf{x}} = \mathbf{A}\mathbf{x} + \mathbf{B}_1\mathbf{w} + \mathbf{B}_2\mathbf{u} \qquad (7)$$
$$\mathbf{z} = \mathbf{C}_1\mathbf{x} + \mathbf{D}_{11}\mathbf{w} + \mathbf{D}_{12}\mathbf{u} \qquad (8)$$
$$\mathbf{y} = \mathbf{C}_2\mathbf{x} + \mathbf{D}_{21}\mathbf{w} + \mathbf{D}_{22}\mathbf{u} \qquad (9)$$

with state $\mathbf{x}$, unknown disturbance $\mathbf{w}$, input $\mathbf{u}$, controlled output $\mathbf{z}$, and measured output $\mathbf{y}$. Under some conditions (see Skogestad and Postlethwaite (2007)), the controller, which minimizes the effect of the disturbances on the output $\mathbf{z}$, can be designed as follows. Given a positive semi definite solution $\mathbf{X}_\infty, \mathbf{Y}_\infty$ of the Riccati equations

$$\mathbf{A}^T\mathbf{X}_\infty + \mathbf{X}_\infty\mathbf{A} + \mathbf{C}_1^T\mathbf{C}_1 +$$
$$\mathbf{X}_\infty(\gamma^{-2}\mathbf{B}_1\mathbf{B}_1^T - \mathbf{B}_2\mathbf{B}_2^T)\mathbf{X}_\infty = 0 \qquad (10)$$

$$\mathbf{A}\mathbf{Y}_\infty + \mathbf{Y}_\infty\mathbf{A}^T + \mathbf{B}_1\mathbf{B}_1^T +$$
$$\mathbf{Y}_\infty(\gamma^{-2}\mathbf{C}_1^T\mathbf{C}_1 - \mathbf{C}_2^T\mathbf{C}_2)\mathbf{Y}_\infty = 0 \qquad (11)$$

and given that the spectral radius $\rho(\mathbf{X}_\infty\mathbf{Y}_\infty) < \gamma^2$, then an observer-controller of the form

$$\dot{\hat{\mathbf{x}}} = \mathbf{A}\hat{\mathbf{x}} + \mathbf{B}_1\gamma^{-2}\mathbf{B}_1^T\mathbf{X}_\infty\hat{\mathbf{x}} + \mathbf{B}_2\mathbf{u} + \mathbf{Z}_\infty\mathbf{L}_\infty(\mathbf{C}_2\hat{\mathbf{x}} - \mathbf{y}) \qquad (12)$$

$$\mathbf{u} = \mathbf{F}_\infty\hat{\mathbf{x}} \quad \text{with} \quad \mathbf{Z}_\infty = (\mathbf{I} - \gamma^{-2}\mathbf{Y}_\infty\mathbf{X}_\infty)^{-1},$$
$$\mathbf{F}_\infty = -\mathbf{B}_2^T\mathbf{X}_\infty, \quad \mathbf{L}_\infty = -\mathbf{Y}_\infty\mathbf{C}_2^T$$

leads to $||\mathbf{T_{zw}}||_\infty < \gamma$. As it is analytically, as well as numerically, very difficult to determine the minimum value γ_0, usually an iterative procedure using the bisection algorithm is used to lower the gain γ and approach γ_0. Most of the control problems meet the conditions for this algorithm or can be transformed to fulfill them (Zhou and Doyle (1998)). We will make use of MATLAB's *Robust Control Toolbox*, which has implemented the presented method. We apply it for the controller design for the case without preview, and for the case with fixed preview based on system augmentation with the Padé approximation.

The controller design for the time delay system (6) is done according to Sename (2007). The starting point of the derivation of this method is a system of the form

$$\dot{\mathbf{x}}(t) = \mathbf{A}_0\mathbf{x}(t) + \mathbf{A}_1\mathbf{x}(t-\tau) + \mathbf{b}u(t) + \mathbf{e}w(t) \qquad (13)$$
$$\mathbf{y}(t) = \mathbf{C}\mathbf{x}(t) + \mathbf{f}w(t) \qquad (14)$$
$$\mathbf{z}(t) = \mathbf{D}\mathbf{x}(t). \qquad (15)$$

The observer controller is assumed to have the following structure

$$\dot{\hat{\mathbf{x}}} = \mathbf{A}_0\hat{\mathbf{x}}(t) + \mathbf{A}_1\hat{\mathbf{x}}(t-\tau) + \mathbf{b}u(t) -$$
$$\mathbf{L}(\mathbf{C}\hat{\mathbf{x}}(t) - \mathbf{y}(t)) + \mathbf{G}\hat{\mathbf{x}}(t) \qquad (16)$$
$$u(t) = \mathbf{K}\hat{\mathbf{x}}(t). \qquad (17)$$

To determine the free parameter matrices $\mathbf{L}, \mathbf{G}$, and $\mathbf{K}$, the extended state $\mathbf{x}_e = [\mathbf{x} \; \mathbf{x} - \hat{\mathbf{x}}]^T$ and the augmented system for the closed loop behavior

$$\dot{\mathbf{x}}_e(t) = \begin{bmatrix} \mathbf{A}_0 + \mathbf{b}\mathbf{K} & -\mathbf{b}\mathbf{K} \\ -\mathbf{G} & \mathbf{A}_0 - \mathbf{L}\mathbf{C} + \mathbf{G} \end{bmatrix}\mathbf{x}_e(t) +$$
$$\begin{bmatrix} \mathbf{A}_1 & 0 \\ 0 & \mathbf{A}_1 \end{bmatrix}\mathbf{x}_e(t-\tau) + \begin{bmatrix} \mathbf{e} \\ \mathbf{e} - \mathbf{L}\mathbf{f} \end{bmatrix}w(t) \qquad (18)$$

are introduced. The goal is to design a controller that stabilizes (18) and restricts $||\mathbf{T_{z_ew}}||_\infty$, so that

$$||\mathbf{T_{z_ew}}||_\infty \leq \gamma \quad \text{with} \quad \mathbf{z}_e = \begin{bmatrix} \mathbf{D} & 0 \\ 0 & \mathbf{I} \end{bmatrix}\mathbf{x}_e. \qquad (19)$$

According to theorem 1 in Sename (2007), such a controller exists if there are, for a given γ, positive definite matrices $\mathbf{P}_c = \mathbf{P}_c^T$, $\mathbf{P}_0 = \mathbf{P}_0^T$, $\mathbf{S}_c$, and $\mathbf{S}_0$ and matrices $\mathbf{X}, \mathbf{Y}$, that satisfy the following equations

$$\mathcal{L}_{OC} = \begin{bmatrix} \mathbf{M}_c & 0 & \mathbf{A}_1\mathbf{P}_c & 0 & \mathbf{E} & \mathbf{P}_c\mathbf{D}^T \\ * & \mathbf{M}_0 & 0 & \mathbf{P}_0\mathbf{A}_1 & \mathbf{P}_0\mathbf{E} - \mathbf{YF} & 0 \\ * & * & -\mathbf{S}_c & 0 & 0 & 0 \\ * & * & * & -\mathbf{S}_0 & 0 & 0 \\ * & * & * & * & -\gamma^2\mathbf{I} & 0 \\ * & * & * & * & * & -\mathbf{I} \end{bmatrix} \prec 0$$
(20)

$$\mathbf{M}_c = \mathbf{A}_0\mathbf{P}_c + \mathbf{P}_c\mathbf{A}_0^T + \mathbf{BX} + \mathbf{X}^T\mathbf{B}^T + \mathbf{S}_c \qquad (21)$$

$$\mathbf{M}_0 = \mathbf{A}_0^T\mathbf{P}_0 + \mathbf{P}_0\mathbf{A}_0 - \mathbf{P}_c^{-1}(\mathbf{BX} + \mathbf{X}^T\mathbf{B}^T)\mathbf{P}_c^{-1} + \\ \mathbf{YC} + \mathbf{C}^T\mathbf{Y}^T + \mathbf{I} + \mathbf{S}_0. \qquad (22)$$

The $*$ denotes the symmetric element, and the observer controller matrices are

$$\mathbf{L} = -\mathbf{P}_0^{-1}\mathbf{Y}, \quad \mathbf{K} = \mathbf{XP}_c^{-1}, \quad \mathbf{G} = -\mathbf{P}_0^{-1}\mathbf{K}^T\mathbf{B}^T\mathbf{P}_c^{-1}.$$

The proof of the theorem can be found in Sename (2007). To minimize the maximal gain γ, the following optimization has to be performed

$$\gamma_0^2 = \min_{\mathbf{P}_0,\mathbf{P}_c,\mathbf{X},\mathbf{Y},\mathbf{S}_c,\mathbf{S}_0} \gamma^2 \qquad (23)$$
$$\text{s.t. } \mathcal{L}_{OC} \prec 0, \mathbf{P}_c \succ 0, \mathbf{P}_0 \succ 0, \mathbf{S}_c \succ 0, \mathbf{S}_0 \succ 0.$$

Due to the term $\mathbf{M}_{nc} = \mathbf{P}_c^{-1}(\mathbf{BX} + \mathbf{X}^T\mathbf{B}^T)\mathbf{P}_c^{-1}$ in (22), the optimization problem (23) is non-convex. Therefore, standard Linear Matrix Inequality (LMI) solvers cannot be used. Instead, a recursive procedure is proposed, which, in each iteration, first determines the critical term $\mathbf{M}_{nc}$ based on values of the previous run and then solves the convexified optimization problem (23) with fixed $\mathbf{M}_{nc}$.

3. CONTROLLER DESIGN

We develop feedback and feedforward controllers for the three cases: no preview, fixed preview, and variable preview of the road profile. As the methods applied require different measured and controlled outputs, we will shortly present the controller design for each case. All models have in common that models for the actuator dynamics or filters for the controlled outputs are not used, in order to keep the design and the parameterization as simple and as comparable as possible.

3.1 Controllers without preview (FB, FF)

The H∞ feedback controller without preview (FB) is designed based on the model (3), and uses the measured output $\mathbf{y}_m$ as in (4). The controlled outputs $\mathbf{z}$ are $\ddot{z}_c, z_w - z_g, z_c - z_w$ and u. The only design parameters are the constant weighting factors $W_{\ddot{z}_c} = 3.5$, $W_{z_w - z_g} = 67$, $W_{z_c - z_w} = 1/0.11$, and $W_u = 0.002$, which were chosen manually to maximize comfort while retaining the level of driving safety of the passive quarter car.

The H∞ feedforward controller without preview (FF) determines the input solely based on the current road profile velocity measurement. Therefore, the model, the controlled outputs $\mathbf{z}$, and the weighting factors are the same as for the feedback controller FB. Only the measured output $\mathbf{y}_m$ is changed to the road profile velocity $\dot{z}_g(t)$.

3.2 Controllers for fixed preview (FB_{fix}, FF_{fix})

The H∞ controller with fixed preview (FB$_{fix}$) consists of a feedback portion, which uses the current measured outputs $\mathbf{y}_m$ as in (4), and of a feedforward portion, which is calculated based on the future road profile velocity $\dot{z}_g(t + \tau)$. The controlled outputs and the weighting functions are the same as for the FB. To enable the preview data to be included in the design, the model (3) is augmented with the model of a Padé approximation as in (5).

The H∞ feedforward controller with preview (FF$_{fix}$) is built the same way as FB$_{fix}$, with the difference that only the previewed road profile velocity $\dot{z}_g(t + \tau)$ is measured.

3.3 Controllers for variable preview (FB_{var}, FF_{var})

The H∞ controller for variable preview times (FB$_{var}$) is designed based on the method developed in Sename (2007) and presented in Section 2.2. As the approach requires a system in the form of (13), (14), and (15), the model (6) is used and the measured and controlled outputs have to be modified. The measured outputs are $\dot{z}_c(t)$, $z_c(t) - z_w(t)$, and $z_g(t + \tau)$. The wheel acceleration $\ddot{z}_w$ cannot be included in the measured output, since it depends on the delayed street profile, which cannot be expressed with (14). In contrast to the other controllers, the street profile z_g is measured instead of the street profile velocity $\dot{z}_g$. This is caused by the structure of the time delay system (6).

Also, the controlled output has to be modified. According to (15), neither the input u nor the disturbance w are allowed to impact the output $\mathbf{z}$. Consequently, we cannot include the chassis acceleration and the input force in $\mathbf{z}$. As the reduction in chassis movement is the main goal of the controller, in the controlled output we replace the chassis acceleration with the chassis velocity. Thus, the controlled outputs for this approach are $\dot{z}_c(t)$ and $z_c(t) - z_w(t)$.

In the case of a pure H∞ feedforward controller (FF$_{var}$), the measured output is reduced to the future road profile $z_g(t + \tau)$.

Due to the new controlled outputs, the weighting functions have to be adjusted for FB$_{var}$ and FF$_{var}$. The weighting for the chassis velocity is set to $W_{\dot{z}_c} = 70$ and the weighting of $z_c - z_w$ is $W_{z_c - z_w} = 10/0.11$. Applying the recursive optimization method described in Section 2.2, an infeasible solution is found with the *YALMIP toolbox* and the solver "sdpt3". The reason for this is the matrix $\mathbf{S}_c$, which is not positive definite. However, for many weighting factors, the resulting controllers can be used, as the closed loop systems are stable according to lemma 1 in Sename (2007). Although the proposed algorithm can result in an infeasible controller, the performance of the feasible controllers can be intuitively adjusted by altering the weighting of the chassis velocity $W_{\dot{z}_c}$: An increase of $W_{\dot{z}_c}$ tends to improve the driving comfort.

4. RESULTS

We investigate the performance of the proposed controllers in simulation with the model of the nonlinear hybrid (NHQC) and nonlinear fully active (NFAQC) quarter car. The road profile we are using reflects a bad country road

traveled at a speed of 50 km/h (see Pellegrini (2012)). We assume that the road profile is known exactly for all simulations. To evaluate the performance achieved, we design the performance criterion $\Gamma(|\cdot|) = 1 - \frac{|\cdot|_{active}}{|\cdot|_{passive}}$, where $|\cdot|_{\{active,passive\}}$ is the Root Mean Square (RMS) value of the quantity under examination of the active and passive quarter car respectively. A positive value of Γ implies an improvement. We use the chassis acceleration $\ddot{z}_c$ as the indicator of comfort, the dynamic wheel load F_{dyn} as the indicator of driving safety, and the suspension deflection $z_c - z_w$ to check whether the suspension limits have been exceeded.

First, we compare the performance of the feedback controllers with the pure feedforward controllers for the NHQC. For this, the nominal time delay for the preview controllers is set to $\tau_{nom} = 0.036\,$s, and the delay is assumed to be exactly known and constant. This equals a preview length of 0.5 m when the vehicle is driven at 50 km/h. The results are shown in table 2. Comparing the

Table 2. Controller performance with time delay $\tau_{nom} = 0.036\,$s (NHQC)

	FB	FF	FB_{fix}	FF_{fix}	FB_{var}	FF_{var}
$\Gamma(\ddot{z}_c)$	62%	60%	67%	67%	62%	60%
$\Gamma(F_{dyn})$	10%	10%	14%	17%	-3%	-4%
$\Gamma(z_c - z_w)$	26%	29%	19%	20%	11%	24%

feedback with the feedforward controllers, we can state that pure feedforward controllers achieve almost the same performance as the feedback controllers. The FF_{fix} even increases driving safety while retaining the same comfort level as the FB_{fix}. Thus, as long as the road profile is known exactly, pure feedforward controllers are sufficient to improve performance. Furthermore, the comparison of FB with FB_{fix} and FF with FF_{fix} shows that including preview information does increase the driving comfort and safety. The comparison of the performance values $\Gamma(\cdot)$ of the FF_{var} and FB_{var} with those of FB, FF, FB_{fix}, and FF_{fix} has limited value, as the controlled outputs and weighting functions had to be chosen in a different way (see section 3.3). Nevertheless, we can state that including the road preview information via a time delay model and using the presented observer controller does not lead to a performance improvement for the NHQC, as the FB_{var} and FF_{var} controllers lead to the same comfort as the FB and FF controller, respectively, but to less driving safety.

In the next step, we examine the influence of the preview length. To do this, we determine the controllers for various constant nominal time delays τ_{nom} and re-test the performance with the profile of the bad country road and the NHQC (see fig. 2). All controllers, except the FF_{fix}, show a minor sensitivity to the preview time. The drop of the FF_{fix} for time delays greater than 0.3 s is based on the Padé approximation. For delays of this length, its order 10 is no longer sufficient. Thus, the performance of FF_{fix} for long preview times can easily be improved by increasing the order of (5). In the case of FB_{fix}, the feedback component compensates for the decline in the feedforward portion. Furthermore, the preview measurement of the road has a positive effect for the FB_{fix}. The highest comfort level is achieved with a preview of 0.036 s. The decline for time delays greater than 0.036 s
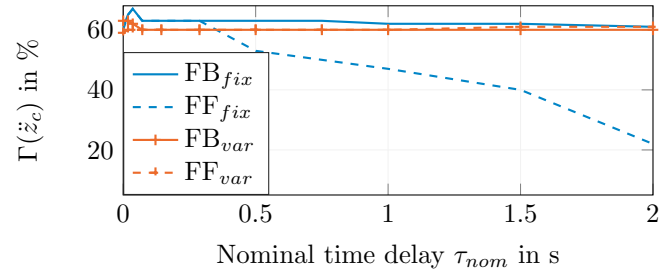

Fig. 2. Comparison of $\Gamma(\ddot{z}_c)$ for varying time delay (NHQC)

is due to the mismatch between the ideal actuator in the design model and the actuators in the NHQC. If the same simulations are performed with a fully active quarter car model, the performance converges with growing preview time, as long as the Padé approximation is good enough (see table 4). The performance of the FB_{var} and FF_{var} controllers is, as desired, robust against variations in the preview time, meaning that it is not even necessary to measure the disturbance in advance.

Next, we check the robustness of the preview controllers considering deviations of the preview time from the nominal value (see fig. 3). We assume that this deviation is known and that it is constant during one simulation run. This deviation can be interpreted as a change in driving speed or preview length. The FB_{fix} and the FF_{fix} are designed for the nominal preview time 0.072 s. Again, the
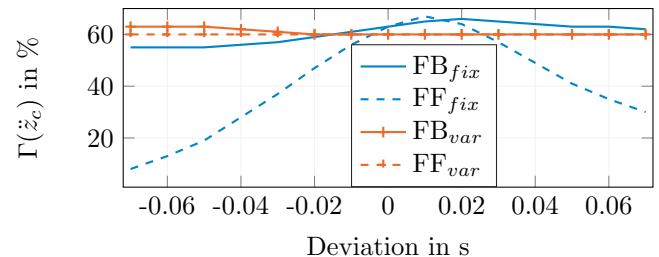
Fig. 3. Comparison of $\Gamma(\ddot{z}_c)$ for deviations from the nominal time delay $\tau_{nom} = 0.072\,$s (NHQC)

performance of the FB_{var} and the FF_{var} is almost independent of the deviation in the time delay. The comfort level of the FF_{fix} degrades rapidly when the absolute deviation from the nominal time delay increases. This drop is partially compensated by the feedback portion in the FB_{fix}. The best performance of the fixed preview controllers is not at the nominal time delay, but at 0.01 s and 0.02 s of deviation. As the actuator dynamics were not considered in the design model (3), the controllers assume that the input force can be realized perfectly, without delay, which is not possible in the NHOC. Thus, at nominal time delay, the actuator acts too slowly to compensate fully for the disturbance. If the time delay is slightly longer than expected, the too slow reaction of the actuator matches the actually required reaction, which improves performance.

Regarding table 2, the improvement achieved using preview information is not significant. Therefore, we take a look at the performance of the controllers simulated with the NFAQC model (see table 3). The FB_{var} and FF_{var}

Table 3. Controller performance with time delay $\tau_{nom} = 0.036\,\text{s}$ (NFAQC)

	FB	FF	FB_{fix}	FF_{fix}	FB_{var}	FF_{var}
$\Gamma(\ddot{z}_c)$	65%	63%	68%	67%	81%	80%
$\Gamma(F_{dyn})$	4%	6%	14%	17%	−12%	−48%
$\Gamma(z_c - z_w)$	23%	25%	15%	16%	11%	20%

gain 19 pp and 20 pp improvement, respectively, whereas the FB and the FF increase $\Gamma(\ddot{z}_c)$ just by 3 pp in comparison to the hybrid quarter car. This shows that the FB_{var} and the FF_{var} only have advantages regarding comfort, if the system model is close enough to the real system dynamics. As the driving safety decreases by more than 50% for the FF_{var}, this controller cannot be used with this parametrization in a real-world application. The FB_{fix} and FF_{fix} do not show any improvement. This is due to their short preview time. Table 4 shows the performance of $\Gamma(\ddot{z}_c)$ for FB_{fix} and FF_{fix} in the case of a time delay of $\tau_{nom} = 0.072\,\text{s}$ and $\tau_{nom} = 0.2\,\text{s}$. The comfort level increases up to 10 pp over that of the controller without preview. Furthermore, road holding and suspension deflection are better than those of FB and FF as well. Thus, the benefit from the road preview data is much greater in the case of a fully active quarter car. In the case of a hybrid quarter car, the performance gain due to preview data is limited as a result of the non ideal actuators.

Table 4. Performance of FB_{fix} and FF_{fix} with $\tau_{nom} = 0.072\,\text{s}$ and $\tau_{nom} = 0.2\,\text{s}$ (NFAQC)

	$\text{FB}_{fix,0.072}$	$\text{FF}_{fix,0.072}$	$\text{FB}_{fix,0.2}$	$\text{FF}_{fix,0.2}$
$\Gamma(\ddot{z}_c)$	73%	73%	75%	74%
$\Gamma(F_{dyn})$	14%	13%	6%	8%
$\Gamma(z_c - z_w)$	27%	28%	31%	31%

5. CONCLUSION AND OUTLOOK

In this paper, we showed how the quarter car can be modeled with road profile preview as a linear time delay system, and how an H∞ observer controller can be designed for this model. Furthermore, we compared the performance of this controller to H∞ controllers without preview and with constant preview modeled via a Padé approximation. The simulation results show that, in contrast to the H∞ controller based on the model with Padé approximation, the H∞ observer controller for time delay systems does work independently of the length of the time delay. However, this comes to the price of a reduced performance, as one fixed controller has to be designed suitable for arbitrary time delays. It was also observed that incorporating the preview data is beneficial, but that unmodeled actuator dynamics can limit the positive effects.

The next step is to test the controllers at the institute's quarter car test stand. Furthermore, an extension of the here used controller design method to time delay systems with a feedthrough of the input and the disturbance to the controlled and measured outputs can enable the use of $\ddot{z}_c$ and $\ddot{z}_w$ as measured and controlled outputs. At last, a controller design method for time delay systems, which is not completely independent of the time delay's value but incorporates it or at least its feasible range, can further improve the performance.

REFERENCES

Akbari, A. and Lohmann, B. (2010). Output feedback H∞ /GH₂ preview control of active vehicle suspensions: A comparison study of LQG preview. *Vehicle System Dynamics*, 48(12), 1475–1494.

Bender, E.K. (1968). Optimum linear preview control with application to vehicle suspension. *Journal of Basic Engineering*, 90(2), 213–221.

Bequette, B.W. (2010). *Process control: Modeling, design, and simulation.* Prentice Hall PTR, Upper Saddle River, NJ, 9th print edition.

Doyle, J.C., Glover, K., Khargonekar, P.P., and Francis, B.A. (1989). State-space solutions to standard H₂ and H∞ control problems. *IEEE Transactions on Automatic Control*, 34(8), 831–847.

Göhrle, C., Schindler, A., Wagner, A., and Sawodny, O. (2014). Design and vehicle implementation of preview active suspension controllers. *IEEE Transactions on Control Systems Technology*, 22(3), 1135–1142.

Hać, A. (1992). Optimal linear preview control of active vehicle suspension. *Vehicle System Dynamics*, 21(1), 167–195.

Hrovat, D. (1997). Survey of advanced suspension developments and related optimal control applications. *Automatica*, 33(10), 1781–1817.

Lauwerys, C., Swevers, J., and Sas, P. (2005). Robust linear control of an active suspension on a quarter car test-rig. *Control Engineering Practice*, 13(5), 577–586.

Mehra, R.K., Amin, J.N., Hedrick, K.J., Osorio, C., and Gopalasamy, S. (1997). Active suspension using preview information and model predictive control. In *Proceedings of the 1997 IEEE International Conference on Control Applications*, 860–865.

Mitschke, M. and Wallentowitz, H. (2014). *Dynamik der Kraftfahrzeuge.* VDI-Buch. Springer Vieweg, Wiesbaden, 5th edition.

Pellegrini, E. (2012). *Model-Based Damper Control for Semi-Active Suspension Systems.* Dissertation, Technical University of Munich, Munich.

Savaresi, S.M., Poussot-Vassal, C., and Spelta, C. (2010). *Semi-Active Suspension Control Design for Vehicles.* Elsevier Professional, 1st edition.

Schindler, A. (2009). *Neue Konzeption und erstmalige Realisierung eines aktiven Fahrwerks mit Preview-Strategie*, volume 31 of *Schriftenreihe des Instituts für Angewandte Informatik - Automatisierungstechnik, Universität Karlsruhe (TH)*. KIT Scientific Publ, Karlsruhe.

Sename, O. (2007). Is a mixed design of observer-controllers for time-delay systems interesting? *Asian Journal of Control*, 9(2), 180–189.

Sename, O. (2001). New trends in design of observers for time-delay systems. *Kybernetika*, 37(4), 427–458.

Skogestad, S. and Postlethwaite, I. (2007). *Multivariable feedback control: Analysis and design.* Wiley, Chichester, 2nd edition.

Unger, A.F. (2012). *Serientaugliche quadratisch optimale Regelung für semiaktive Pkw-Fahrwerke*, volume 66 of *Audi-Dissertationsreihe*. Cuvillier, Göttingen, 1st edition.

Zhou, K. and Doyle, J.C. (1998). *Essentials of robust control.* Prentice Hall, Upper Saddle River, NJ.

References

Own Publications

[117] J. N. Strohm and F. Christ. Preview H∞ Control of a Hybrid Suspension System. *9th IFAC Symposium on Advances in Automotive Control, IFAC-PapersOnLine,* 52.5 (2019), 237–242 (cf. pp. 31, 32, 37, 39).

[118] J. N. Strohm and B. Lohmann. Optimal Feedforward Preview Control by FIR Filters. *20th IFAC World Congress 2017, IFAC-PapersOnLine,* 50.1 (2017), 5115–5120 (cf. pp. 27, 28, 35, 36, 40).

[119] J. N. Strohm and B. Lohmann. Vorausschauende Störgrößenaufschaltung für die Schwingungsdämpfung am Viertelfahrzeug. *at - Automatisierungstechnik,* 65.8 (2017), 596–607 (cf. pp. 28–30, 37, 38, 40).

[120] J. N. Strohm and B. Lohmann. A Fast Convergence FxLMS Algorithm for Vibration Damping of a Quarter Car. In: *2018 IEEE Conference on Decision and Control (CDC).* IEEE, 2018, 6094–6100 (cf. pp. 29, 37, 39).

[121] J. N. Strohm, D. Pech, and B. Lohmann. A Proactive Nonlinear Disturbance Compensator for the Quarter Car. *International Journal of Control, Automation and Systems,* 18.8 (2020), 2012–2026 (cf. pp. 30, 38–40).

Other Publications

[1] J. Adamy. *Nichtlineare Systeme und Regelungen.* Berlin, Heidelberg: Springer Berlin Heidelberg, 2014 (cf. p. 30).

[2] O. Ajala, D. Bestle, and J. Rauh. Modelling and Control of an Electro-Hydraulic Active Suspension System. *Archive of Mechanical Engineering,* LX.1 (2013) (cf. p. 12).

[3] A. Akbari and B. Lohmann. Output feedback H∞ /GH 2 preview control of active vehicle suspensions: A comparison study of LQG preview. *Vehicle System Dynamics,* 48.12 (2010), 1475–1494 (cf. pp. 25, 32, 37).

[4] C. Arana, S. A. Evangelou, and D. Dini. Series Active Variable Geometry Suspension for Road Vehicles. *IEEE/ASME Transactions on Mechatronics,* 20.1 (2015), 361–372 (cf. p. 3).

[5] S. Barton-Zeipert. Fahrbahnprofilerfassung für ein aktives Fahrwerk. PhD thesis. Hamburg: Helmut-Schmidt-Universität, 2014 (cf. p. 24).

[6]   E. K. Bender. Optimum Linear Preview Control With Application to Vehicle Suspension. *Journal of Basic Engineering,* 90.2 (1968), 213–221 (cf. pp. 21, 23, 24, 37, 38).

[7]   B. W. Bequette. *Process control: Modeling, design, and simulation.* 9th print. Prentice-Hall international series in the physical and chemical engineering sciences. Upper Saddle River, NJ: Prentice Hall PTR, 2010 (cf. p. 24).

[8]   C. Briat. *Linear parameter-varying and time-delay systems: Analysis, observation, filtering & control.* Vol. 3. Advances in delays and dynamics. Heidelberg: Springer, 2015 (cf. p. 41).

[9]   J. C. Burgess. Active adaptive sound control in a duct: A computer simulation. *The Journal of the Acoustical Society of America,* 70.3 (1981), 715–726 (cf. pp. 29, 36).

[10] B. K. Cho. Active suspension controller design using MPC with preview information. *KSME International Journal,* 13.2 (1999), 168–174 (cf. pp. 25, 37).

[11] H. D. Choi, C. J. Lee, and M. T. Lim. Fuzzy Preview Control for Half-vehicle Electro-hydraulic Suspension System. *International Journal of Control, Automation and Systems,* 16.5 (2018), 2489–2500 (cf. pp. 25, 32, 37).

[12] ClearMotion Inc., ed. *Proactive Ride.* 2018. URL: https://www.clearmotion. com/technology (cf. p. 3).

[13] C. R. Cutler and B. L. Ramaker. Dynamic matrix control - A computer control algorithm. *Joint Automatic Control Conference,* 17 (1980) (cf. pp. 9, 35).

[14] S. Cytrynski, U. Neerpasch, R. Bellmann, and B. Danner. Das aktive Fahrwerk des neuen GLE von Mercedes-Benz. *ATZ - Automobiltechnische Zeitschrift,* 120.12 (2018), 42–45 (cf. p. 3).

[15] J. Deutscher and B. Lohmann. Flatness based asymptotic disturbance rejection for linear and nonlinear systems. In: *European Control Conference (ECC), 2003.* 2003, 3183–3188 (cf. p. 30).

[16] S. Devasia, D. Chen, and B. Paden. Nonlinear inversion-based output tracking. *IEEE Transactions on Automatic Control,* 41.7 (1996), 930–942 (cf. p. 35).

[17] J. C. Dixon. *The shock absorber handbook.* 2nd ed. Wiley-Professional engineering publishing series. Chichester, England: John Wiley, 2007 (cf. pp. 1, 2).

[18] M. Donahue and J. K. Hedrick. Implementation of an Active Suspension Preview Controller for Improved Ride Comfort. In: *Diploma Thesis.* 2001 (cf. p. 24).

[19] J. C. Doyle, K. Glover, P. P. Khargonekar, and B. A. Francis. State-space solutions to standard H_2 and H_∞ control problems. *IEEE Transactions on Automatic Control,* 34.8 (1989), 831–847 (cf. p. 22).

[20] F. Dunne and L. Y. Pao. Optimal blade pitch control with realistic preview wind measurements. *Wind Energy,* 19.12 (2016) (cf. p. 27).

[21] M. M. ElMadany, B. A. Al Bassam, and A. A. Fayed. Preview Control of Slow-active Suspension Systems. *Journal of Vibration and Control,* 17.2 (2010), 245–258 (cf. pp. 25, 37).

[22] Feng Tyan, Yu-Fen Hong, Shun-Hsu Tu, and Wes S. Jeng. Generation of Random Road Profiles. *CSME,* 4.2 (2009), 151–156 (cf. p. 19).

[23] M. Fliess, J. Lévine, P. Martin, and P. Rouchon. Sur les systèmes non linéaires différentiellement plats. (On differentially flat nonlinear systems). *Comptes Rendus de l'Académie des Sciences. Série I,* (1992) (cf. p. 9).

[24] M. Fliess, J. Lévine, P. Martin, and P. Rouchon. Flatness and defect of non-linear systems: Introductory theory and examples. *International Journal of Control,* 61.6 (1995), 1327–1361 (cf. p. 9).

[25] N. J. Ford, D. V. Savostyanov, and N. L. Zamarashkin. On the Decay of the Elements of Inverse Triangular Toeplitz Matrices. *SIAM Journal on Matrix Analysis and Applications,* 35.4 (2014), 1288–1302 (cf. p. 27).

[26] E. Fridman. *Introduction to Time-Delay Systems: Analysis and Control.* Systems & Control. Cham and s.l.: Springer International Publishing, 2014 (cf. p. 11).

[27] M. Fröhlich. *Ein robuster Zustandsbeobachter für ein semiaktives Fahrwerkregelsystem: Zugl.: München, Techn. Univ., Diss., 2008.* Als Ms. gedr. Vol. 675. Fortschritt-Berichte VDI Reihe 12, Verkehrstechnik/Fahrzeugtechnik. Düsseldorf: VDI Verl., 2008 (cf. p. 22).

[28] D. Fu, Y. Bai, and M. Sun. Delay-dependent H∞ dynamic output feedback control for systems with time-varying delay. In: *2009 IEEE International Conference on Control and Automation.* IEEE, 2009, 1184–1189 (cf. p. 41).

[29] W. S. Gan, S. Mitra, and S. M. Kuo. Adaptive feedback active noise control headset: Implementation, evaluation and its extensions. *IEEE Transactions on Consumer Electronics,* 51.3 (2005), 975–982 (cf. p. 36).

[30] Z. Gan, A. J. Hillis, and J. Darling. Adaptive control of an active seat for occupant vibration reduction. *Journal of Sound and Vibration,* 349 (2015), 39–55 (cf. p. 36).

[31] K. Garret. Simpler Controls Would Mean Safer Cars. *new scientist,* 65.931 (1975) (cf. p. 2).

[32] R. D. Gitlin, H. C. Meadors, and S. B. Weinstein. The Tap-Leakage Algorithm: An Algorithm for the Stable Operation of a Digitally Implemented, Fractionally Spaced Adaptive Equalizer. *Bell System Technical Journal,* 61.8 (1982), 1817–1839 (cf. pp. 29, 36).

[33] C. Göhrle. *Methoden und Implementierung einer vorausschauenden Fahrwerksregelung für aktive und semi-aktive Federungssysteme: Zugl.: Stuttgart, Univ., Diss., 2014.* Vol. 19. Steuerungs- und Regelungstechnik. Aachen: Shaker, 2014 (cf. pp. 25, 37).

[34] C. Göhrle, A. Schindler, A. Wagner, and O. Sawodny. Design and Vehicle Implementation of Preview Active Suspension Controllers. *IEEE Transactions on Control Systems Technology,* 22.3 (2014), 1135–1142 (cf. p. 25).

[35] C. Göhrle, A. Schindler, A. Wagner, and O. Sawodny. Road Profile Estimation and Preview Control For Low-Bandwidth Active Suspension Systems. *IEEE/ ASME Transactions on Mechatronics,* 20.5 (2015), 2299–2310 (cf. pp. 23, 40).

[36] G. H. Golub and C. F. van Loan. *Matrix computations.* 3. Aufl., [Nachdr.] Johns Hopkins studies in the mathematical sciences. Baltimore: Johns Hopkins Univ. Press, 2007 (cf. p. 24).

[37] C. Graf, R. Kieneke, and J. Maas. Online force estimation for an active suspension control. In: *2012 IEEE/ASME International Conference on Advanced Intelligent Mechatronics (AIM).* IEEE, 2012, 544–549 (cf. p. 22).

[38] B. L. J. Gysen, T. P. J. van der Sande, J. J. H. Paulides, and E. A. Lomonova. Efficiency of a Regenerative Direct-Drive Electromagnetic Active Suspension. *IEEE Transactions on Vehicular Technology,* 60.4 (2011), 1384–1393 (cf. p. 3).

[39] B. Gysen, J. Paulides, J. Janssen, and E. A. Lomonova. Active Electromagnetic Suspension System for Improved Vehicle Dynamics. *IEEE Transactions on Vehicular Technology,* 59.3 (2010), 1156–1163 (cf. p. 12).

[40] A. Hać. Adaptive Control of Vehicle Suspension. *Vehicle System Dynamics,* 16.2 (1987), 57–74 (cf. pp. 21, 23).

[41] A. Hać. Optimal Linear Preview Control of Active Vehicle Suspension. *Vehicle System Dynamics,* 21.1 (1992), 167–195 (cf. pp. 24, 37).

[42] R. J. Hampo and K. A. Marko. Investigation of the Application of Neural Networks to Fault Tolerant Control of an Active Suspension System. In: *1992 American Control Conference.* IEEE, 1992, 11–15 (cf. p. 40).

[43] S. S. Haykin. *Adaptive filter theory.* 5. ed. Always learning. Upper Saddle River, NJ: Pearson, 2014 (cf. pp. 29, 36).

[44] K. Howard. Active suspension. *Motor Sport,* 2001.12 (2001) (cf. p. 2).

[45] D. Hrovat. Survey of Advanced Suspension Developments and Related Optimal Control Applications. *Automatica,* 33.10 (1997), 1781–1817 (cf. p. 21).

[46] B. Huang, C.-Y. Hsieh, F. Golnaraghi, and M. Moallem. A Methodology for Optimal Design of a Vehicle Suspension System With Energy Regeneration Capability. *Journal of Vibration and Acoustics,* 137.5 (2015), 51014 (cf. p. 3).

[47] L. R. Hunt, G. Meyer, and R. Su. Noncausal inverses for linear systems. *IEEE Transactions on Automatic Control,* 41.4 (1996), 608–611 (cf. p. 35).

[48] International Organization for Standardization. *Mechanical vibration and shock – Evaluation of human exposure to whole-body vibration.* 1997-05 (cf. p. 19).

[49] A. Isidori. *Nonlinear control systems.* 3. ed. Communications and control engineering series. Berlin: Springer, 2002 (cf. pp. 7, 9).

[50] C. Jablonowski, J. Schmitt, and A. Obermüller. Das Fahrwerk des neuen Audi A8. *ATZextra,* 23.S9 (2018), 14–19 (cf. p. 3).

[51] W. D. Jones. Easy Ride - Bose Corp. uses speaker technology to give cars adaptive suspension. *IEEE Spectrum,* 42.3 (2005), 12–14 (cf. p. 16).

[52] G. Kannan, A. A. Milani, I. M. S. Panahi, and N. Kehtarnavaz. Performance enhancement of adaptive Active Noise Control systems for fMRI machines. *Conference proceedings : 32nd Annual International Conference of the IEEE Engineering in Medicine and Biology Society. IEEE Engineering in Medicine and Biology Society. Annual Conference,* 2010 (2010), 4327–4330 (cf. p. 36).

[53] D. Karnopp. Active Damping in Road Vehicle Suspension Systems. *Vehicle System Dynamics,* 12.6 (1983), 291–311 (cf. p. 12).

[54] D. Karnopp, M. J. Crosby, and R. A. Harwood. Vibration Control Using Semi-Active Force Generators. *Journal of Engineering for Industry,* 96.2 (1974), 619 (cf. p. 21).

[55] D. E. Kirk. *Optimal Control Theory: An Introduction.* Dover Books on Electrical Engineering. Newburyport: Dover Publications, 2004 (cf. p. 24).

[56] G. Koch, E. Pellegrini, S. Spirk, N. Pletschen, and B. Lohmann. *Actuator Control for a Hybrid Suspension System.* Vol. 6. Lehrstuhl für Regelungstechnik, 2011 (cf. p. 17).

[57] G. Koch. Adaptive control of mechatronic vehicle suspension systems. PhD thesis. München: Technische Universität München, 2011 (cf. p. 17).

[58] G. Koch, O. Fritsch, and B. Lohmann. Potential of Low Bandwidth Active Suspension Control with Continuously Variable Damper. *IFAC Proceedings Volumes,* 41.2 (2008), 3392–3397 (cf. p. 17).

[59] G. Koch, O. Fritsch, and B. Lohmann. Potential of low bandwidth active suspension control with continuously variable damper. *Control Engineering Practice,* 18.11 (2010), 1251–1262 (cf. pp. 16, 22).

[60] G. Koch and T. Kloiber. Driving State Adaptive Control of an Active Vehicle Suspension System. *IEEE Transactions on Control Systems Technology,* 22.1 (2014), 44–57 (cf. p. 40).

[61] G. Koch, T. Kloiber, and B. Lohmann. Nonlinear and filter based estimation for vehicle suspension control. In: *49th IEEE Conference on Decision and Control (CDC).* IEEE, 2010, 5592–5597 (cf. p. 22).

[62] G. Koch, S. Spirk, and B. Lohmann. Reference model based adaptive control of a hybrid suspension system. *IFAC Proceedings Volumes,* 43.7 (2010), 312–317 (cf. p. 23).

[63] J.-H. Koo and M. Ahmadian. A qualitative analysis of groundhook tuned vibration absorbers for controlling structural vibrations. *Proceedings of the Institution of Mechanical Engineers, Part K: Journal of Multi-body Dynamics,* 216.4 (2005), 351–359 (cf. p. 21).

[64] P. Krauze and J. Kasprzyk. Vibration control in quarter-car model with magnetorheological dampers using FxLMS algorithm with preview. In: *2014 European Control Conference (ECC)*. IEEE, 2014, 1005–1010 (cf. pp. 26, 36, 38, 39).

[65] R. Krebs. *Fünf Jahrtausende Radfahrzeuge: 2 Jahrhunderte Straßenverkehr mit Wärmeenergie. Über 100 Jahre Automobile.* Berlin, Heidelberg: Springer Berlin Heidelberg, 1994 (cf. p. 1).

[66] S.-M. Kuo and D. R. Morgan. *Active noise control systems: Algorithms and DSP implementations.* A Wiley-Interscience publication. New York, NY: Wiley, 1996 (cf. pp. 10, 26, 29, 36, 41).

[67] R. G. Langlois, D. M. Hanna, and R. J. Anderson. Implementing Preview Control on an Off-Road Vehicle with Active Suspension. *Vehicle System Dynamics,* 20.sup1 (1992), 340–353 (cf. p. 24).

[68] C. Lauwerys, J. Swevers, and P. Sas. Robust linear control of an active suspension on a quarter car test-rig. *Control Engineering Practice,* 13.5 (2005), 577–586 (cf. p. 22).

[69] H. Le Nguyen, K.-S. Hong, and S. Park. Road-frequency adaptive control for semi-active suspension systems. *International Journal of Control, Automation and Systems,* 8.5 (2010), 1029–1038 (cf. p. 23).

[70] J. Lévine. *Analysis and Control of Nonlinear Systems: A Flatness-based Approach.* Mathematical Engineering. Berlin, Heidelberg: Springer-Verlag Berlin Heidelberg, 2009 (cf. pp. 9, 30).

[71] Z. Li, I. Kolmanovsky, E. Atkins, J. Lu, D. Filev, and J. Michelini. Cloud aided semi-active suspension control. In: *2014 IEEE Symposium on Computational Intelligence in Vehicles and Transportation Systems (CIVTS)*. IEEE, 2014, 76–83 (cf. p. 38).

[72] B. Lohmann. Flatness Based Disturbance Compensation. *Scientific Report, Institute of Automation, University of Bremen,* (2002) (cf. p. 30).

[73] N. Louam, D. A. Wilson, and R. S. Sharp. Optimal Control of a Vehicle Suspension Incorporating the Time Delay between Front and Rear Wheel Inputs. *Vehicle System Dynamics,* 17.6 (1988), 317–336 (cf. pp. 25, 37).

[74] G. Ludyk. *Theoretische Regelungstechnik 1: Grundlagen, Synthese linearer Regelungssysteme.* Springer-Lehrbuch. Berlin and Heidelberg: Springer, 1995 (cf. p. 28).

[75] C. C. MacAdam. Application of an Optimal Preview Control for Simulation of Closed-Loop Automobile Driving. *IEEE Transactions on Systems, Man, and Cybernetics,* 11.6 (1981), 393–399 (cf. p. 27).

[76] J. M. Maciejowski. *Predictive control: With constraints.* Harlow: Prentice Hall, 2002 (cf. p. 9).

[77] K. M. Madhavan Rathai, M. Alamir, and O. Sename. Experimental Implementation of Model Predictive Control Scheme for Control of Semi-active Suspension System. *IFAC-PapersOnLine,* 52.5 (2019), 261–266 (cf. p. 23).

[78] K. M. Madhavan Rathai, M. Alamir, O. Sename, and R. Tang. A Parameterized NMPC Scheme for Embedded Control of Semi-active Suspension System. *IFAC-PapersOnLine,* 51.20 (2018), 301–306 (cf. pp. 25, 37).

[79] G. Marro, D. Prattichizzo, and E. Zattoni. Convolution profiles for right inversion of multivariable non-minimum phase discrete-time systems. *Automatica,* 38.10 (2002), 1695–1703 (cf. p. 35).

[80] W. Matschinsky. *Radführungen der Straßenfahrzeuge: Kinematik, Elasto-Kinematik und Konstruktion.* 3., aktualisierte und erweiterte Auflage. Berlin, Heidelberg: Springer-Verlag Berlin Heidelberg, 2007 (cf. p. 14).

[81] R. K. Mehra, J. N. Amin, K. J. Hedrick, C. Osorio, and S. Gopalasamy. Active suspension using preview information and model predictive control. In: *Proceedings of the 1997 IEEE International Conference on Control Applications.* 1997, 860–865 (cf. pp. 25, 37).

[82] M. Mitschke and H. Wallentowitz. *Dynamik der Kraftfahrzeuge.* 5., überarb. u. erg. Aufl. VDI-Buch. Wiesbaden: Springer Vieweg, 2014 (cf. pp. 13, 16, 19).

[83] A. Moran and M. Nagai. Optimal Preview Control of Rear Suspension Using Nonlinear Neural Networks. *Vehicle System Dynamics,* 22.5-6 (1993), 321–334 (cf. pp. 25, 38).

[84] A. Moran and M. Nagai. Optimal Active Control of Nonlinear Vehicle Suspensions Using Neural Networks. *JSME international journal. Ser. C, Dynamics, control, robotics, design and manufacturing,* 37.4 (1994), 707–718 (cf. p. 24).

[85] M. M. Morato, M. Q. Nguyen, O. Sename, and L. Dugard. Design of a fast real-time LPV model predictive control system for semi-active suspension control of a full vehicle. *Journal of the Franklin Institute,* 356.3 (2019), 1196–1224 (cf. p. 37).

[86] M. Münster, U. Mair, H.-J. Gilsdorf, A. Thomä, C. Müller, M. Hippe, and J. Hoffmann. Elektromechanische aktive Aufbaukontrolle. *ATZ - Automobiltechnische Zeitschrift,* 111.9 (2009), 644–649 (cf. p. 3).

[87] J. Nagumo and A. Noda. A learning method for system identification. *IEEE Transactions on Automatic Control,* 12.3 (1967), 282–287 (cf. pp. 29, 36).

[88] K. S. Narendra and K. Parthasarathy. Identification and control of dynamical systems using neural networks. *IEEE transactions on neural networks,* 1.1 (1990), 4–27 (cf. p. 40).

[89] K. Ogata. *Discrete time control systems.* Englewood Cliffs, NJ: Prentice-Hall, 1987 (cf. p. 8).

[90] K. Ogata. *Modern control engineering.* 4. ed., international ed. Upper Saddle River, NJ: Prentice Hall, 2002 (cf. p. 8).

[91] J.-E. Oh, S.-H. Park, J.-S. Hong, and J. Shin. Active vibration control of flexible cantilever beam using piezo actuator and Filtered-X LMS algorithm. *KSME International Journal,* 12.4 (1998), 665–671 (cf. p. 36).

[92] A. Olbrot. Stabilizability, detectability, and spectrum assignment for linear autonomous systems with general time delays. *IEEE Transactions on Automatic Control,* 23.5 (1978), 887–890 (cf. p. 11).

[93] J. Paschedag. Aktive Schwingungsisolation in Kfz-Motoraufhängungen – Systemkonfiguration und Methoden. PhD Thesis. München: Technische Universität München, 2008 (cf. p. 36).

[94] E. Pellegrini. Model-Based Damper Control for Semi-Active Suspension Systems. PhD Thesis. München: Technische Universität München, 2012 (cf. p. 17).

[95] N. Pletschen. Nonlinear H2 control of a low-bandwidth active vehicle suspension system using Takagi-Sugeno methods. In: *Advanced Vehicle Control AVEC'16.* Ed. by J. Edelmann, M. Plöchl, and P. E. Pfeffer. CRC Press/Balkema, P.O. Box 11320, 2301 EH Leiden, The Netherlands: Crc Press, 2016, 663–672 (cf. pp. 22, 23).

[96] N. Pletschen and K. J. Diepold. Nonlinear state estimation for suspension control applications: A Takagi-Sugeno Kalman filtering approach. *Control Engineering Practice,* 61 (2016), 292–306 (cf. pp. 22, 40).

[97] M. Pyper, W. Schiffer, and W. Schneider. *ABC - Active Body Control: Von der Blattfederung zum aktiven System für mehr Fahrsicherheit und Fahrkomfort.* Vol. 241. Die Bibliothek der Technik. München: Verl. moderne industrie AG & Co. KG, 2003 (cf. pp. 2, 17).

[98] S. Rajala, T. Roinila, M. Vilkko, O. Ajala, and J. Rauh. H ∞ Control Design of a Novel Active Quarter-Car Suspension System. *IFAC-PapersOnLine,* 50.1 (2017), 14519–14524 (cf. p. 22).

[99] K. M. M. Rathai, O. Sename, and M. Alamir. GPU-Based Parameterized NMPC Scheme for Control of Half Car Vehicle With Semi-Active Suspension System. *IEEE Control Systems Letters,* 3.3 (2019), 631–636 (cf. pp. 23, 37).

[100] P. Rouchon, M. Fliess, J. L. Évine, and P. Martin. Flatness and motion planning : the car with n trailers. In: *In Proc. European Control Conference.* 1993, 1518–1522 (cf. p. 9).

[101] M. Sambur. Adaptive noise canceling for speech signals. *IEEE Transactions on Acoustics, Speech, and Signal Processing,* 26.5 (1978), 419–423 (cf. p. 36).

[102] D. Sammier, O. Sename, and L. Dugard. Skyhook and H∞ Control of Semi-active Suspensions: Some Practical Aspects. *Vehicle System Dynamics,* 39.4 (2003), 279–308 (cf. p. 22).

[103] S. M. Savaresi, C. Poussot-Vassal, and C. Spelta. *Semi-Active Suspension Control Design for Vehicles.* 1. Ed. s.l.: Elsevier professional, 2010 (cf. p. 12).

[104] A. Schindler. *Neue Konzeption und erstmalige Realisierung eines aktiven Fahrwerks mit Preview-Strategie: Univ. (TH), Diss.–Karlsruhe, 2009.* Vol. 31. Schriftenreihe des Instituts für Angewandte Informatik - Automatisierungstechnik, Universität Karlsruhe (TH). Karlsruhe: KIT Scientific Publ, 2009 (cf. pp. 24, 27).

[105]   K. Schlacher and M. Schöberl. Construction of flat outputs by reduction and elimination. *IFAC Proceedings Volumes,* 40.12 (2007), 693–698 (cf. p. 9).

[106]   O. Sename. Is a Mixed Design of Observer-Controllers for Time-Delay Systems Interesting? *Asian Journal of Control,* 9.2 (2007), 180–189 (cf. pp. 31, 32).

[107]   O. Sename. New trends in design of observers for time-delay systems. *Kybernetika,* 37.4 (2001), [427]–458 (cf. p. 12).

[108]   K. Sharma, D. A. Crolla, and D. A. Wilson. The design of a fully active suspension system incorporating a Kalman filter for state estimation. In: *International Conference on Control '94.* IEE, 1994, 344–349 (cf. p. 22).

[109]   R. S. Sharp and D. A. Crolla. Road Vehicle Suspension System Design - a review. *Vehicle System Dynamics,* 16.3 (1987), 167–192 (cf. p. 12).

[110]   R. S. Sharp and S. A. Hassan. On the Performance Capabilities of Active Automobile Suspension Systems of Limited Bandwidth. *Vehicle System Dynamics,* 16.4 (1987), 213–225 (cf. p. 16).

[111]   R. S. Sharp and C. Pilbeam. On the Ride Comfort Benefits available from Road Preview with Slow-active Car Suspensions. *Vehicle System Dynamics,* 23.sup1 (1994), 437–448 (cf. pp. 25, 37).

[112]   H. J. Sira-Ramirez, A. Z. Matamoros-Sanchez, and R. M. Goodall. Flatness Based Control of a Suspension System: A GPI Observer Approach. In: *World Congress.* Ed. by B. Sergio. IFAC proceedings volumes. IFAC, Elsevier, 2011, 11103–11108 (cf. p. 9).

[113]   S. Skogestad and I. Postlethwaite. *Multivariable feedback control: Analysis and design.* 2. ed., reprinted with corr. Chichester: Wiley, 2007 (cf. p. 22).

[114]   S. Spirk. *Modulare vertikaldynamische Regelungskonzepte für ein hybrid aktuiertes Fahrwerk.* Fahrzeugtechnik. München: Dr. Hut, 2016 (cf. pp. 18, 24, 38, 39).

[115]   S. Spirk and B. Lohmann. *Controlling an active suspension using methods of optimal control: Final program and book of abstracts : Grand Wailea Waldorf Astoria Resort, Maui Hawaii, December 10-13, 2012.* [Piscataway, N.J.]: IEEE, 2012 (cf. pp. 23, 37).

[116]   R. Streiter. ABC Pre-Scan im F700. *ATZ - Automobiltechnische Zeitschrift,* 110.5 (2008), 388–397 (cf. p. 38).

[122]   J. Sun and Q. Yang. Research on Least Means Squares adaptive control for automotive active suspension. In: *2008 IEEE International Conference on Industrial Technology.* IEEE, 2008, 1–4 (cf. p. 23).

[123]   T. Takagi and M. Sugeno. Fuzzy identification of systems and its applications to modeling and control. *IEEE Transactions on Systems, Man, and Cybernetics,* SMC-15.1 (1985), 116–132 (cf. p. 23).

[124]   M. Takegaki and K. Matsui. A Design Method of Optimal Feedforward Compensator. *Transactions of the Society of Instrument and Control Engineers,* 21.4 (1985), 367–373 (cf. p. 35).

[125] Tenneco Inc., ed. *ACOCAR: Fully Active Suspension System.* 2011. URL: https://www.tenneco.com/assets/1/7/ACOCAR_Brochure.pdf (cf. p. 3).

[126] A. G. Thompson. An Active Suspension with Optimal Linear State Feedback. *Vehicle System Dynamics,* 5.4 (1976), 187–203 (cf. p. 21).

[127] A. G. Thompson, B. R. Davis, and C. E. M. Pearce. An Optimal Linear Active Suspension with Finite Road Preview. In: SAE Technical Paper Series. SAE International, Warrendale, PA, United States, 1980 (cf. pp. 12, 24, 37, 38).

[128] M. Tomizuka. "Optimum Linear Preview Control With Application to Vehicle Suspension"—Revisited. *Journal of Dynamic Systems, Measurement, and Control,* 98.3 (1976), 309 (cf. pp. 24, 37, 38).

[129] H. E. Tseng and D. Hrovat. State of the art survey: Active and semi-active suspension control. *Vehicle System Dynamics,* 53.7 (2015), 1034–1062 (cf. pp. 12, 16).

[130] J. C. Tudon-Martinez, S. Fergani, O. Sename, J. J. Martinez, R. Morales-Menendez, and L. Dugard. Adaptive Road Profile Estimation in Semiactive Car Suspensions. *IEEE Transactions on Control Systems Technology,* 23.6 (2015), 2293–2305 (cf. pp. 24, 38).

[131] A. F. Unger. *Serientaugliche quadratisch optimale Regelung für semiaktive Pkw-Fahrwerke: Zugl: München, Techn. Univ., Diss., 2012.* 1. Aufl. Vol. 66. Audi-Dissertationsreihe. Göttingen: Cuvillier, 2012 (cf. pp. 21, 22).

[132] M. Valášek, M. Novák, Z. Šika, and O. Vaculín. Extended Ground-Hook - New Concept of Semi-Active Control of Truck's Suspension. *Vehicle System Dynamics,* 27.5-6 (1997), 289–303 (cf. p. 21).

[133] VDI-Fachbereich Schwingungstechnik. *Human exposure to mechanical vibrations - Whole-body vibration.* Berlin, 2012 (cf. p. 19).

[134] S. Vosen. Hybrid energy storage systems for stand-alone electric power systems: Optimization of system performance and cost through control strategies. *International Journal of Hydrogen Energy,* 24.12 (1999), 1139–1156 (cf. p. 27).

[135] B. Wagner. *Analytische und iterative Verfahren zur Inversion linearer und nichtlinearer Abtastsysteme: Univ., Diss.–Erlangen-Nürnberg, 1998.* Als Ms. gedr. Vol. 763. Fortschritt-Berichte VDI Reihe 8, Meß-, Steuerungs- und Regelungstechnik. Düsseldorf: VDI-Verl., 1999 (cf. p. 35).

[136] B. Widrow. Adaptive Filters. In: *Aspects of network and system theory.* Ed. by R. E. Kalman and N. DeClaris. New York: Holt Rinehart Winston, 1971, 563–587 (cf. p. 10).

[137] B. Widrow and M. E. Hoff. Adaptive Switching Circuits. In: *1960 IRE WESCON Convention Record, Part 4.* New York: IRE, 1960, 96–104 (cf. p. 10).

[138] J.-D. Wu and R.-J. Chen. Application of an active controller for reducing small-amplitude vertical vibration in a vehicle seat. *Journal of Sound and Vibration,* 274.3-5 (2004), 939–951 (cf. p. 36).

[139] W. Xue, K. Li, Q. Chen, and G. Liu. Mixed FTS/ H∞ control of vehicle active suspensions with shock road disturbance. *Vehicle System Dynamics,* 57.6 (2018), 841–854 (cf. p. 12).

[140] M. Yamashita, K. Fujimori, C. Uhlik, R. Kawatani, and H. Kimura. H_∞ control of an automotive active suspension. In: *29th IEEE Conference on Decision and Control.* IEEE, 1990, 2244–2250 vol.4 (cf. p. 22).

[141] Y. Yokoya, K. Asami, T. Hamajima, and N. Nakashima. Toyota Electronic Modulated Suspension (TEMS) System for the 1983 Soarer. In: SAE Technical Paper Series. SAE International400 Commonwealth Drive, Warrendale, PA, United States, 1984 (cf. p. 2).

[142] F. Yu and D. A. Crolla. State Observer Design for an Adaptive Vehicle Suspension. *Vehicle System Dynamics,* 30.6 (1998), 457–471 (cf. p. 22).

[143] M. Yu, C. Arana, S. A. Evangelou, D. Dini, and G. D. Cleaver. Parallel Active Link Suspension: A Quarter-Car Experimental Study. *IEEE/ASME Transactions on Mechatronics,* 23.5 (2018), 2066–2077 (cf. p. 3).

[144] C. Yue, T. Butsuen, and J. K. Hedrick. Alternative Control Laws for Automotive Active Suspensions. *Journal of Dynamic Systems, Measurement, and Control,* 111.2 (1989), 286 (cf. p. 21).

[145] ZF Friedrichshafen AG, ed. *Völlig entspannt: ZF entkoppelt Insassen mit vollaktivem Fahrwerksystem sMOTION.* 15.06.2018. URL: https://press.zf.com/press/de/releases/release_2933.html (cf. p. 3).

[146] K. Zhou and J. C. Doyle. *Essentials of robust control.* Upper Saddle River, NJ: Prentice Hall, 1998 (cf. p. 22).

[147] Q. Zou and S. Devasia. Preview-Based Optimal Inversion for Output Tracking: Application to Scanning Tunneling Microscopy. *IEEE Transactions on Control Systems Technology,* 12.3 (2004), 375–386 (cf. p. 35).